

## **UC Davis**

### **UC Davis Electronic Theses and Dissertations**

#### **Title**

The Genetic Regulation of Wood Vessel Anatomical Traits in Populus

#### **Permalink**

<https://escholarship.org/uc/item/56f1p3bb>

#### **Author**

Rodriguez-Zaccaro, Fresia Daniela

#### **Publication Date**

2022

Peer reviewed|Thesis/dissertation

The Genetic Regulation of Wood Vessel Anatomical Traits in *Populus*

By

FRESIA DANIELA RODRIGUEZ-ZACCARO  
DISSERTATION

Submitted in partial satisfaction of the requirements for the degree of

DOCTOR OF PHILOSOPHY

in

Plant Biology

in the

OFFICE OF GRADUATE STUDIES

of the

UNIVERSITY OF CALIFORNIA

DAVIS

Approved:

---

Andrew T. Groover (Chair)

---

Gail Taylor

---

Maciej Zwieniecki

Committee in Charge

2022

## Table of Contents

<b>Acknowledgements and Dedication</b> .....	iii
<b>Abstract</b> .....	iv
<b>Introduction</b> .....	1
<b>Chapter 1</b> .....	26
Wood and water: How trees modify wood development to cope with drought	
<b>Chapter 2</b> .....	51
Genetic regulation of vessel morphology in Populus	
<b>Chapter 3</b> .....	81
A systems genetic analysis of vessel traits in poplar	
<b>Chapter 4</b> .....	135
The effects of genotype and drought on tree physiology and wood anatomy	
<b>Conclusions</b> .....	179

## **Acknowledgements**

This work would have not been possible without the support of the many kind and talented researchers who helped and advised me throughout my time as a graduate student. I want to especially thank my advisor, Andrew Groover, for his patience, kindness, and willingness to always lend a helping hand. I am truly grateful for his thoughtful advice and words of encouragement during stressful times. I want to thank my dissertation committee, Gail Taylor and Maciej Zwieniecki, for their advice and support. Suzanne Gerttula and Héloïse Bastiaanse are thanked for generously instructing me in valuable laboratory techniques and statistical methods. I am grateful to Courtney Canning for substantial assistance in setting up experiments and keeping my trees alive. I want to thank Isabelle Henry and Meric Lieberman for their invaluable assistance involving chapter editing, RNA-sequencing and sequence data processing. Nancy Zaragoza, Haley Harrison, Aedric Lim, Pakeeza Azizpor, and Lucy Sullivan are also thanked for the countless hours spent helping me in the greenhouse and laboratory.

## **Dedication**

Le dedico este trabajo a mi mamá Daniela Zaccaro, a mis abuelitos Esterina y Ramón Galo, y a mi familia. Todos son importantes para mí. Los quiero mucho.

## Abstract

Vessel elements are highly lignified, tube-like cells that serve as the primary water transporting conduits in angiosperm wood. These cells stack end-on-end to form larger structures known as vessels, which provide a low-resistance pathway for the movement of water from roots to leaves. The dimensions and distribution of vessels in wood (vessel anatomy) directly influence water transport efficiency, ultimately affecting tree photosynthetic capacity and growth. Vessel anatomy is also a factor that contributes to the vulnerability of trees to drought-induced cavitation, a process that can lead to lethal hydraulic failure. The genetic regulation of wood anatomy and related physiological traits is not very well understood. A detailed review of wood structure, function, drought acclimation, and implications for forest tree survival can be found in Chapter 1 of this dissertation. Chapters 2 to 4 consist of three studies that make use of a unique *Populus deltoides* × *nigra* pedigree carrying genomically defined insertions and deletions that generate gene dosage variation. In Chapter 2, we found that all examined wood traits are under genetic control, showing moderate heritabilities ranging from 0.32 to 0.53. We found significant line-dependent trait variation and significant correlations between most examined traits and gene dosage at specific genomic regions. In Chapter 3, we studied whole transcriptome gene expression in wood forming tissues and integrated our analyses with our previous trait-dosage correlations to find putative mechanisms and specific candidate genes related to trait variation. In particular, we found evidence for tree height-independent regulation of vessel traits. Lastly, in Chapter 4 we found evidence of gene dosage-dependent variation in vessel anatomy-related physiological traits, including vulnerability to drought-induced cavitation. Understanding the genetic regulation of vessel traits in wood will be vital for the development of successful mitigation strategies under current and future climate change-related drought.

## **Introduction**

### *Trees and drought*

Trees are vital components of numerous ecosystems worldwide. At the ecosystem scale, trees can modulate temperatures, influence hydrological, nitrogen and carbon cycles, and act as keystone organisms that help maintain species diversity (Bond et al. 2007; Pastor and Post 1986; Manning et al. 2006). Globally, forest trees have a major role in carbon sequestration, serving as a sink for an estimated 26% of the world's yearly carbon emissions from 2000 to 2007 (Pan et al. 2011). The impact of trees on the global economy is significant, with the wood-based industry contributing over \$1.52 trillion to national economies in 2015 (FAO 2022). Tree growth and survival across many natural ecosystems, including forests harvested for wood products, are largely limited by water availability (Lambers and Oliveira 2019). Accordingly, climate change-associated heat and drought have been linked to a significant rise in world-wide tree mortality (Allen et al. 2010). Projected climate change scenarios involving increasingly severe and frequent drought events are expected to continue this trend throughout the 21<sup>st</sup> century (McDowell and Allen 2015). Drought can directly kill or reduce the fitness of trees through two non-mutually exclusive physiological mechanisms: carbon starvation and hydraulic failure. Carbon starvation involves the avoidance of desiccation through stomatal closure at the cost of carbon assimilation, restricting the production of necessary sugars. Hydraulic failure involves the embolism-induced obstruction of water flow between roots and water-demanding tissues, resulting in desiccation (McDowell et al. 2008). Susceptibility to hydraulic failure is partially determined by wood anatomy, which includes the dimensions and distributions of water-conducting cells (see "*Wood vessel anatomy affects tree hydraulic function*" below). The study of wood anatomical traits, then, can provide valuable insights into how trees will cope in future climate scenarios. Trees within the *Populus* genus (poplar trees) are particularly well suited as a

system in which to study wood traits. Compared to other forest trees, *Populus* species and hybrids are relatively fast growing, have short generation times, can be easily vegetatively propagated, and respond quickly to experimental treatments. The genetic dissection of traits is facilitated in *Populus* through the availability of a completely sequenced genome, ease of genetic transformation and substantial genetic and phenotypic variation within and across populations (Ellis et al. 2010).

### *The vascular cambium and the structure of wood*

All plant growth ultimately originates from indefinitely maintained stem cell-containing regions called meristems. The shoot and root apices contain the primary meristems that generate all above and below ground axial growth, respectively. Ultimately derived from the primary meristems, the vascular cambium is a secondary meristem that is responsible for most plant radial growth. This includes the production of secondary phloem (or inner bark) towards the outside and of secondary xylem (or wood) towards the inside of stems and roots (Bennet and Leyser 2006). The vascular cambium expands outwards while leaving new xylem behind through periclinal divisions, while maintaining continuity through anticlinal divisions. The vascular cambium (or cambial zone) is composed of fusiform and ray initials, along with their immediate derivatives. In angiosperms, the derivatives of fusiform initials differentiate on the xylem side into axial parenchyma cells, fiber cells, or tracheary elements, which include vessel elements and occasionally tracheids (Carlquist 2001). Ray initial derivatives differentiate into ray parenchyma cells. Axial and ray parenchyma cells are organized into longitudinal strands and transverse rays, respectively, and constitute the metabolically active living tissue of wood. Together, axial and radial parenchyma tissues form a highly interconnected network and function as water and nonstructural carbohydrate reservoirs. Parenchyma tissues likely play a role in

embolism refilling and ion-mediated changes in water flow (Slupianek et al. 2021). Fibers cells have thick and highly lignified secondary cell walls and specialize in structural and mechanical support. Typically dead at functional maturity, these cells are highly elongated due to extensive axially oriented intrusive growth during their development (Thomas 1977). Lastly, vessel elements are tube-like cells that function as the primary water transporting conduits in angiosperm wood. Broadly, vessel element development from fusiform derivatives involves rapid and dramatic radial expansion, the deposition of a highly lignified secondary cell wall, and programmed cell death, producing a dead but functionally mature conductive cell (Dejardin et al. 2010). The axially located end walls of developing vessel elements are degraded during cell autolysis, forming openings known as perforation plates (Yata et al. 1970). Individual vessel elements are connected at perforation plates to form larger structures called vessels, which provide a pathway for the upward movement of water under tension. Openings in the secondary cell wall known as pits allow for the lateral flow of water between vessel elements, and between vessel elements and parenchyma cells. Unlike open perforation plates, pits are sealed with water-permeable pit membrane structures, which generate some resistance to water flow (Choat et al. 2006).

### *Wood hydraulic function*

Arranged in a complex interconnected network, vessels in wood provide a low-resistance pathway for the long-distance transport of water and solutes from roots to leaves. The upward flow of water is predominantly driven by capillary forces generated in transpiring leaves. When stomata are open, water evaporates from air-water menisci in mesophyll cell walls into leaf intercellular spaces. As menisci become more concave due to water evaporation, the surface tension of water resists this deformation, generating negative pressure. This negative pressure

pulls water up through the xylem network as an unbroken column held together by cohesion (Brown 2013). More broadly, the movement of xylem sap is driven by a water potential gradient across the soil-tree-atmosphere continuum, with water moving from a region of relatively high water potential (i.e., irrigated soil) to very low water potential (i.e., the atmosphere). Xylem sap, then, is transported under large negative pressures in a metastable state (Lambers and Oliveira 2019). Under increasingly dry conditions the upward flow of water can be impeded by the formation and spread of air pockets within the xylem network, eventually leading to lethal hydraulic failure (Barigah et al. 2013). Air pocket formation is caused by cavitation, which is the phase change of water from liquid to gas. Cavitation during drought is thought to be the consequence of air-seeding from adjacent air-filled cells through shared pit membranes. As water availability decreases, xylem sap pressure becomes sufficiently negative to force an air bubble from an adjacent air-filled space into a functioning vessel. This air bubble serves as a nucleation site for cavitation (Cochard 2006).

#### *Wood vessel anatomy affects tree hydraulic function*

Wood vessel anatomy directly affects the ability of trees to efficiently move water from roots to shoots. Greater water transport efficiency (quantified as a volumetric flow rate) ultimately allows for increased photosynthetic rates and growth (Campanello et al. 2008). However, high water transport efficiency has been associated with an increased risk of cavitation and embolism formation during freeze-thaw cycles and drought (Li and Wang 2019; Gleason et al. 2016). Vessel cross-sectional width (termed vessel diameter) has been extensively linked to tree hydraulic function, with larger vessels allowing for more efficient transport of water at the cost of decreased safety from cavitation (Hacke et al. 2016). The positive relationship between vessel width and volumetric flow rate has been at least partially explained through the Hagen-

Poiseuille law, which states that the flow rate of a liquid moving through a tube is proportional to the fourth power of the conduit radius (Elmore and Ewers 1986). Due to their more extensive pitted wall area, larger vessels could be more prone to air-seeding during drought when compared to more narrow vessels, leading to greater risk of cavitation (Wheeler et al. 2005). The number of vessels per unit area of cross-sectional xylem (known as vessel frequency or density) is generally strongly negatively correlated to mean vessel diameter in tree stems. Consequently, greater vessel frequencies are often linked to lower water transport efficiency and increased safety to cavitation (Sperry et al. 2008). Greater vessel frequencies can also independently contribute to hydraulic safety and efficiency by ensuring that a greater percentage of vessels remain functional after cavitation and embolism occur (Tyree et al. 1994). Vessel diameter often decreases, while vessel frequency increases in woody stems as a response to drought and other stressors (see “Environmental effects on wood anatomy” below). Interestingly, some tropical trees have been shown to respond to high salinity or dry conditions by significantly increasing vessel number with minimal change to vessel diameter, increasing both transport efficiency and safety from cavitation (Schmitz et al. 2006; Verheyden et al. 2005).

Less well-studied traits include vessel clustering (or vessel grouping) and cross-sectional vessel shape. Vessel grouping is a proxy for the extent of interconnectivity of the xylem network through shared pits (Scholz et al. 2013). Greater vessel grouping has been related to increased stem hydraulic conductivity through the decrease in flow path resistance and increased capacity to modulate flow through sap ionic concentrations (Loepfe et al. 2007; Nardini et al 2012). Greater vessel grouping indices have been correlated to either increased or decreased resistance to cavitation across different studies. Greater vessel grouping could lead to increased resistance to cavitation due to the presence of alternate water pathways that can circumvent embolism

blockage (Smith et al. 2013; Carlquist 1984). Other studies have suggested that greater vessel grouping can lead to decreased resistance to cavitation through an increased likelihood of embolism spread within a highly interconnected xylem network (Guet et al. 2015, Loepfe et al. 2007). The precise relationship between vessel grouping and vulnerability to cavitation is likely species dependent and could be related to the distribution of vessel sizes within sapwood. The functional significance of vessel shape in wood is not very well understood. However, microchannel fluid flow theory suggests that vessels that are closer to perfect cross-sectional circularity allow for more efficient water transport compared to other shapes (Zhao et al. 2019). Vessel shape could also affect the likelihood of conduit implosion under tension, with more circular sections of vessels capable of evenly distributing loading stress (Grigorenko and Rozhok 2014).

#### *Environmental effects on wood anatomy*

Water availability is often the most important limiting factor for tree growth and productivity (Lambers and Oliveira 2019). Consequently, much attention has been given to the effects of water stress on tree and wood development. Drought has been shown to induce the formation of wood with decreased vessel diameters and increased vessel frequencies in relation to well-watered controls. The magnitude of this response is highly variable across different poplar tree genotypes. Cao et al. (2013) found that *P. deltoides* × *P. nigra* hybrids developed wood with greater vessel frequency and lower vessel diameters under drought, while *P. cathayana* showed no response. Fichot et al. (2009) found variable wood anatomy responses across six *P. deltoides* × *P. nigra* genotypes, ranging from no response to high wood plasticity under drought. Similarly, the degree of vessel frequency increase under drought varied significantly between different *P. nigra* genotypes, with a genotype originating from a wet site

showing the greatest response (Wildhagen et al. 2018). The magnitude of this response can also vary depending on season, with vessels produced during early summer showing a greater response to drought than those produced in late summer (Arend and Fromm 2007). Drought-induced alterations in wood anatomy have been linked to changes in hydraulic function, with studies reporting significant reductions in water transport efficiency and increases in resistance to cavitation in drought-treated plants (Plavcova and Hacke 2012; Awad et al. 2010). Accordingly, this response has been interpreted as a mechanism through which trees can become resistant to drought-induced hydraulic failure, with the ability to acclimate seen as an adaptive trait (Arend and Fromm 2007). Why some genotypes or species have greater wood developmental plasticity under drought is not very well understood from either an evolutionary or genetic perspective. Presumably, xylem plasticity could evolve in populations exposed to variable levels of water availability or extreme temperature fluctuations, as generally speaking, a limited potential for acclimation could have detrimental consequences for fitness (Martinez-Meier et al. 2008).

Drought has also been shown to significantly affect pit structure, with specific effects occurring in a genotype-dependent manner. Drought was related to increases in maximum pit pore size in *P. tremuloides* and increases in percentage of porous pit membranes in both *P. tremuloides* and *P. balsamifera* (Hillabrand et al. 2016). These pit structural changes can potentially result in greater vulnerability to cavitation through increased likelihood of air seeding through larger and more numerous pit pores (Hacke et al. 2001). Drought-induced cell wall composition changes have also been reported. Drought stress produced thicker secondary cell walls in fibers, with reduced expression of secondary cell wall biosynthesis genes (Yu et al. 2021). In eucalyptus trees, drought induced an increase of lignin content in vessel secondary walls in a species-dependent manner (Moulin et al 2022). Increased lignin content in vessels as a

result of drought has been interpreted as adaptation that helps reduce vulnerability to implosion under extreme tension (Hillabrand et al. 2019).

Environmental stressors such as high salinity and freezing temperatures can induce the production of wood with a similarly altered vessel anatomy. High salinity can significantly reduce water potential in soil, disrupting the pressure gradient that drives the movement of water into roots (Boursiac et al. 2005). This reduces the flow of sap through the xylem and the ability of living cells to take up water, resulting in desiccation (Sobrado 2001). A high salt treatment applied to *P. × canescens* resulted in the production of wood with smaller and more numerous vessels, along with a decrease in xylem radial growth. The same treatment did not induce these alterations in the more salt-tolerant *P. euphratica* (Junghans et al. 2006). Similarly, exposure to high salinity in horse chestnut (*Aesculus hippocastanum*) resulted in decreased vessel diameter and increased vessel frequency (Eckstein et al. 1976). Salt stress-induced alterations in wood anatomy have been directly related to decreased xylem osmotic potential, along with lower K<sup>+</sup> concentrations in stems. Interestingly, anatomical changes have often been limited to vessels, with little to no size alterations reported for fiber or ray cells (Janz et al. 2011; Escalante-Estrada et al. 2009).

The non-living vessel network in wood can become embolized due to freeze-thaw induced cavitation. In addition, wood structure and composition can be modified by freezing conditions. In eucalyptus hybrid, chilling temperatures resulted in thicker and more lignified xylem cell walls and a significant decrease of vessel and fiber lumen diameters (Ployet et al. 2018). Cell wall modifications involving increased lignin and hemicellulose content have been related to increased resistance to frost (LeGall et al. 2015; Burke et al. 1976). Variations in vessel width and frequency have been widely reported in natural populations across temperature

gradients, with trees experiencing colder temperatures often showing smaller and more numerous vessels, often with shorter vessel lengths and increased lignification (Pandey et al. 2020; Baas and Wheeler, 2011). Poplar hybrids with narrow vessels showed lower degrees of freeze-thaw induced embolism. Safe narrow vessels could be a vital adaptive trait in boreal environments (Schreiber et al. 2013).

*Exploring the genetic regulation of wood vessel anatomical traits through molecular approaches*

Molecular studies that examine wood anatomy predominantly focus on vessel cross-sectional diameter and frequency, two traits that are often highly negatively correlated and likely difficult to disentangle genetically. As previously mentioned, fully differentiated vessel elements in wood are the result of a sequence of developmental steps, including cell fate determination, cell expansion, secondary cell wall deposition and programmed cell death (Jin and Fan 2009). The final diameter of a vessel element is likely determined by outward expansion generated by turgor pressure inside the developing cell, and cell wall properties that restrict said expansion. Turgor pressure is ultimately modulated by the ability of water to move into developing xylem cells. Aquaporins are membrane-bound channel proteins that can facilitate the movement of water into and out of cells and are coded for by genes in the PIP (PLASMA MEMBRANE INTRINSIC PROTEIN) and TIP (TONOPLAST INTRINSIC PROTEIN) families, among others. PIP1 and PIP2 are expressed in woody poplar stems (Secchi and Zwieniecki 2010). PIP2;3, PIP2;5 and TIP2;1 are highly expressed in the cambial zone, developing xylem cells and parenchyma rays in hybrid poplar stems. High expression of these genes in contact cells (parenchyma ray cells that share a pit with vessel elements) was more consistent than in isolation cells (ray cells not in direct contact with vessel elements), suggesting that rays serve as water reservoirs for vessel elements. Expression of these genes in the cambium was widened under high water and nitrogen

conditions. Trees with wider aquaporin expression produced wider and less numerous vessels, suggesting that aquaporin-mediated water transport plays a role in rapid vessel expansion and vessel number determination (Almeida-Rodriguez and Hacke 2012).

Osmotic adjustment within developing xylem cells likely also has an important role in the modulation of turgor pressure and cell expansion. Potassium ( $K^+$ ) transport has been shown to modulate turgor and cell expansion in guard cells, with an influx of  $K^+$  driving an influx of water into cells (Kwak et al. 2001).  $K^+$  varies seasonally in poplar hybrid cambium, with the highest content measured during spring and summer, during early wood formation, and the lowest during the fall and winter, during latewood formation.  $K^+$  content was strongly correlated to osmotic potential, with greater  $K^+$  related to lower osmotic potentials (Wind et al. 2004). Likewise, increased  $K^+$  concentration in the cambium and wood forming tissues through nutrient treatment has been related with increased vessel size, while treatment with  $K^+$  channel blockers resulted in significantly smaller vessels (Langer et al. 2002), suggesting that this osmolyte plays an important role in cell expansion. A recent study identified a potential plasma membrane localized  $K^+$  transporter in developing poplar xylem. A loss of function mutant showed smaller and less numerous vessels, while an overexpressor showed larger and more numerous vessels (Ribeiro et al. 2020).

The primary cell wall of a developing vessel element limits turgor-driven expansion and presumably helps determine the final diameter of a vessel. Primary cell walls are composed of cellulose microfibrils organized in a net-like structure, which is in turn embedded in a pectin matrix and cross-linked by hemicelluloses, primarily xyloglucan (Cosgrove 1997). The ability of the cell wall to expand, termed cell wall plasticity, depends on the structure and orientation of cellulose microfibrils and how they interact with other wall polysaccharides. In particular, the

activity of cell wall modifying enzymes that disrupt links between hemicelluloses and microfibrils can affect how pliable a cell wall is to turgor pressure (Mellerowicz 2006). Proposed models suggest that the breakage of hemicellulose cross-links (or separation from microfibrils) is required to allow microfibrils to move apart and allow expansion (Carpita and Gibeaut 1993). In particular, xyloglucan endotransglycosylases (XETs), which cut and rejoin cross-linking hemicelluloses, have been shown to increase primary cell wall extensibility (Van Sandt et al. 2007). Expansins disrupt hemicellulose-microfibril bonding in a PH dependent manner and are similarly related to cell wall expansion (McQueen and Cosgrove 1994). Both XETs and expansins are primarily expressed in the vascular cambium and developing wood in stems (Bourquin et al. 2002; Wang et al. 2010). However, not many studies directly link primary cell wall remodeling in the cambial zone to ultimate vessel size and frequency.

Alterations in secondary cell wall biosynthesis-related genes have been shown to affect wood vessel anatomy, suggesting that secondary cell wall deposition has a role in determining the final diameter and frequency of vessels. XND1 (XYLEM NAC DOMAIN 1) is a negative regulator of genes involved in secondary cell wall synthesis (Zhong et al. 2021). Overexpression of this gene in poplar stems resulted in decreased cell division rates from the cambium, as well as reduced vessel diameters and frequencies in relation to controls. XND1 expression was greatest in cells within the expansion zone, in the early stages of secondary cell wall deposition (Grant et al. 2010). ERF (ETHYLENE RESPONSE FACTOR) genes have been shown to reduce xylem cell lignification. Overexpression of this gene in poplar resulted in reduced vessel diameters and increased vessel frequencies (Wessels et al. 2019). MYB2 is a transcription factor shown to regulate genes in the monolignol biosynthesis pathway. Overexpression of this gene in stems

resulted in increased vessel lumen areas, decreased vessel frequencies and a reduction in vessel grouping (De Micco et al. 2012).

The degree of vessel grouping in wood ultimately depends on the regulation of cell fate determination from the cambium. Cell fate determination and spatial patterning in wood have been associated with auxin transport and concentration gradients. Namely, chemically induced auxin accumulation in the vascular cambium resulted in the production of bands of highly clustered vessel elements in poplar wood and the formation of large areas containing only fiber cells (Junghans et al. 2003; Johnson et al. 2018). The genetic regulation of vessel shape (which includes circularity) is poorly understood. Variation in this trait could be determined by differences in primary cell wall structure across radial and tangential walls, leading to differences in anisotropic expansion that result in varied degrees of cell elongation. Likewise, secondary cell wall formation could also play a role in final cell shape. Cellulose deficient IRX (IRREGULAR XYLEM) mutants, for example, are characterized by thin, irregularly shaped secondary cell walls (Hao and Mohnen 2014).

#### *Exploring the genetic regulation of wood vessel traits through quantitative genetics approaches*

Most biologically important traits in plants are quantitative and likely controlled by numerous genes with minor effects as well as by the environment (Ikram and Chardon 2010). Consequently, quantitative genetics approaches can provide valuable insights into the genetic regulation of wood development. Three useful techniques include the estimation of heritability of traits through pedigrees and clones, quantitative trait loci (QTL) mapping and genome-wide association studies (GWAS). However, studies that examine poplar wood vessel anatomical traits through these approaches are limited. Broad sense heritability estimates represent the proportion of phenotypic variation of a trait within a population that can be attributed to genetic

as opposed to environmental factors. Because wood anatomical traits are known to be highly environmentally plastic, obtaining heritability estimates can be crucial for selective breeding for trait improvement (Schmidt et al. 2019). Many studies focus on wood density, specific gravity and fiber dimensions, considered important factors for wood quality (Pande 2011; Pliura et al. 2007; Beaudon et al. 1992; Yanchuk et al. 1984), while a limited amount focus on vessel traits, mainly vessel element length and diameter (Pande and Dhiman 2011). QTL mapping and GWAS approaches can help identify loci that are significantly correlated to traits of interest, which can lead to the identification of candidate genes. These methods can help estimate the magnitude of the effect of genomic regions on trait variation and generally elucidate the genetic architecture of traits and (Mauricio 2001; Cortes et al. 2021). To date, very few of these studies have focused on poplar wood vessel anatomy. A recent GWAS analysis on *P. trichocarpa* reported a single significant association with intermediate vessel element width (Chhetri et al. 2020).

#### *Transcriptomic approaches and gene dosage effects*

Groups of genes interact in complex regulatory networks that influence the phenotypes of organisms. Whole-genome transcriptome gene expression studies have provided some recent insight into the regulatory gene networks associated with vessel anatomy. A differential expression study involving drought treated and well-watered controls suggested that an antagonistic effect between ABA signaling and secondary cell wall formation could be related to smaller and more numerous vessels seen in drought-stressed wood (Yu et al. 2021). Mature poplar wood, which contains wider and less numerous vessels compared to juvenile wood showed extensive over-expression of turgor maintenance and cell expansion related genes (Luo et al. 2021). However, elucidating the genetic architecture, regulatory pathways and mechanisms that determine wood anatomical trait variation has been limited by a lack of suitable germplasm

resources. Substantial phenotypic and genetic variation is crucial for the effective functional genomic dissection of traits. Such variation might not be readily found in natural populations, as mutations affecting important traits might be strongly selected against or show meiotic instability. Gene dosage (or gene copy number) has been related to important quantitative trait variation in plants (Liu et al. 2003). Gene dosage alterations have been shown to induce not only cis, but numerous trans gene expression effects, suggesting that dosage disruption of a few genes can have large effects on complex regulatory pathways (Guo and Birchler 1994). Likewise, dosage alterations of genes coding for protein subunits have been shown to affect the function of whole multi subunit proteins due to stoichiometric imbalances (Birchler and Veitia 2014). Although gene dosage represents an important source of genetic variation its effects on wood anatomy and related physiological traits are currently poorly understood. Exploring the relationship between dosage variation and wood vessel anatomy, then, can provide invaluable new insights into the genetic control of these traits.

#### *Utilizing a unique poplar dosage mutant pedigree*

The following chapters will consist of a review of the relationship between wood traits and drought (Chapter I), and three related studies making use of a unique dosage mutant poplar pedigree for trait dissection (Chapters II, III and IV). First developed and described by Henry et al. (2015), this pedigree was produced by crossing two female *P. deltoides* with a male *P. nigra*'s gamma-irradiated pollen. Approximately 800 F1 individuals were completely sequenced to determine the exact locations and sizes of gamma irradiation-induced insertions and deletions. In Chapter II, 201 F1 progeny lines were used to estimate the phenotypic and genetic variance of wood and stem traits. Additionally, dosage dependent QTL analyses were conducted to test for significant correlations between trait variation and relative gene dosage throughout the genome.

In Chapter III, an RNA-seq study was conducted on the wood-forming tissues of 33 lines included in the previous chapter (many selected due to extreme wood phenotypes and the presence of indels spanning dosage QTLs). The goal of this study was to identify and functionally characterize gene groups or networks associated to wood and stem trait variation, and to identify candidate genes within networks. Lastly, Chapter IV involves a preliminary study exploring the relationship between gene dosage and physiological traits related to wood anatomy. A subset of 8 lines included in Chapters II and III were chosen due to the presence of insertions or deletions spanning a wood anatomy dQTL identified in Chapter II (including 2 non-lesion controls). The aim was to determine if traits like vulnerability to cavitation ( $P_{50}$ ) and stomatal conductance (Gs) differ significantly across lesion type and treatment (severe drought vs. well-watered conditions).

## REFERENCES

- Allen, C., Macalady, A., Chenchouni, H., Bachelet, D., McDowell, N., Vennetier, M. et al. (2010). A global overview of drought and heat-induced tree mortality reveals emerging climate change risks for forests. *Forest Ecology and Management* 259, 660-684.
- Almeida-Rodriguez, A., and Hacke, U. (2012). Cellular localization of aquaporin mRNA in hybrid poplar stems. *American Journal of Botany* 99, 1249-1254.
- Arend, M., and Fromm, J. (2007). Seasonal change in the drought response of wood cell development in poplar. *Tree Physiology* 27, 985-992.
- Awad, H., Barigah, T., Badel, E., Cochard, H., and Herbette, S. (2010). Poplar vulnerability to xylem cavitation acclimates to dryer soil conditions. *Physiologia Plantarum* 139, 280-288.
- Baas, P., and Wheeler, E. (2011). "Wood anatomy and climate change," in *Climate Change, Ecology and Systematics*, ed. T. Hodkinson, M. Jones, S. Waldren, J. Parnell (Cambridge, UK: Cambridge University Press), 141-155.

- Barigah, T., Charrier, O., Douris, M., Bonhomme, M., Herbette, S., Ameglio, T. et al. (2013). Water stress-induced xylem hydraulic failure is a causal factor of tree mortality in beech and poplar. *Annals of Botany* 112, 1431-1437.
- Beaudon, M., Hernandez, R., Koubaa, A., Poliquin, J. (1992). Interclonal, intraclonal and within tree variation in wood density of poplar hybrid clones. *Wood and Fiber Science* 24, 147-153.
- Bennet, T., and Leyser, O. (2006). Something on the side: axillary meristems and plant development. *Plant Molecular Biology* 60, 843-854.
- Birchler, J., and Veitia, R. (2014). "The gene balance hypothesis: dosage effects in plants," in *Plant Epigenetics and Epigenomics*, ed. P. McKeown (Totowa, NJ: Humana Press), 25-32.
- Bond, B., Meinzer, F., and Brooks, R. (2007). "How Trees Influence the Hydrological Cycle in Forest Ecosystems," in *Hydroecology and Ecohydrology: Past, Present and Future*, ed. P. Wood, D. Hannah, J. Sadler (Hoboken, NJ: John Wiley & Sons), 7-28.
- Bourquin, V., Nishikubo, N., Abe, H., Brumer, H., Denman, S., Eklund, M. et al. (2002). Xyloglucan endotransglycosylases have a function during the formation of secondary cell walls of vascular tissues. *The Plant Cell* 14, 3073-3088.
- Boursiac, Y., Chen, S., Luu, D., Sorieul, M., van den Dries, N., and Maurel, C. (2005) Early effects of salinity on water transport in *Arabidopsis* roots. Molecular and cellular features of aquaporin expression. *Plant Physiology* 139, 790-805.
- Brown, H. (2013). The theory of the rise of sap in trees: some historical and conceptual remarks. *Physics in Perspective* 15, 320-358.
- Burke, M., Gusta, L., Quamme, H., Weiser, C., and Li, P. (1976). Freezing and injury in plants. *Annual Review of Plant Physiology* 27, 507-528.
- Campanello, P., Gatti, G., and Goldstein, G. (2008). Coordination between water transport efficiency and photosynthetic capacity in canopy tree species at different growth irradiances. *Tree Physiology* 28, 85-94.

- Cao, X., Jia, J., Zhang, C., Li, H., Liu, T., Jiang, X., et al. (2013). Anatomical, physiological and transcriptional responses of two contrasting poplar genotypes to drought and re-watering. *Physiologia Plantarum* 151, 480-494.
- Carlquist, S. (2001). Comparative wood anatomy. Berlin: Springer-Verlag.
- Carlquist, S. (1984). Vessel grouping in dicotyledon wood. *Aliso* 10, 505-525.
- Carpita, N., and Gibeaut, D. (1993). Structural models of primary cell walls in flowering plants: Consistency of molecular structure with the physical properties of the walls during growth. *Plant Journal* 3, 1-30.
- Chhetri, H., Furches, A., Macaya-Sanz, D., Walker, A., Kainer, D., Jones, P., et al. (2020). Genome-wide association study of wood anatomical and morphological traits in *Populus trichocarpa*. *Frontiers in Plant Science* 11, doi: 10.3389/fpls.2020.545748.
- Choat, B., Brodie, T., Cobb, A., Zwieniecki, M., and Holbrook, M. (2006). Direct measurements of intervessel pit membrane hydraulic resistance in two angiosperm tree species. *American Journal of Botany* 93, 993-1000.
- Cochard, H. (2006). Cavitation in trees. *Comptes Rendus Physique* 7, 1018-1026.
- Cortes, L., Zhang, Z., and Ju, Y. (2021). Status and prospects of genome-wide association studies in plants. *The Plant Genome* 14, e20077.
- Cosgrove, D. (1997). Assembly and enlargement of primary cell wall in plants. *Annual Review of Cell Developmental Biology* 13, 171-201.
- Dejardin, A., Laurans, F., Arnaud, D. Breton, C., Pilate, G., and Leple, J. (2010). Wood formation in angiosperms. *Comptes Rendus Biologies* 333, 325-334.
- De Micco, V., Ruel, K., Joseleau, J., Grima-Pattenati, J., and Aronne, G. (2012). Xylem anatomy and cell wall ultrastructure of *Nicotiana tabacum* after lignin genetic modification through transcriptional activator EgMYB2. *IAWA Journal* 33, 269-286.
- Eckstein, D., Liese, W., and N. Parameswaran. 1976. On the structural changes in wood and bark of a salt-damaged horse chestnut tree. *Holzforschung* 30:173-178.

- Ellis, B., Jansson, S., Strauss, S., and Tuskan, G. (2010). “Why and how *Populus* became a model tree,” in *Genetics and Genomics of Populus*, ed. S. Jansson, R. Bhalerao, A. Groover (New York, NY: Springer), 3-14.
- Elmore, G., and Ewers, F. (1986). Fluid flow in the outermost xylem increment of a ring-porous tree, *Ulmus americana*. *American Journal of Botany* 73, 1771-1774.
- Escalante, M., Lautner, S., Nehls, U., Selle, A., Teuber, M., Schnitzler, J. et al. (2009). Salt stress affects xylem differentiation of gray poplar (*Populus × canescens*). *Planta* 229, 299-309.
- FAO: Food and Agriculture Organization of the United Nations. (2022). The State of the World’s Forests. <https://www.fao.org/3/cb9360en/cb9360en.pdf> [Accessed July 15, 2022].
- Fichot, R., Laurans, F., Monclus, R., Moreau, A., Pilate, G., and Brignolas, F. (2009). Xylem anatomy correlates with gas exchange, water-use efficiency and growth performance under contrasting water regimes: evidence from *Populus deltoides × Populus nigra* hybrids. *Tree Physiology* 29, 1537-1549.
- Gleason, S., Westoby, M., Jansen, S., Choat, B., Hacke, U., Pratt, R., et al. (2016). Weak tradeoff between xylem safety and xylem-specific hydraulic efficiency across the world’s woody plant species. *New Phytologist* 209, 123-136.
- Grant, E., Fujino, T., Beers, E., and Brunner, A. (2010). Characterization of NAC domain transcription factors implicated in control of vascular cell differentiation in *Arabidopsis* and *Populus*. *Planta* 232, 337-352.
- Grigorenko, Y. and Rozhok, L. (2014). Applying discrete fourier series to solve problems of the stress state of hollow noncircular cylinders. *International Applied Mechanics* 50, 105-127.
- Guet, J., Fichot, R., Lédée, C., Laurans, F., Cochard, H., Delzon, S., Bastien, C., and Brignolas, F. (2015). Stem xylem resistance to cavitation is related to xylem structure but not to growth and water-use efficiency at the within-population level in *Populus nigra* L. *Journal of Experimental Botany* 66, 4643-4652.

- Guo, M., and Birchler, J. (1994). Trans-acting dosage effects on the expression of model gene systems in maize aneuploids. *Science* 266, 1999-2002.
- Hacke, U., Spicer, R., Schreiber, S., and Plavcova, L. (2016). An ecophysiological and developmental perspective on variation in vessel diameter. *Plant, Cell and Environment* 40, 831–845.
- Hacke, U., Stiller, V., Sperry, J., Pitterman, J., and McCulloh, K. (2001). Cavitation fatigue. Embolism and refilling cycles can weaken the cavitation resistance of xylem. *Plant Physiology* 125, 779-786.
- Hao, Z. and Mohnen, D. (2014). A review of xylan and lignin biosynthesis: Foundation for studying *Arabidopsis* irregular xylem mutants with pleiotropic phenotypes. *Critical Reviews in Biochemistry and Molecular Biology* 49, 212-241.
- Henry, I., Zinkgraf, M., Groover, A., and Comai, L. (2015). A system for dosage-based functional genomics in poplar. *The Plant Cell* 27, 2370-2383.
- Hillabrand, R., Hacke, U., and Lieffers, V. (2019). Defoliation constrains xylem and phloem functionality. *Tree Physiology* 39, 1099-1108.
- Hillabrand, R., Hacke, U., and Lieffers, V. (2016). Drought-induced xylem pit membrane damage in aspen and balsam poplar. *Plant, Cell and Environment* 39, 2210-2220.
- Ikram, S. and Chardon, F. (2010). “Plant quantitative traits,” in *Encyclopedia of Life Sciences*, (Hoboken, NJ: John Wiley and Sons), 1-9.
- Janz, D., Lautner, S., Wildhagen, H., Behnke, K., Schnitzler, J., Rennenber, H. et al. (2012). Salt stress induces the formation of a novel type of ‘pressure wood’ in two *Populus* species. *New Phytologist* 194, 129-141.
- Jin, Z., and Fan, R. (2009). Ultrastructural analysis of the differentiation process of secondary xylem vessel element in *Populus deltoides*. *Frontiers of Forestry in China* 4, 284.
- Johnson, D., Eckart, P., Alsamadisi, N., Noble, H., Martin, C., and Spicer, R. (2018). Polar auxin transport is implicated in vessel differentiation and spatial patterning during secondary growth in *Populus*. *American Journal of Botany* 105, 186-196.

- Junghans, U., Polle, A., Duchting, P., Weiler, E., Kuhlman, B., Gruber, F. et al. (2006). Adaptation to high salinity in poplar involves changes in xylem anatomy and auxin physiology. *Plant, Cell and Environment* 29, 1519-1531.
- Junghans, U., Langenfeld-Heyser, R., Polle, A., and Teichmann, T. (2003). Effect of auxin transport inhibitors and ethylene on the wood anatomy of poplar. *Plant Biology* 6, 22-29.
- Kwak, J., Murata, Y., Baizabal-Aguirre, V., Merrill, J., Wang, M., Kemper, A., et al. (2001). Dominant negative guard cell K<sup>+</sup> channel mutants reduce inward-rectifying K<sup>+</sup> currents and light-induced stomatal opening in *Arabidopsis*. *Plant Physiology* 127, 473-485.
- Lambers, H., and Oliveira, R. (2019). "Plant Water Relations," in *Plant Physiological Ecology*, ed. H. Lambers and R. Oliveira (Berlin, Germany: Springer), 187-263.
- Langer, K., Ache, P., Geiger, D., Stinzinger, A., Arend, M., Wind, C. et al. (2002). Poplar potassium transporters capable of controlling K<sup>+</sup> homeostasis and K<sup>+</sup>-dependent xylogenesis. *The Plant Journal* 32, 997-1009.
- LeGall, H., Phillippe, F., Domon, J., Gillet, F., Pelloux, J., and Rayon, C. (2015). Cell wall metabolism in response to abiotic stress. *Plants* 4, 112-166.
- Li, Z., and Wang, C. (2019). Research progress on responses of xylem of woody plants to freeze-thaw embolism. *Chinese Journal of Plant Ecology* 43, 635-647.
- Liu, J., Cong, B., and Tanksley, S. (2003). Generation and analysis of an artificial gene dosage series in tomato to study mechanisms by which cloned quantitative trait locus fw2.2 controls fruit size. *Plant Physiology* 132, 292-299.
- Loepfe, L., Martinez-Vilalta, J., Pinol, J., and Mencuccini, M. (2007). The relevance of xylem network structure for plant hydraulic efficiency and safety. *Journal of Theoretical Biology* 247, 788-803.
- Luo, L., Zhu, J., Gui, J., Yin, T., Luo, W., Liu, J., et al. (2021). A comparative analysis of transcription networks active in juvenile and mature wood in *Populus*. *Frontiers in Plant Science* 12, doi:10.3389/fpls.2021.675075.

- Manning, A., Fischer, J., and Lindenmayer, D. (2006). Scattered trees are keystone structures- implications for conservation. *Biological Conservation* 132, 311-321.
- Martinez-Meier, A., Sanchez, L., Pastorino, M., Gallo, L., and Rozenberg, P. (2008) What is hot in tree rings? The wood density of surviving Douglas-firs to the 2003 drought and heat wave. *Forest Ecology and Management* 256, 837-843.
- Mauricio, R. (2001). Mapping quantitative trait loci in plants: uses and caveats for evolutionary biology. *Nature Reviews Genetics* 2, 370-381.
- McDowell, N. and Allen, C. (2015). Darcy's law predicts widespread forest mortality under climate warming. *Nature Climate Change* 5, 669.
- McDowell, N., Pockman, W., Allen, C., Breshears, D., Cobb, N., Kolb, T. et al. (2008). Mechanisms of plant survival and mortality during drought: Why do some plants survive while others succumb to drought? *New Phytologist* 178, 719-739.
- McQueen-Mason, S., and Cosgrove, D. (1994). Disruption of hydrogen bonding between plant cell wall polymers by proteins that induce wall extension. *PNAS* 91, 6574-6578.
- Mellerowicz, E. (2006). "Woody wall formation," in *The Science and Lore of the Plant Cell Wall: Biosynthesis, Structure and Function*, ed. T. Hayashi (Boca Raton, FL: Brown Walker Press), 267-294.
- Nardini, A., Dimasi, F., Klepsch, M., and Jansen, S. (2012). Ion-mediated enhancement of xylem hydraulic conductivity in four *Acer* species: relationships with ecological and anatomical features. *Tree Physiology* 32, 1434-1441.
- Moulin, J., Ribeiro, D., Vidaurre, G., Mulin, L., and Moreira, S. (2022). Effects of drought stress on the formation and lignification of eucalyptus wood cells. *IAWA Journal* 0, 1-13.
- Novaes, E., Osorio, L., Drost, D., Miles, B., Boaventura-Novaes, Benedict, C. et al. (2009). Quantitative genetic analysis of biomass and wood chemistry of *Populus* under different nitrogen levels. *New Phytologist* 182, 878-890.

- Pan, Y., Birdsey, R., Fang, J., Houghton, R., Kauppi, P. Kurz, W., et al. (2011). A large and persistent carbon sink in the world's forests. *Science* 333, 988-993.
- Pande, P. (2011). Variations in wood properties and growth in some clones of *Populus deltoides* Bartr. ex Marsh. *American Journal of Plant Sciences* 2, 644-649
- Pande, P. and Dhiman, R. (2011). Performance and variability patterns in wood properties and growth traits in the parents, F1 and F2 generation hybrid clones of *Populus deltoides*. *Journal of Forestry Research* 22, 379-385.
- Pandey, M., Pathak, M., and Shrestha, B. (2020). Morphological and wood anatomical traits of *Rhododendron lepidotum* Wall ex G. Don along the elevation gradients in Nepal Himalayas. *Arctic, Antarctic and Alpine Research* 53, 35-47.
- Pastor, J., and Post, W. (1986). Influence of climate, soil moisture and succession of forest carbon and nitrogen cycles. *Biogeochemistry* 2, 3-27.
- Plavcova, L., and Hacke, U. (2012). Phenotypic and developmental plasticity of xylem in hybrid poplar saplings subjected to experimental drought, nitrogen fertilization, and shading. *Journal of Experimental Botany* 63, 6481-6491.
- Pliura, A., Zhang, S., MacKay, J., and Bousquet, J. (2007). Genotypic variation in wood density and growth traits of poplar hybrids at four clonal trials. *Forest Ecology and Management* 238, 92-106.
- Ployet, R., Soler, M., Carocha, V., Ladouce, N., Alves, A., Rodrigues, J. et al. (2018). Long cold exposure induces transcriptional and biochemical remodelling of xylem secondary cell wall in *Eucalyptus*. *Tree Physiology* 38, 409-422.
- Ribeiro, C., Conde, D., Balmant, K., Dervinis, C., Johnson, M., McGrath, A. et al. (2020). The uncharacterized gene EVE contributes to vessel element dimensions in *Populus*. *PNAS* 117, 5059-5066.
- Sauter J. (2000) Photosynthate allocation to the vascular cambium: facts and problems. In: Savidge R.A., Barnett J.R., Napier R. (Eds), *Cell and molecular biology of wood formation*. BIOS Scientific Publishers, Oxford, UK: pp. 71-83.

- Sauter J., and Kloth, S. (1986). Plasmodesmatal frequency and radial translocation rates in ray cells of poplar (*Populus x canadensis* Moench ‘robusta’). *Planta*, 168, 377-380
- Schmidt, P., Hartung, J., Bennewitz, J., and Piepho, H. (2019). Heritability in plant breeding on a genotype difference basis. *Genetics* 212, 991-1008.
- Schmitz, N., Verheyden, A., Beeckman, H., Kairo, J., and Koedam, N. (2006). Influence of a salinity gradient on the vessel characters of a mangrove species *Rhizophora mucronata*. *Annals of Botany* 98, 1321-1330.
- Scholz, A., Klepsch, M., Karimi, Z., and Jansen, S. (2013). How to quantify conduits in wood? *Frontiers in Plant Science* 4, 56. doi: 10.3389/fpls.2013.00056.
- Schreiber, S., Hamann, A., Hacke, U., and Thomas, B. (2013). Sixteen years of winter stress: an assessment of cold hardiness, growth performance and survival of hybrid poplar clones at a boreal planting site. *Plant, Cell and Environment* 36, 419-428.
- Słupianek, A., Dolzblasz, A., and Sokołowska, K. (2021). Xylem parenchyma-role and relevance in wood functioning in trees. *Plants* 10, 1247.
- Smith, M., Fridley, J., Yin, J., and Bauerle, T. (2013). Contrasting xylem vessel constraints on hydraulic conductivity between native and non-native woody understory species. *Frontiers in Plant Science* 4, 486.
- Sobrado, M. (2001) Hydraulic properties of a mangrove *Avicennia germinans* as affected by NaCl. *Biologia Plantarum* 44, 435-438.
- Sperry, J., Meinzer, F., and McCulloh, K. (2008). Safety and efficiency conflicts in hydraulic architecture: scaling from tissues to trees. *Plant, Cell and Environment* 31, 632-645.
- Thomas, R. (1977). “Wood: structure and chemical composition,” in *Wood Technology: Chemical Aspects*, ed. I. Goldstein (Washington D.C.: ACS Publications), 1-23.
- Tyree, M., Davis, S., and Cochard, H. (1994). Biophysical perspectives of xylem evolution: is there a tradeoff of hydraulic efficiency for vulnerability to dysfunction? *IAWA Journal* 15, 335-360.

- Verheyden, A., De Ridder, F., Shmitz, N., Beeckman, H., and Koedam, N. (2005). High-resolution time series of vessel density in Kenyan mangrove trees reveal a link with climate. *New Phytologist* 167, 425-435.
- Van Sandt, V., Suslov, D., Verbelen, J., and Vissenberg, K. (2007). Xyloglucan endotransglucosylase activity loosens a plant cell wall. *Annals of Botany* 100, 1467-1473.
- Wang, G., Gao, Y., Wang, J., Yang, L., Song, R., Li, X. et al. (2010). Overexpression of two cambium-abundant Chinese fir (*Cunninghamia lanceolata*)  $\alpha$ -expansin genes ClEXPA1 and ClEXPA2 affect growth and development in transgenic tobacco and increase the amount of cellulose in stem cell walls. *Plant Biotechnology Journal* 9, 486-502.
- Wessels, B., Seyfferth, C., Escamez, S., Vain, T., Antos, K, Vahala, J., et al. (2019). An AP2/ERF transcription factor ERF139 coordinates xylem cell expansion and secondary cell wall deposition. *New Phytologist* 224, 1585-1599.
- Wheeler, J., Sperry, J., Hacke, U., and Hoang, N. (2005). Inter-vessel pitting and cavitation in woody Rosaceae and other vesselled plants: a basis for a safety versus efficiency trade-off in xylem transport. *Plant, Cell and Environment* 28, 800-812.
- Wind, C., Arend, M., and Fromm, J. (2004). Potassium-dependent cambial growth in Poplar. *Plant Biology* 6, 30-37.
- Wildhagen, H., Paul, S., Allwright, M., Smith, H., Malinowska, M., Schnabel, S., et al. (2018). Genes and gene clusters related to genotype and drought-induced variation in saccharification potential, lignin content and wood anatomical traits in *Populus nigra*. *Tree Physiology* 38, 320-339.
- Yanchuk, A., Dancik, B., and Micko, M. (1984). Variation and heritability of wood density and fibre length of trembling aspen in Alberta, Canada. *Silvae Genetica* 33, 11-16.
- Yata, S., Itoh, T., and Kishima, T. (1970). Formation of perforation plates and bordered pits in differentiating vessel elements. *Wood Research: Bulletin of the Research Institute Kyoto University* 50, 1-11.

Yu, D., Janz, D., Zienkiewicz, K., Herrfurth, C., Feussner, I., Chen, S., et al. (2021). Wood formation under severe drought invokes adjustment of hormonal and transcriptional landscape in poplar. *International Journal of Molecular Sciences* 22, 9899.

Zhao, X., Guo, P., and Peng, H. (2019). An ignored anatomical variable: pore shape shows a nonrandom variation pattern in xylem cross-sections. *Nordic Journal of Botany* 37, e02249.

Zhong, R., Kandasamy, M., and Ye, Z. (2021). XND1 regulates secondary wall deposition in xylem vessels through inhibition of VND functions. *Plant and Cell Physiology* 62, 53-65.

## **Chapter 1. Wood and water: How trees modify wood development to cope with drought**

**F. Daniela Rodriguez-Zaccaro, Andrew Groover**

*(Adapted from a previously published manuscript)*

### **Societal impact statement**

Drought plays a conspicuous role in forest mortality and is expected to become more severe in future climate scenarios. Recent surges in drought-associated forest tree mortality have been documented worldwide. For example, recent droughts in California and Texas killed approximately 129 million and 300 million trees, respectively. Drought has also induced acute pine tree mortality across east-central China, and across extensive areas in southwest China. Understanding the biological processes that enable trees to modify wood development to mitigate the adverse effects of drought will be crucial for the development of successful strategies for future forest management and conservation.

### **Summary**

Drought is a recurrent stress to forests, causing periodic forest mortality with enormous economic and environmental costs. Wood is the water-conducting tissue of tree stems, and trees modify wood development to create anatomical features and hydraulic properties that can mitigate drought stress. This modification of wood development can be seen in tree rings where not only the amount of wood but also the morphology of the water-conducting cells are modified in response to environmental conditions. In this review, we provide an overview of how trees conduct water, and how trees modify wood development to affect water conduction properties in response to drought. We discuss key needs for new research, and how new knowledge of wood formation can play a role in the conservation of forests under threat by climate change.

## INTRODUCTION

Water is key to forest growth and survival. Drought and heat-induced forest mortality have affected forests worldwide (Allen et al. 2010) and is expected to worsen through the 21st century (McDowell & Allen, 2015). For example, severe drought was associated with the death of more than 129 million trees in California from 2010 to 2017, 300 million trees in Texas in 2011 (USGCRP 2018), and 40 to 80% stand level mortality of *Cedrus atlantica*-dominated forests in Algeria (Bentouati 2008). Droughts have induced tree mortality of *Pinus tabulaeformis* across 0.5 million hectares in east-central China (Wang et al. 2007) and across extensive areas of *Pinus yunnanensis* in southwest China (Li 2003). Drought is expected to affect global processes including carbon cycles as well as regional issues including hydrology and water availability (Adams et al., 2010). Covering about 30% of the global land area (FAO 2018), forests can remove large amounts of carbon dioxide (CO<sub>2</sub>) from the atmosphere (Bonan 2008), totaling 3,300 tera-grams of CO<sub>2</sub> annually from 1993 to 2003 (IPCC 2007). Anthropogenic CO<sub>2</sub> emissions can be partially counteracted by forest carbon uptake, and 11% of U.S. CO<sub>2</sub> emissions were offset by net storage of atmospheric carbon by forests from 1990 to 2015 (USGCRP 2018). Drought, however, is expected to decrease forest carbon sequestration through diminished gross primary production and increased tree mortality (Pan et al. 2011). These drought-induced effects on trees can also disrupt hydrologic cycles by decreasing the flux of water to the atmosphere through reduced transpiration (Reed et al. 2014).

In contrast to more intensively cultivated agricultural crops, the majority of forests harvested for timber and other products are not irrigated, and survival and yields for forest industry are limited by water availability. In an ecological sense, water availability has myriad impacts on both industrial and natural forests. Namely, drought-induced tree mortality can

directly and indirectly alter many ecosystem services provided by forests. These services include primary and secondary forest products, carbon storage, water yield and quality, recreational value, and wildlife habitat (USFS 2016). Primary and secondary forest products in particular represent a significant part of the global economy, with production and trade valued at \$227 billion in 2016 (FAO 2018). Trees weakened by drought stress show increased mortality due to biotic factors, as dramatically illustrated by large-scale losses to bark beetles in North America (Bentz et al. 2010; Logan et al. 2017). Drought and associated-forest mortality are a primary driver of catastrophic wildfire that affected 9.8 million acres in the United States in 2017 alone (<https://www.nifc.gov/fireInfo/nfn.htm>). Our current understanding of how trees respond and succumb to drought is incomplete. Physiologically, drought stress can cause direct mortality of trees through at least two, non-exclusive mechanisms (McDowell et al. 2008). The first is through “carbon starvation,” where closing of stomata pores in leaves minimizes water loss to transpiration but also limits the entry of CO<sub>2</sub> necessary for photosynthesis into the leaf, leading to mortality over time. The second is through hydraulic failure, which is dictated in part by wood anatomy.

In this paper, we discuss the important role of wood formation in determining how trees respond to drought. Wood is the water-conducting tissue of tree stems, and trees modify wood formation in response to drought to produce wood with hydraulic properties that mitigates the likelihood of hydraulic failure. In the following sections, we present the complex mechanisms of water conduction and drought response in trees through integration of knowledge of wood development, wood anatomy and tree physiology.

## WOOD STRUCTURE AND FUNCTION

Wood, also known as secondary xylem, is the product of the vascular cambium (Figure 1.1), a lateral meristem whose initials divide to produce daughter cells that differentiate into wood and secondary phloem (the inner bark) (Larson 1994). Fusiform and ray initials produce an axial and radial set of tissues, respectively. The radial tissues consist of rays, whose cells play roles in storage, biochemistry, and lateral transport of water and nutrients in the stem. The axial tissues include tracheary elements, the cells directly responsible for water conduction. Tracheary elements are among the most developmentally plastic plant cells, showing amazing diversity in morphology across plant lineages, different stages of plant growth, and different environmental conditions. In gymnosperm trees (e.g., pines) the axial tissues of wood are composed primarily of tracheids, a type of tracheary element that provides mechanical support (Figure 1.1c).

Tracheids are long cells (up to 6 mm) (Sperry et al. 2006) that interconnect with each other through pits, which are cell wall perforations that allow water to flow between cells. In most angiosperm trees (e.g., broadleaved trees such as poplars), water conduction is achieved by the vessel element (Figure 1.1f), a type of tracheary element that can join end-on-end with other vessel elements to produce longer conduits termed vessels (Sperry et al. 2006). During vessel element differentiation, the end walls are degraded resulting in low resistance of water flow between cells within the vessel. While vessel elements have a secondary cell wall similar to tracheids, the mechanical strength of angiosperm wood comes from the production of another cell type, the fiber. Central to the function of both tracheids and vessel elements, pits are perforations through cell walls connecting tracheary elements to each other or other cell types. Pits are formed in specific locations of tracheary elements in which secondary cell wall deposition is prevented by recently uncovered molecular mechanisms (see below). A simple pit

is formed by the localized, partial degradation of primary cell wall, leaving a fine mesh of material that allows passage of water but inhibits passage of air bubbles. Some gymnosperms, including conifer species, can form more specialized pits, containing a flap like structure (torus-margo) that can seal the pit against the surrounding cell wall to prevent the spread of air bubbles. The development of this complex wood tissue system is modified in response to environmental conditions, including drought, to balance tradeoffs between the efficiency of water conduction and risk of failure during water stress. To understand the ramifications of these modifications, it is first necessary to consider how water is transported through the woody tissues of trees stems.

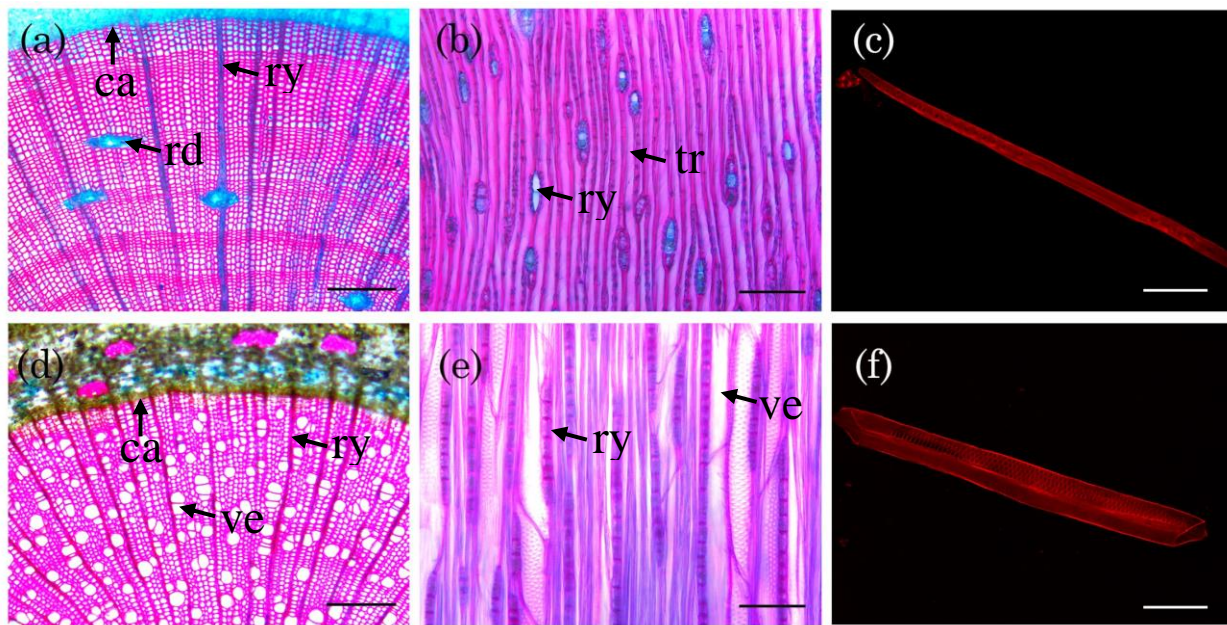


**FIGURE 1.1|** Transverse stem sections of a gymnosperm species, *Pinus radiata* (a) and an angiosperm hybrid, *Populus deltoides* × *Populus nigra* (d); scale bars are 200 μm. Tangential stem sections of *Pinus radiata* (b) and *P. deltoides* × *P. nigra* (e); scale bars are 100 μm. Single *Pinus radiata* tracheid (c) and *P. deltoides* × *P. nigra* vessel element (f); scale bars are 100 μm. Cambium (ca); Resin duct (rd); Ray (ry); tracheid (tr)

## HOW WATER IS TRANSPORTED IN TREES

Trees move water from roots to leaves, sometimes spanning hundreds of feet. Notably, the coast redwood (*Sequoia sempervirens*), the tallest tree species in the world, can reach heights

of 100 m or more. The ascent of sap (water and solutes) in trees is ultimately the result of the molecular properties of water. Hydrogen bonds that form between water molecules give rise to the property of cohesion, while hydrogen bonds between water and tracheary element cell walls give rise to the property of adhesion. Together, cohesion and adhesion allow water to move upward inside tracheary elements against the force of gravity in a process known as the cohesion-tension mechanism of water transport (Dixon and Joly 1895; Pickard 1981). The force moving water from roots to shoots is largely generated by capillary action in the leaves, specifically in the walls of mesophyll cells (Figure 1.2). Water evaporates (transpires) when leaf stomata are open during the day (Figure 1.2), generating a force (tension, or negative pressure) that pulls water by cohesion through the xylem.

## **THE INTERPLAY OF WOOD DEVELOPMENT, WOOD ANATOMY AND PHYSIOLOGY**

As previously mentioned, drought-induced tree mortality can be caused by two non-mutually exclusive physiological mechanisms: carbon starvation and hydraulic failure (McDowell et al. 2008). Hydraulic failure involves the loss of vascular function when air bubbles (emboli) form and spread throughout the xylem, producing breaks in the otherwise continuous water column (Figure 1.3). Air-filled xylem is unable to transport water, leading to desiccation and death (Barigah et al. 2013). Air bubbles in the xylem are the result of cavitation (the phase change of water from liquid to gas) under large negative pressures inside the xylem during water stress (as low as  $-11$  MPa in some species) (Jacobsen et al. 2007). Xylem sap is kept in a metastable liquid state due to the lack of nucleation sites, which initiates the phase change into gas (Tyree and Sperry 1989). Drought-induced cavitation likely occurs when an air bubble enters the system through a pit from an adjacent air-filled space and serves as a nucleation site for

cavitation (Cochard et al. 1992; Crombie et al. 1985; Sperry and Tyree 1990). Specifically, air-seeding occurs when the difference in pressure between both sides of the pit becomes sufficiently large (Figure 1.3), with larger pit pores at greater risk. The differences between angiosperm and conifer pit anatomy result in slightly different air-seeding mechanisms, but ultimately air-seeding in both taxa is driven by the difference in pressure between both sides of the pit. Variation in the morphology and arrangement of tracheary elements can have large impacts on water transport and risk of cavitation under water stress. The Hagen-Poiseuille equation predicts that hydraulic conductivity of vessels increases with the 4th power of diameter, meaning that small changes in diameter have large effects on conductivity. For example, it would take 16 vessels of 10  $\mu\text{m}$  diameter to equal the flow rate of a single 20  $\mu\text{m}$  diameter vessel. However, increased diameter also elevates the risk of cavitation and air embolism, and thus there is a tradeoff between hydraulic conductivity and drought-induced cavitation (Hacke et al. 2017; Tyree and Zimmermann 2002; Wheeler et al. 2005). Wider vessels might be more vulnerable to cavitation through an increased chance of a rare large pore in a pit membrane that enables air-seeding (Christman et al. 2012). The interplay of wood anatomy and drought response is best studied in angiosperm trees, where the risk of hydraulic failure is highly correlated with the diameter, number, and spacing of vessels (McDowell et al. 2008; Tyree and Sperry 1989; Venturas et al. 2017). Vessel trait properties thus represent a balance of optimizing water flow rates with the risk of hydraulic failure and can be dramatically altered during development to in response to water stress and other ongoing environmental changes (Venturas et al. 2017).

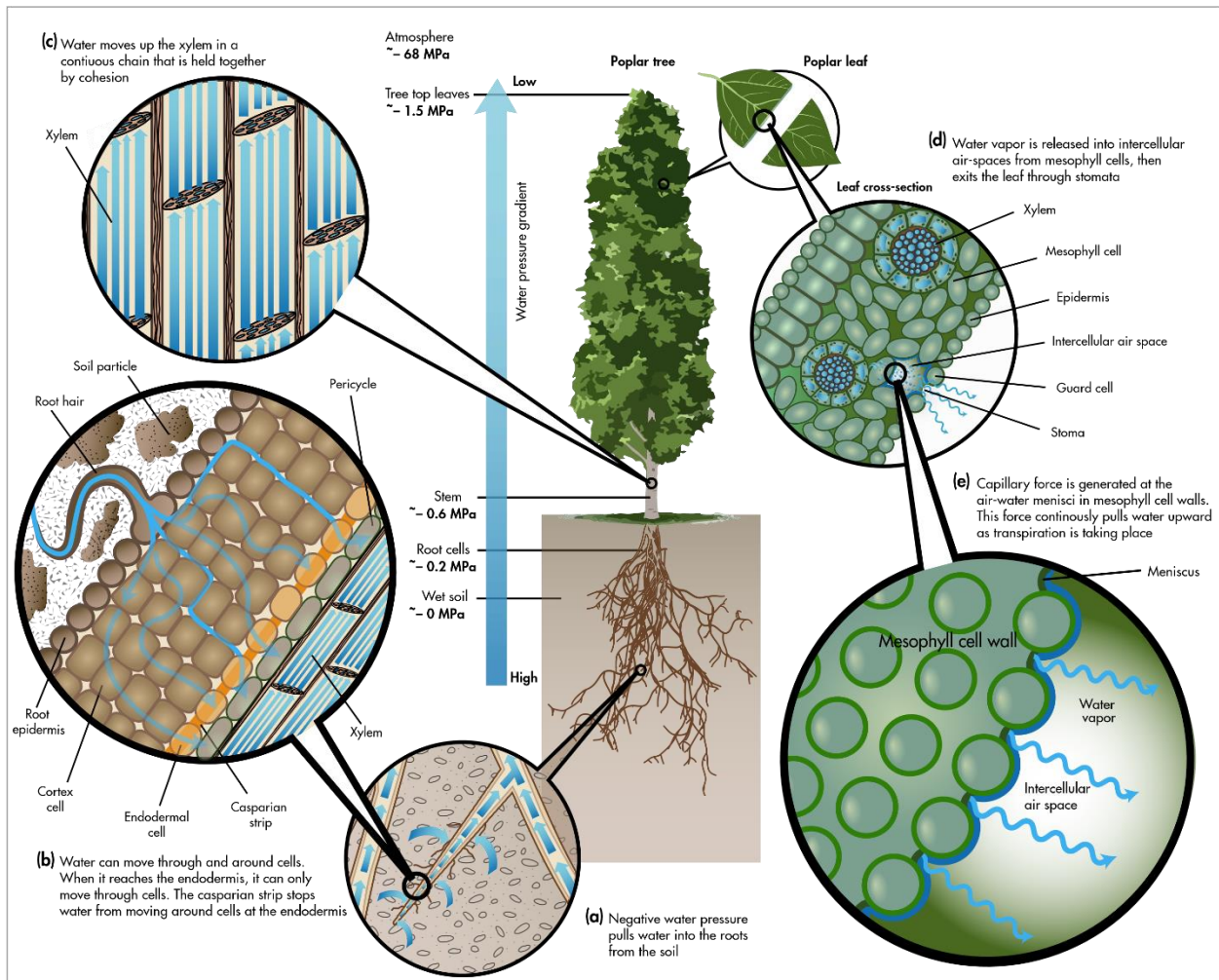


**FIGURE 1.2|** The path of water through a tree, and the cohesion-tension mechanism of water transport. (a) Water moves into the roots when root cell water potential is lower than soil water potential; (b) water moves through (symplastic movement) and around (apoplastic movement) the cells in the root cortex. The pathway of water around cells is blocked by the casparian strip at the endodermis, forcing water to take the symplastic pathway through the endodermal cells and enabling regulated entry of minerals and solutes into the vascular system (Karahara et al. 2004); (c) water moves into the xylem, where water pressure becomes progressively negative with increasing height; (d, e) water escapes the tree as vapor through stomata in the leaves. Water vapor pressure in the atmosphere is almost always extremely negative compared to leaf vapor pressure, driving evaporation from the leaf mesophyll cell walls

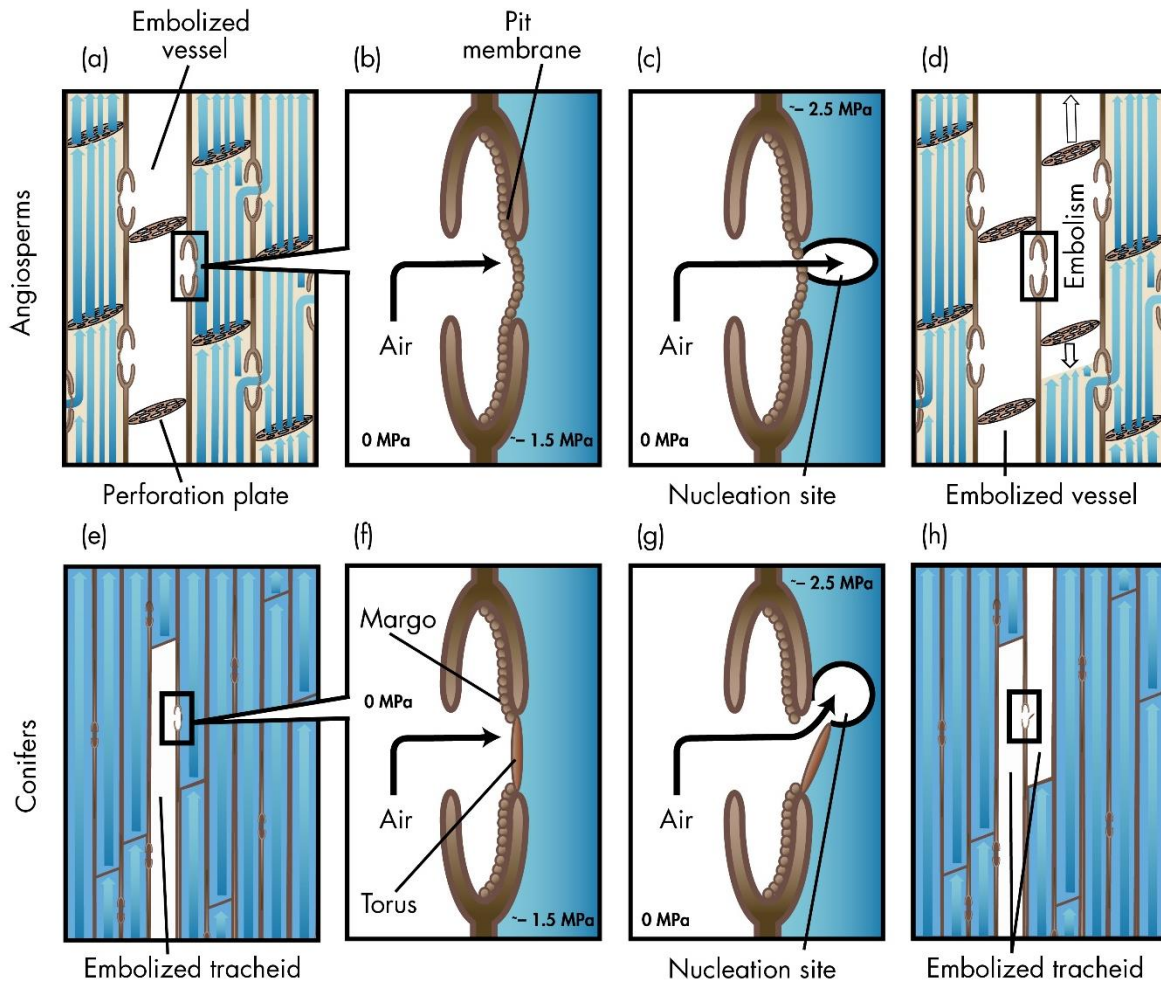


**FIGURE 1.3** Drought-induced cavitation through the air-seeding mechanism in angiosperms and conifers. Inter-vessel (a) and intertracheary pits (e) allow lateral movement of water between cells. The pit membrane stops air from an embolized vessel from entering an adjacent water-filled vessel (b). Similarly, the torus of a conifer pit stops air from spreading into an adjacent functioning tracheid (f). As water stress increases, pressure inside the functioning vessel further decreases (becomes more negative) while the embolized vessel remains at atmospheric pressure. The difference in pressure between both sides of the pit membrane becomes large enough to force an air bubble through a pore. (c) A large difference in pressure can also tear or deform the conifer torus, allowing air bubbles through (g). An air bubble serves as a nucleation point for cavitation, producing an embolism, or air-pocket (d, h). Greater connectivity between vessel elements allows for the rapid spread of the embolism (d). Emboli in tracheids will not spread as readily due to the low connectivity between each cell (h)

## **THE DEVELOPMENTAL STAGES OF TRACHEARY ELEMENT**

### **DIFFERENTIATION**

Ultimately, the morphology and water-conducting properties of a tracheary element can be traced back to its initial differentiation, which can be broadly described by sequential morphological events leading to a functioning cell (Figure 1.4). The first event is specification of a cell produced by a fusiform initial to differentiate as a tracheary element, as opposed to some other cell type. Next is the radial expansion of the nascent tracheary element. This radial expansion is most dramatic in vessel elements, which can expand up to a 100-fold over the cambial initial. The next most conspicuous stage of development involves the production of a thick, lignified cell wall. Secondary cell wall synthesis is excluded from localized areas that will ultimately become pits interconnecting adjoining cells. As differentiation progresses, hydrolytic enzymes are sequestered in the vacuole of the cell. The dramatic end to this complex developmental process is programmed cell death, which is affected by the rapid rupture of the vacuole, resulting in mixing of the hydrolytic contents of the vacuole with the cytoplasm (Groover and Jones 1999). The final product of differentiation is a hollow cell corpse defined by secondary cell wall. Some aspects of tracheary element differentiation are relatively well described. The biosynthesis of the secondary cell wall has been particularly well studied, in part because of its economic value as a major constituent of woody biomass utilized by forest industries. For example, genes encoding biosynthetic enzymes and cell wall-related transcription factors have been characterized (Carpita 2011; Turner and Somerville 1997), and transcriptional networks regulating cell wall synthesis have been modeled (Taylor-Teeple et al. 2015). In contrast, our understanding of the traits influencing water conduction and drought response is at best fragmentary and in some cases completely lacking. Below we focus on three key unresolved

research questions: (a) How do trees sense and transmit signals to change wood development in response to water stress? (b) How is pit formation altered to mitigate cavitation vulnerability in response to water stress? and (c) How is the diameter of differentiating tracheary elements modified in response to drought stress? Examples are presented from angiosperm wood development, for which we have the most complete studies.

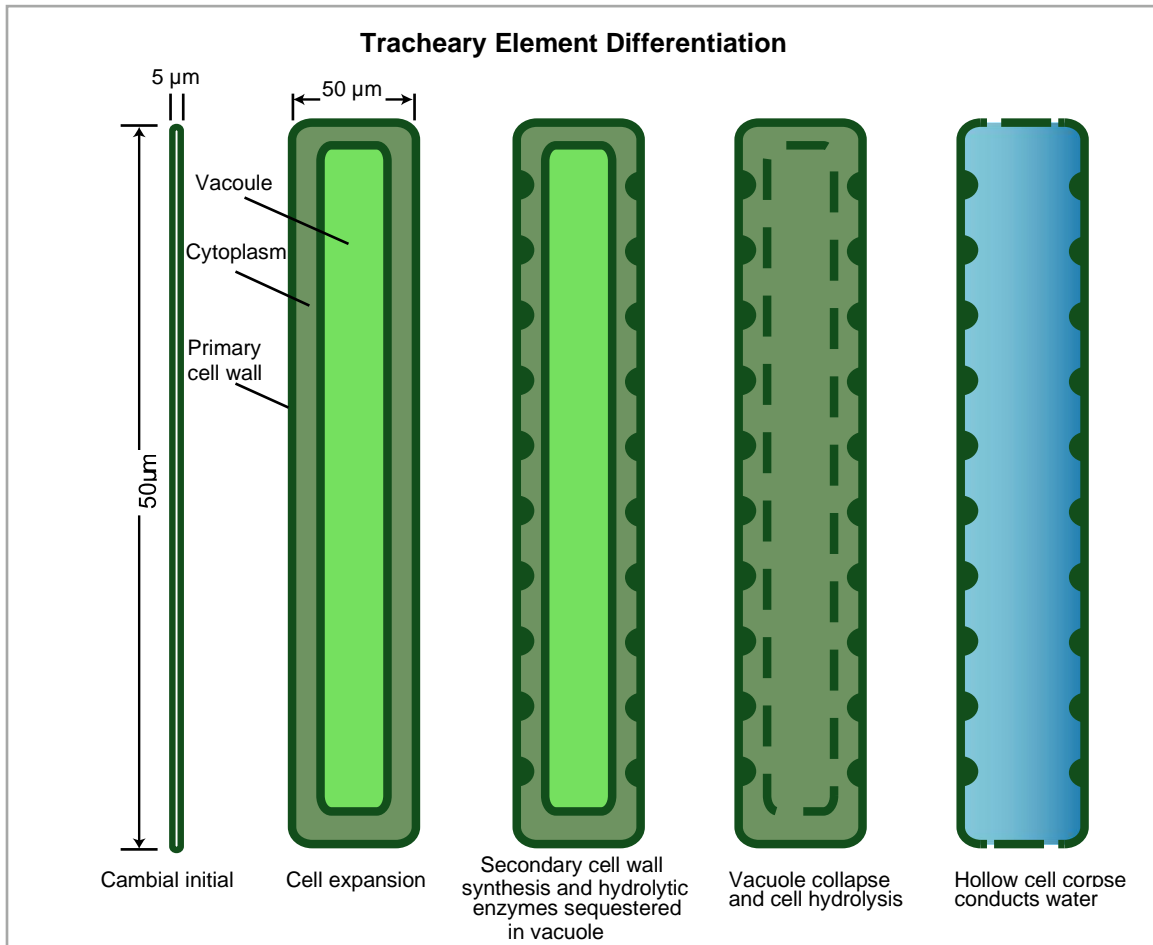


**FIGURE 1.4** Sequential events defining the differentiation of tracheary elements (left to right). Cambial initials divide one or more times to produce a daughter that acquires the cell fate of a vessel element. The cell undergoes radial expansion driven by turgor pressure to a diameter reflective of growth conditions and water stress. Secondary cell wall is deposited between the plasma membrane and primary cell wall. At the same time, hydrolytic enzymes are produced and sequestered within vacuoles. Programmed cell death results in the rapid collapse of vacuoles, mixing hydrolytic enzymes in the vacuoles with the cytoplasm, resulting in hydrolysis of the cell contents. End walls and primary cell walls are variously hydrolyzed depending on the species, developmental Cambial initial Cell expansion Secondary cell wall Vacuole collapse Hollow cell corpse Tracheary Element Differentiation 5 µm stage and other factors. The final product is a hollow cell corpse

## **HOW DO TREES SENSE AND TRANSMIT SIGNALS TO CHANGE WOOD DEVELOPMENT IN RESPONSE TO WATER STRESS?**

Trees sense water stress and transmit signals to coordinate physiological responses (e.g. closing stomata) and changes in growth, including wood development. Multiple non-exclusive mechanisms have been suggested for sensing of water stress, but a primary mechanism appears to be the sensing of stress at the individual cell level by plasma membrane-localized receptors (Osakabe et al. 2013). An example is sensing of osmotic changes resulting from water stress by transmembrane histidine kinase K<sup>+</sup> transporters (HKT1-like proteins) that have been shown to activate intracellular water stress signaling mechanisms in both poplar (Bertheau et al. 2015; Cheddor et al. 2005; Héricourt et al. 2016) and eucalyptus (Liu et al. 2001). Interestingly, K<sup>+</sup> levels peak in the cell expansion zone of the cambium, and cambial K<sup>+</sup> levels correlate with seasonal changes in vessel element diameter in poplar (Ache et al. 2010; Arend et al. 2005; Fromm 2010; Langer et al. 2002; Wind et al. 2004), potentially linking HKT1-like intracellular signaling to tissue-level changes in wood development. As potassium is a primary osmoticum in plant cells (Wang et al. 2013), these observations are also consistent with potassium potentially playing a causative role as an osmoticum affecting turgor and ultimately diameter growth of differentiating vessels in response to water stress (see below). The hormone ABA has been implicated as a primary signal of water stress in plants including trees, coordinating responses including stomatal closure, reduced growth, and changes in wood development. Like other plants, ABA levels are elevated in poplar under water stress (Chen et al. 2002; Jia et al. 2017). Treatment with ABA results in poplar stems with smaller diameter and more frequent vessel elements (Popko et al. 2010), similar to developmental changes seen in response to water stress. ABA elicits changes in large number of genes associated with stress response (Fujita et al. 2011),

resulting in the observed complex changes in physiology and development. Interestingly, epigenetic factors have been shown in poplar to play roles in changing gene expression or maintaining a “memory” of previous water stress (Raj et al. 2011).

### *Perspectives*

Currently a large base of knowledge about water stress at the molecular, genetic and cell biology levels in model crop plants is largely untranslated to trees. While physiology studies are numerous in trees, much of that knowledge remains unconnected to mechanisms. A major challenge is thus to comprehensively describe for at least one tree species the mechanistic basis of water stress sensing, signal transduction, and how signals are translated in physiological and developmental responses.

## **HOW IS PIT FORMATION ALTERED TO MITIGATE CAVITATION VULNERABILITY IN RESPONSE TO WATER STRESS?**

Recent research has detailed molecular mechanisms regulating where and how pits form in the secondary cell walls of Arabidopsis vessels. Deposition of cellulose microfibrils in secondary cell walls is directed by a plasma membrane-localized cellulose synthase complexes that track microtubules. Protein complexes containing MICROTUBULE DEPLETION DOMAIN1 (MIDD1) and RHORELATED PROTEIN FROM PLANTS11 (ROP11) actively promote the disassembly of cortical microtubules and thus exclude cellulose synthase complexes and secondary cell wall formation in regions destined to become pits (Oda and Fukuda 2013; Oda et al. 2010; Sasaki et al. 2017). Interestingly, mutation or changes in expression of these and MIDD1/ROP11 interacting proteins can dramatically change the spacing and size of pits (Nagashima et al. 2018). Mathematical modeling shows that pit formation has features consistent with a classical Turing reaction diffusion mechanism (Nagashima et al. 2018).

## *Perspectives*

While these molecular details are exciting, it is currently unknown how this mechanism is modified to produce variation in the spacing or size of pits in nature, or how variation is ultimately linked to physiological properties of water transport or hydraulic failure during water stress. One critical area for new research is to examine how components of the MIDD1/ROP11 complex are modified during water stress to change pit patterning and size. Another need is to determine the range of natural variation in genes encoding components of the MIDD1/ROP11 mechanism, and to what degree they predict variation in pit properties in nature. Both of these questions are now highly tractable, including determining natural variation using existing genome wide association populations in poplar.

### **HOW IS THE DIAMETER OF DIFFERENTIATING TRACHEARY ELEMENTS MODIFIED IN RESPONSE TO DROUGHT STRESS?**

The diameter of tracheary elements (most dramatically in vessel elements) is correlated with both water conduction and cavitation vulnerability. The change in wood development in response to water stress can be striking, for example in poplar the diameter, number and clustering of vessel elements produced all change in response to water stress (Fichot et al. 2009). Unfortunately, the regulation of tracheary element diameter and frequency are among the most poorly understood aspects of tracheary element differentiation. Understanding the molecular regulation of vessel element diameter is thus a crucial area for new research to understand how physiological changes during drought translate into compensating features of wood anatomy.

Cell expansion in plant cells is driven by turgor, and turgor-driven swelling is the only known mechanism that could potentially drive tracheary element expansion. Water crosses the plasma membrane and enters a cell when the concentration of solutes inside the cell is greater

than that outside of the cell, causing the cell to swell. How much and in what dimensions the cell expands is determined not only by solute concentrations but also by the resistance of the cell wall. Turgor is an active process that occurs while the plasma membrane is intact, and thus the final diameter of a tracheary element is realized while the cell is still living, prior to programmed cell death. Also, because the secondary cell wall is rigid, expansion and the final diameter of the cell must be realized before secondary cell wall synthesis is complete.

A number of possible mechanisms might control the final diameter of the developing tracheary element, but ultimately the diameter is a function of the turgor pressure in the differentiating cell and the rigidity of the cell wall. The primary walls of cells within the cambial zone are relatively thin and pliable, and it can be deduced that the primary cell wall must be dramatically extended during tracheary element expansion. For example, to expand from a 5 to 50  $\mu\text{m}$  diameter, the cell must extend 10-fold in circumference and add 10-fold more cell wall material to maintain a constant cell wall thickness. One outstanding question is whether the secondary cell wall plays a role in restricting cell expansion. One observation arguing against that possibility is presented by *Arabidopsis* irregular xylem (*irx*) mutants, which have weakened secondary walls but do not have enlarged vessel elements (Turner and Somerville 1997). Similarly, downregulation of homologous genes in poplar results in mechanically weakened secondary cell walls, but only a ~5% increase in vessel element diameter (Li et al. 2011). It would thus appear that the primary wall or even pressure from surrounding cells, and not the secondary cell wall, may be the determinants of resistance against turgor during vessel element differentiation.

The best conceptual models for vessel element primary cell wall expansion are given by the classical auxin-mediated extensibility of primary cell walls by a pH and expansion-dependent

mechanism. Auxin is well known to affect cell wall extensibility in an expansin-dependent manner by lowering apoplastic pH in the “acid growth” hypothesis (Barbez et al. 2017). Auxin has long been implicated in vessel element differentiation, with auxin transport suggested as both a mechanism for interconnecting files of vessel elements as well as influencing the morphology of differentiating vessel elements (Barbez et al. 2017; Hacke et al. 2017; Spicer et al. 2013). In the zinnia in vitro system, auxin is required to induce vessel element differentiation, and increasingly acidic pH in vessel increases vessel element diameter (Roberts and Haigler 1994). Intriguingly, treatment of poplar stems with an inhibitor of polar auxin transport results in the development of wood with smaller and more clustered vessels, similar to what is seen in response to water stress (Johnson et al. 2018).

Regulation of solute concentration and turgor during tracheary element expansion has several features that make this a primary candidate regulatory mechanism controlling final diameter. Perhaps the best studied example of turgor regulation is given by guard cells which control the aperture of stomata in leaves. Guard cells increase turgor pressure by the regulated influx of solutes, namely  $K^+$  and sugars, which leads to the influx of water that causes the cell to swell (Kim et al. 2010). Poplar trees treated with ABA have wood with decreased  $K^+$  levels (Wind et al. 2004). Experimental depletion of  $K^+$  results in poplar wood with changes in the distribution and size of vessels elements (Fromm 2010; Wind et al. 2004), similar to what is seen in response to drought. Potassium and sugar levels are also both correlated with changes in tracheary element diameter occurring during seasonal changes in poplar (Ache et al. 2010). Mechanistically, a poplar  $K^+$  channel was identified that could play a causative role in regulating  $K^+$  levels and turgor in differentiating vessels (Arend et al. 2005; Langer et al. 2002).

Importantly, both ABA and changes in K<sup>+</sup> and sugar levels provide potential mechanisms interconnecting tree physiology during water stress with the development of tracheary elements.

### *Perspectives*

There are a number of challenges in providing a comprehensive understanding of the regulation of vessel element diameter. In vitro systems for the study of vessel element differentiation (e.g., the Zinnia system) lack the tissue-level context of normal vessel element differentiation and may be of limited utility. New approaches enabling the experimental manipulation, cell biology and imaging of differentiating vessel elements within living stems are thus needed. Computed tomography (CT) and other imaging approaches capable of visualizing cells deep within tissue could be used in conjunction with genetically encoded sensors or molecular probes against putative osmolytes, for example, to better understand the dynamics of expansion and the basis for the driving force of osmotic pressure. Potential surprises could include a relatively rapid expansion of vessels, and cooperation from neighboring ray cells in providing osmoticum.

### **CONCLUSIONS**

The scale of societal, economic and ecological impacts of forest mortality and yield losses caused by heat and drought stress require coordinated responses at levels ranging from local and national governments to intergovernmental bodies, to individual land managers. Complex decision making regarding forest management needs to be supported by the best possible science. Unfortunately, we currently have major knowledge gaps regarding the biology underlying water and abiotic stress responses in trees.

Importantly, new integrative approaches that cross traditional disciplines are needed to link how trees perceive water stress, transmit stress signals, and coordinate changes in

development and physiology. Even now basic questions about the interaction of wood development and physiology remain, including how changes in wood development impact growth and survival over longer time periods. The explosion of information about water and abiotic stress responses in crops and model plants has largely not been extended to trees. Indeed, perennial plants likely have unique attributes not found in herbaceous annuals that require direct research efforts. Even within tree species, it remains debatable to what extent findings in model trees like poplar will translate to other species. Most dramatically, gymnosperms and angiosperm trees have distinct wood types and other differences that likely require independent research efforts.

Understanding the biological factors underlying the responses of individual trees, tree species and forests to drought stress will enable new approaches for predicting and mitigating the future effects of drought. For wood biology, understanding the mechanisms underlying tracheary element morphology is now technically tractable using molecular, cell biology and genomic tools. But these mechanisms must then be interpreted in terms of physiology and ultimately whole tree responses to the environment. These efforts will require increased cooperation from researchers in previously disparate fields including tree physiology, anatomy, genomics and cell biology. Perhaps the most challenging will be to translate these basic findings into real solutions for predicting and mitigating drought, for example through direct selection of trees for breeding and restoration based on molecular markers rather than traditional tree breeding.

## **REFERENCES**

- Ache, P., Fromm, J., and Hedrich, R. (2010). Potassium-dependent wood formation in poplar: seasonal aspects and environmental limitations. *Plant Biology* 12, 259-267.
- Adams, H. D., Macalady, A. K., Breshears, D. D., Allen, C. D., Stephenson, N. L., Saleska, et al. (2010). Climate-induced tree mortality: Earth system consequences. *Eos* 91, 153-154.

- Allen, C., Macalady, A., Chenchouni, H., Bachelet, D., McDowell, N., Vennetier M, et al. (2010). A global overview of drought and heat-induced tree mortality reveals emerging climate change risks for forests. *Forest Ecology and Management* 259, 660-684.
- Arend, M., Stinzinger, A., Wind, C., Langer, K., Latz, A., Ache, P., et al. (2005). Polar-localized poplar K<sup>+</sup> channel capable of controlling electrical properties of wood-forming cells. *Planta* 223, 140.
- Barbez, E., Dunser, K., Gaidora, A., Lendl, T., and Busch, W. (2017). Auxin steers root cell expansion via apoplastic pH regulation in *Arabidopsis thaliana*. *Proceedings of the National Academy of Sciences* 114, 4884–4893.
- Barigah, T., Charrier, O., Douris, M., Bonhomme, M., Herbette, S., Améglio, T., et al. (2013). Water stress-induced xylem hydraulic failure is a causal factor of tree mortality in beech and poplar. *Annals of Botany* 112, 1431-1437.
- Bentouati, A. (2008). La situation du cedre de l'Atlas dan les Aures (Algerie). *Foret Méditerranéen* 29, 203-208.
- Bentz, B., Régnière, J., Fettig, C., Hansen, E., Hayes, J., Hicke, J., et al. (2010). Climate change and bark beetles of the western United States and Canada: Direct and indirect effects. *BioScience* 60, 602-613.
- Bertheau, L., Djeghdir, I., Foureau, E., Cheddor, F., Glevarec, G., Oudin, A., et al. (2015). Insights into B-type RR members as signaling partners acting downstream of HPt partners of HK1 in the osmotic stress response in *Populus*. *Plant Physiology and Biochemistry* 94, 244-252.
- Bonan, G. (2008). Forests and climate change: forcings, feedbacks and the climate benefits of forests. *Science* 320, 1444–1449.
- Carpita, N. (2011). Update on Mechanisms of Plant Cell Wall Biosynthesis: How plants make cellulose and other (1->4)- $\beta$ -d-glycans. *Plant Physiology* 155, 171-184.
- Cheddor, F., Bénédicti, H., Depierreux, C., Delmotte, F., Morabito, D., Carpin, S. (2005). Osmotic stress sensing in *Populus*: Components identification of a phosphorelay system. *FEBS Letters* 580, 77-81.

- Chen, S., Li, J., Wang, T., Wang, S., Polle, A., and Hüttermann, A. (2002). Osmotic stress and ion-specific effects on xylem abscisic acid and the relevance to salinity tolerance in poplar. *Journal of Plant Growth Regulation* 21, 224-233.
- Christman, M., Sperry, J., and Smith, D. (2012). Rare pits, large vessels and extreme vulnerability to cavitation in a ring-porous tree species. *New Phytologist* 193, 713-720.
- Cochard, H., Cruiziat, P., and Tyree, M. (1992). Use of positive pressures to establish vulnerability curves: further support for the air-seeding hypothesis and implications for pressure-volume analysis. *Plant Physiology* 100, 205-209.
- Crombie, D., Hipkins, M., and Milburn, J. (1985). Gas penetration of pit membranes in the xylem of *Rhododendron* as the cause of acoustically detectable sap cavitation. *Functional Plant Biology* 12, 445-453.
- Dixon, H., and Joly, J. (1895). On the ascent of sap. *Philosophical Transactions of the Royal Society of London* 186, 563-576.
- FAO: Food and Agriculture Organization of the United Nations (2018). *The State of the World's Forests 2018 - Forest pathways to sustainable development*. Rome. Licence: CC BY-NC-SA 3.0 IGO.
- Fichot, R., Laurans, F., Monclus, R., Moreau, A., Pilate, G., and Brignolas, F. (2009). Xylem anatomy correlates with gas exchange, water-use efficiency and growth performance under contrasting water regimes: evidence from *Populus deltoides* × *Populus nigra* hybrids. *Tree Physiology* 29, 1537-1549.
- Fromm, J. (2010). Wood formation of trees in relation to potassium and calcium nutrition. *Tree Physiology* 30, 1140-1147.
- Fujita, Y., Fujita, M., Shinozaki, K., and Yamaguchi-Shinozaki, K. (2011). ABA-mediated transcriptional regulation in response to osmotic stress in plants. *Journal of Plant Research* 124, 509-525.
- Groover, A., and Jones, A. (1999). Tracheary element differentiation uses a novel mechanism coordinating programmed cell death and secondary cell wall synthesis. *Plant Physiology* 119, 375-384.

- Hacke, U., Spicer, R., Schreiber, S., Plavcová, L. (2017). An ecophysiological and developmental perspective on variation in vessel diameter. *Plant, Cell & Environment* 40, 831-845.
- Héricourt, F., Chefdor, F., Djeghdir, I., Larcher, M., Lafontaine, F., Courdavault, V., et al. (2016). Functional divergence of poplar histidine-aspartate kinase HK1 paralogs in response to osmotic stress. *International Journal of Molecular Sciences* 17, 2061.
- IPCC: Intergovernmental Panel on Climate Change. (2007). *Climate Change 2007: The Physical Science Basis. Contribution of Working Group I to the Fourth Assessment Report of the IPCC*. In S. Solomon, D. Qin, M. Manning, Z. Chen, M. Marquis, K.B. Averyt, M. Tignor and H.L. Miller, eds. Cambridge, UK: Cambridge University Press. 996 pp
- Jacobsen, A., Pratt, R., Ewers, F., and Davis, S. (2007). Cavitation resistance among 26 chaparral species of southern California. *Ecological Monographs* 77, 99-115.
- Jia, J., Zhou, J., Shi, W., Cao, X., Luo, J., Polle, A., et al. (2017). Comparative transcriptomic analysis reveals the roles of overlapping heat-/drought-responsive genes in poplars exposed to high temperature and drought. *Scientific Reports* 7, 43215.
- Johnson, D., Eckart, P., Alsamadisi, N., Noble, H., Martin, C., and Spicer, R. (2018). Polar auxin transport is implicated in vessel differentiation and spatial patterning during secondary growth in *Populus*. *American Journal of Botany* 105, 186-196.
- Karahara, I., Ikeda, A., Kondo, T., and Uetake, Y. (2004). Development of the casparian strip in primary roots of maize under salt stress. *Planta* 219, 41-47.
- Kim, T., Böhmer, M., Hu, H., Nishimura, N., and Schroeder, J. (2010). Guard cell signal transduction network: Advances in understanding abscisic acid, CO<sub>2</sub>, and Ca<sup>2+</sup> signaling. *Annual Review of Plant Biology* 61, 561-591.
- Langer, K., Ache, P., Geiger, D., Stinzinger, A., Arend, M., Wind, C., et al. (2002). Poplar potassium transporters capable of controlling K<sup>+</sup> homeostasis and K<sup>+</sup>-dependent xylogenesis. *Plant Journal* 32, 997-1009.

- Larson, P. R. (1994). *The Vascular Cambium: Development and Structure*. Berlin, Heidelberg: Springer-Verlag.
- Li, L. (2003). *Major forest disease and insect pests in China*. Beijing: Beijing Forestry Publishing House.
- Li, Q., Min, D., Wang, J., Peszlen, I., Horvath, L., Horvath, B., et al. (2011). Down-regulation of glycosyltransferase 8D genes in *Populus trichocarpa* caused reduced mechanical strength and xylan content in wood. *Tree Physiology* 31, 226-236.
- Liu, W., Fairbairn, D., Reid, R., and Schachtman, D. (2001). Characterization of two HKT1 homologues from *Eucalyptus camaldulensis* that display intrinsic osmosensing capability. *Plant Physiology*, 127, 283-294
- Logan, T., Beverly, E., Arjan, J., and Jeffrey, A. (2017). Tree mortality from fires, bark beetles, and timber harvest during a hot and dry decade in the western United States (2003–2012). *Environmental Research Letters* 12, 065005
- McDowell, N., and Allen, C. (2015). Darcy's law predicts widespread forest mortality under climate warming. *Nature Climate Change* 5, 669.
- McDowell, N., Pockman, W., Allen, C., Breshears, D., Cobb, N., Kolb, T., et al. (2008). Mechanisms of plant survival and mortality during drought: Why do some plants survive while others succumb to drought? *New Phytologist* 178, 719-739.
- Nagashima, Y., Tsugawa, S., Mochizuki, A., Sasaki, T., Fukuda, H., and Oda, Y. (2018). A Rho-based reaction-diffusion system governs cell wall patterning in metaxylem vessels. *Scientific Reports* 8, 11542-11542
- Oda, Y., and Fukuda, H. (2013). Rho of plant GTPase signaling regulates the behavior of Arabidopsis Kinesin-13A to establish secondary cell wall patterns. *The Plant Cell*, 25(11), 4439-4450.
- Oda, Y., Iida, Y., Kondo, Y., and Fukuda, H. (2010). Wood cell-wall structure requires local 2D-microtubule disassembly by a novel plasma membrane-anchored protein. *Current Biology* 20, 1197–1202

- Osakabe, Y., Yamaguchi-Shinozaki, K., Shinozaki, K., and Tran, L. (2013). Sensing the environment: Key roles of membrane-localized kinases in plant perception and response to abiotic stress. *Journal of Experimental Botany* 64, 445-458.
- Pan, Y., Birdsey, R., Fang, J., Houghton, R., Kauppi, P., Kurz, W., et al. (2011). A large and persistent carbon sink in the world's forests. *Science* 333, 988–993.
- Pickard, W. (1981). The ascent of sap in plants. *Progress in Biophysics and Molecular Biology*, 37, 181-229.
- Popko, J., Hänsch, R., Mendel, R., Polle, A., and Teichmann, T. (2010). The role of abscisic acid and auxin in the response of poplar to abiotic stress. *Plant Biology* 12, 242-258.
- Raj, S., Bräutigam, K., Hamanishi, E., Wilkins, O., Thomas, B., Schroeder, W., et al. (2011). Clone history shapes *Populus* drought responses. *Proceedings of the National Academy of Sciences, USA*, 108, 12521-12526.
- Reed, D., Ewers, B., and Pendall, E. (2014). Impact of mountain pine beetle induced mortality on forest carbon and water fluxes. *Environmental Research Letters* 9, 105004.
- Roberts, A., and Haigler, C. (1994). Cell expansion and tracheary element differentiation are regulated by extracellular pH in mesophyll cultures of *Zinnia elegans* L. *Plant Physiology* 105, 699-706.
- Sasaki, T., Fukuda, H., and Oda, Y. (2017). CORTICAL MICROTUBULE DISORDERING1 is required for secondary cell wall patterning in xylem vessels. *The Plant Cell* 29, 3123–3139.
- Sperry, J., Hacke, U., and Pittermann, J. (2006). Size and function in conifer tracheids and angiosperm vessels. *American Journal of Botany* 93, 1490-1500.
- Sperry, J., and Tyree, M. (1990). Water stress induced xylem embolism in three species of conifers. *Plant, Cell and Environment*, 13, 427-436.
- Spicer, R., Tisdale-Orr, T., and Talavera, C. (2013). Auxin-responsive DR5 promoter coupled with transport assays suggest separate but linked routes of auxin transport during woody stem development in *Populus*. *PLoS ONE* 8, e72499

- Taylor-Teeple, M., Lin, L., de Lucas, M., Turco, G., Toal, T. W., Gaudinier, A., et al. (2015). An *Arabidopsis* gene regulatory network for secondary cell wall synthesis. *Nature* 517, 571-575.
- Turner, S., and Somerville, C. (1997). Collapsed xylem phenotype of *Arabidopsis* identifies mutants deficient in cellulose deposition in the secondary cell wall. *The Plant Cell* 9, 689-701.
- Tyree, M., and Sperry, J. (1989). Vulnerability of xylem to cavitation and embolism. *Annual Review of Plant Physiology and Plant Molecular Biology* 40, 19-36.
- Tyree, M., and Zimmermann, M. (2002). Xylem structure and the ascent of sap. Heidelberg, Berlin: Springer-Verlag.
- USFS. (2016). Effects of drought on forests and rangelands in the United States: A comprehensive science synthesis. [J. M. Vose, J. Clarke, C. Luce, & T. Patel-Weynand (Eds.)]. Washington, DC: U.S. Department of Agriculture, Forest Service. <https://doi.org/10.2737/WO-GTR-93b>
- USGCRP (2018). Impacts, Risks, and Adaptation in the United States: Fourth National Climate Assessment, Volume II [D. Reidmiller, C. Avery, D. Easterling, K. Kunkel, K. Lewis, T. Maycock, and B. Stewart (eds.)]. Washington, DC: U.S. Global Change Research Program. <https://doi.org/10.7930/NCA4.2018>.
- Venturas, M., Sperry, J., and Hacke, U. (2017). Plant xylem hydraulics: What we understand, current research, and future challenges. *Journal of Integrative Plant Biology* 59, 356–389.
- Wang, H., Zhang, Z., Kong, X., Lui, S., and Shen, Z. (2007). Preliminary deduction of potential distribution and alternative hosts of invasive pest, *Dendroctonus valens* (Coleoptera: Scolytidae). *Scientia Silvae Sinicae* 143, 71-76.
- Wang, M., Zheng, Q., Shen, Q., and Guo, S. (2013). The critical role of potassium in plant stress response. *International Journal of Molecular Sciences* 14, 7370-7390.
- Wheeler, J. K., Sperry, J. S., Hacke, U. G., and Hoang, N. (2005). Inter-vessel pitting and cavitation in woody Rosaceae and other vesselless plants: A basis for a safety versus efficiency trade-off in xylem transport. *Plant, Cell and Environment* 28, 800-812.

Wind, C., Arend, M., and Fromm, J. (2004). Potassium-dependent cambial growth in poplar. *Plant Biology* 6, 30-37.

## **Chapter 2. Genetic regulation of vessel morphology in *Populus***

**F. Daniela Rodriguez-Zaccaro, Isabelle Henry, Andrew Groover**

*(Adapted from a previously published manuscript)*

### **Abstract**

During secondary growth, forest trees can modify the anatomy of the wood produced by the vascular cambium in response to environmental conditions. Notably, the trees of the model angiosperm genus, *Populus*, reduce the risk of cavitation and hydraulic failure under water stress by producing water-conducting vessel elements with narrow lumens, which are more numerous and more interconnected with each other. Here, we determined the genetic architecture of vessel traits affecting hydraulic physiology and resilience to water stress. Vessel traits were measured for clonally replicated genotypes of a unique *P. deltoides x nigra* population carrying genomically-defined insertions and deletions that create gene dosage variation. We found significant phenotypic variation for all traits measured (mean vessel diameter, height-corrected mean vessel diameter, vessel frequency, height-corrected vessel frequency, vessel grouping index, and mean vessel circularity), and that all traits were under genetic control and showed moderate heritability values, ranging from 0.32 to 0.53. Whole-genome scans of correlations between gene dosage and phenotypic traits identified quantitative trait loci for tree height, mean vessel diameter, height-corrected mean vessel diameter, height-corrected vessel frequency, and vessel grouping index. Our results demonstrate that vessel traits affecting hydraulic physiology are under genetic control, and both pleiotropic and trait-specific quantitative trait loci are found for these traits.

### **INTRODUCTION**

Wood (secondary xylem) is the water conducting tissue of tree stems, and the anatomical features of wood can have profound effects on water transport as well as vulnerability to hydraulic

failure during water stress (Rodriguez-Zaccaro and Groover, 2019). Vessel elements are the primary water conducting cells in most angiosperms, including trees of the model genus *Populus*. Vessel differentiation starts with the commitment of terminal cell fate and cessation of cell division, followed by cell expansion, construction of a rigid secondary cell wall, and programmed cell death to produce a water conducting cell corpse (Groover and Jones, 1999; Turner et al., 2014). In *Populus* stems undergoing secondary growth, vessel elements differentiate from xylem mother cells derived from fusiform initials of the vascular cambium and join end-on-end to create longer water conducting tubes termed vessels (Larson, 1994; Sperry et al., 2006). Pits between adjacent vessel elements and between vessel elements and other cells such as ray parenchyma provide additional routes for water to pass both between and out of vessel elements. Importantly, secondary growth can be altered to produce wood anatomy and vessel morphologies that mitigate water stress during drought or maximize water conduction for fast growth under permissive conditions (Tyree 1989; Tyree et al. 1989; Tyree and Zimmermann 2002). To what degree these changes reflect passive or indirect responses of development to environmental conditions, as opposed to genetically regulated responses, remains unclear.

Together, the anatomical properties of vessels have a profound effect on water conduction physiology (Rodriguez-Zaccaro and Groover, 2019). Vessel lumen diameter directly affects the rate of water transport through secondary xylem, with wider vessels contributing to greater water transport efficiency. This can be partially explained through the Hagen-Poiseuille law, modeling the volumetric flow rate of a liquid moving through a tube as being proportional to the fourth power of the radius of the tube (Venturas et al. 2017). Consequently, a small increase in vessel width can produce a large increase in water flow and allow for greater photosynthesis and growth rates (Brodribb and Feild 2000). Larger vessel diameters, however, have been associated with

greater vulnerability to cavitation due to drought and other abiotic stressors (Hacke et al. 2016; Gleason et al. 2016). Cavitation results in the formation of air-pockets within the xylem network, which can lead to lethal hydraulic failure (Tyree 1989). Vessel frequency (VF), which is the number of vessels within a given area of xylem, and vessel grouping index (VGI), a measure of vessel clustering and interconnectivity, can also affect hydraulic function. A greater VF can increase water transport efficiency and buffer the xylem network from hydraulic failure by allowing for a larger fraction of smaller diameter vessels that remain functional under water stress compared to lower VF xylem (Baas et al. 1983; Villar-Salvador et al. 1997). Similarly, a greater VGI can lead to increased hydraulic efficiency and mitigate the effects of cavitation by providing xylem sap alternate routes to bypass embolized vessels (Carlquist 1984; Lens et al. 2010). Greater VGI, however, has also been related to increased vulnerability to cavitation due to a likely increase in the probability of embolism spread in a more interconnected xylem network (Loepfe et al. 2007). A trait that has not been as well studied in the context of hydraulic function is vessel shape or cross-sectional circularity. According to microchannel fluid mechanics, a more circular conduit is able to transport fluids more efficiently than conduits with more irregular shapes (White 2011). Vessel circularity has also been related to safety from water stress, with more circular vessels able to withstand large negative pressures within the xylem network without imploding and disrupting water transport (Cochard et al. 2004). Non-lumen fraction (NF) is the proportion of xylem area that is not made up of vessel lumen area. This trait has been previously positively related to wood mechanical strength and density (Searson et al. 2004; Zanne et al. 2010), an important trait that helps determine commercial wood quality.

Several stem and wood anatomical traits have been shown to be correlated to each other (von Arx et al. 2013; Hajek et al. 2014), although cause and effect for these correlations is not

known. For example, MVD and VF are often negatively correlated (Chauhan et al. 1999; Sellin et al. 2008). Some studies have suggested that this correlation is the result of a trade-off between hydraulic conductivity and mechanical support in stems (Wagner et al. 1998; Barbour and Whitehead 2003); a positive correlation leading to larger and more numerous vessels could result in mechanically weaker stems that are selected against. MVD and VF are also known to predictably scale with tree height; larger trees tend to have wider and less numerous vessels compared to smaller trees at the same sampling height (Olson et al. 2014). Some hydraulic optimality models suggest that vessel width and quantity are influenced by height. The Hagen-Poiseuille law predicts that longer conduits are more resistant to flow than shorter conduits of equal diameter. Wider vessels, then, are thought to compensate for the decrease in water transport efficiency that would otherwise result from the longer conductive pathways necessarily present in taller trees (Olson and Rosell 2013). However, the correlation between tree height and vessel traits is not perfect, and it is unclear to what degree the observed variation in vessel traits could be the result of genetic regulation independent from tree size.

The regulation of cell expansion and final diameter in vessel elements likely involves the regulation of cell turgor and cell wall expansion. The experimental manipulation of potassium, a primary osmoticum of plant cells likely involved in cell turgor regulation, can be used to alter the diameter of differentiating vessel elements (Cutter and Murphey, 1977). However, there is less evidence that manipulation of secondary cell wall formation can have similar effects. For example, well-characterized *irregular xylem (irx)* mutants with physically compromised vessels with crumpled cell walls are not significantly defective in terms of cell diameter (Turner and Somerville 1997). Whether turgor regulation, cell wall regulation, or other unknown factors such as the timing of transition from cell division to cell expansion are the most critical factors influencing final cell

diameter and morphology remains uncertain. One reason for this knowledge gap is that experimental systems to investigate the genetic and genomic properties of vessel element morphology within relevant species, including forest trees, have been historically lacking.

We previously developed *Populus* germplasm with the goal of performing functional genomic experiments directly in a forest tree species with extensive secondary growth and wood formation. To create this resource, pollen from a *P. nigra* male tree was irradiated to create chromosomal breaks prior to crossing with two *P. deltoides* females to produce a large F1 hybrid population (Henry et al. 2015). The insertions and deletions in each F1 individual create structural variation and associated gene dosage variation in the affected regions. Insertions and deletions were genomically mapped for each F1 individual, allowing genome-wide surveys linking gene dosage variation with phenotypes to identify dosageQTL (dQTL) (Bastiaanse et al. 2019; Bastiaanse et al. 2021). The genetic architecture of multiple biomass and phenology-related traits were previously dissected using this resource, including the identification of dQTL for multiple traits, and demonstrated that gene dosage is a major source of phenotypic variation in this population (Bastiaanse et al., 2019; Bastiaanse et al. 2020). These results are relevant to natural genetic variation in *Populus* where, similar to other plant species that have been surveyed, structural and gene dosage variation is prevalent (Pinosio et al., 2016; Zhang et al., 2019).

Here we used the same poplar irradiation hybrid germplasm to estimate the genetic architecture of prominent vessel element and stem traits including mean vessel diameter (MVD), vessel frequency (VF), vessel grouping index (VGI), mean vessel circularity (MVC), tree height (TH), non-lumen fraction (NF) and bark thickness (BT). We report correlations among all traits measured, including tree height and vessel traits. All traits showed modest heritabilities, indicating that there is a significant genetic component underlying the observed phenotypic variation for

vessel traits. Additionally, dQTL are reported for MVD, tree height-corrected MVD (cMVD), tree height-corrected VF (cVF) and VGI. We provide evidence of dQTL commonly shared by correlated traits, as well as trait-specific dQTL, suggesting independent regulation of both correlated and uncorrelated traits. Together, our results show that vessel traits are under genetic regulation and not simply a passive consequence of tree height, and that systems genetic approaches could now be used to further dissect these traits and identify candidate genes using this same genomics resource.

## **MATERIALS AND METHODS**

### *Plant Materials*

A subset of 201 poplar hybrid genotypes was included from a larger dosage mutant pedigree developed and described by Henry and colleagues (2015). Briefly, the pedigree was produced by crossing two female *Populus deltoides* with gamma-irradiated pollen of a male *P. nigra*. The F1 hybrids were then completely sequenced using Illumina short reads. Relative sequencing read coverage values were used to detect insertions and deletions (indel mutations) across F1 hybrids, that together cover the entire poplar genome multiple times. The pedigree consists of nearly 800 replicated lines maintained in an outdoor plantation at the US Forest Service Institute of Forest Genetics in Placerville, CA.

All lines within the subset were clonally propagated through stem cuttings from the field in multiple replicates (ramets) during the spring of 2018. Cuttings were planted with rooting hormone (Bontone) in individual 2.83 L pots filled with horticultural soil (Sunagro Sunshine Mix #4) and fertilizer (Osmocote, approximately 14g per kg soil) inside a greenhouse at the IFG. After a 2 month growth period, 3 healthy clonal replicates per line were randomly selected to include in a randomized complete block design. Plants were grown in a lathe house for 3 months, harvested,

and moved inside a greenhouse to coppice and grown for a second 3 month period before harvesting a second time. Both crops were kept under well-watered conditions using a drip-irrigation system and monitored for stem height and diameter growth until the end of the growing season in the fall of 2018. Greenhouse trees were kept at a near constant temperature of 23 °C. All analyses and results involve the latter greenhouse-grown crop. A 6 to 8 cm woody stem segment was harvested from each tree at a fixed height of 10 cm from the point of emergence from the original cutting. Stems were immediately stored in a 60% ethyl alcohol solution in 50 mL Falcon tubes.

### *Histology*

Stem internodes were cut in 40 µm thick cross-sections with a sliding microtome (Spencer Lens) or a vibratome (Vibratome Series 1000). Sections were stained with and mounted in a mixture of phloroglucinol and Astra Blue, which stain lignin and cellulose, respectively. Sections were then photographed at X5 or X10 magnification under a microscope with a digital camera with standardized settings (Leica Microsystems). A 100 µm scale bar was included in each image, adjusted for specific magnification. Lastly, a high quality micrograph of each replicate within a line was selected for image analysis.

### *Image Analysis*

Stem cross-section micrographs were processed using Fiji ImageJ software (v2) to obtain wood anatomical trait data. Images were spatially calibrated using the known scale bar length to determine the number of pixels per micrometer. Bark thickness was calculated as the average distance between the cambial zone and the outer cork in unprocessed images. All non-xylem areas (bark and pith) were then manually cut out of the image before converting to grayscale. Images were divided into a “foreground” consisting of vessel lumens, and a “background” made up of

non-vessel lumen area, by setting a standardized pixel thresholding value. Vessel lumen area and circularity values were obtained directly through the Analyze Particles tool, with equivalent circle vessel diameters calculated from vessel lumen areas (Scholz et al. 2013). A mean vessel diameter and mean vessel circularity value was calculated for each image. A vessel frequency value was calculated for each image by dividing the number of vessels (obtained through the Analyze Particles tool) by the total xylem area ( $\text{mm}^2$ ). NF was calculated by multiplying the mean vessel area by vessel frequency (Scholz et al. 2013). A vessel grouping index value was obtained for each image by dividing the number of vessels by the number of vessel groups. A vessel group consists of anything from a solitary vessel to any number of clustered vessels with secondary walls that are in contact (Carlquist 2001). Vessel groups were counted manually using the Multi-point tool.

#### *Height corrected traits*

Because tree height is correlated with vessel diameter (Olson and Rosell, 2013), cMVD, and cVF values were calculated for each tree to assess the portion of trait variation that cannot be explained by height. The log<sub>10</sub> of the final tree height at harvest was plotted against the log<sub>10</sub> of each trait. The equation describing the linear regression of each plot was used to obtain expected trait values predicted from tree height. Expected values were subtracted from observed trait values to obtain residual values that were used as height-corrected trait data. Lines with residual values near 0 were considered to have vessel trait values expected for their height. Lines with significantly higher residual values for MVD, for example, were considered to have unusually wide vessels for their height.

#### *Estimating Broad-sense Heritability*

The broad-sense heritability ( $H^2$ ) of each trait was estimated using the repeatability function in the CRAN heritability R package (version 1.3) developed by Kruijer et al. (2015).

Repeatability, or intraclass correlation, is considered the broad-sense heritability, and was calculated by dividing the total genetic variance by the total phenotypic variance of a trait. The total genetic variance was estimated by subtracting the mean sums of squares for genotype and residual error obtained from an analysis of variance and dividing the results by the number of clonal replicates in each line. The total phenotypic variance was calculated by adding the total genetic variance to the mean sums of squares of the residual error (Kruijer et al. 2015).

### *Statistical Analysis*

Trait data were transformed, when appropriate, through Box-Cox power transformations. Pearson's correlation tests were run to determine the relationship between all trait combinations. An ANOVA-based analysis was performed on each trait in base R, with genotype and final tree height at harvest as independent factors in each model, with the exception of height-corrected traits which involved only a genotype factor. Tree height was also treated as a dependent variable in a separate model with genotype as the sole independent factor. Each analysis was followed by a Tukey's honest significance post hoc test.

Dosage dependent quantitative trait locus analyses (dQTL) were performed on all traits. The start and end sites of all the indels of the genotypes included in the analysis were used to create the boundaries of genomic bins, as previously described (Bastiaanse et al., 2019; Bastiaanse et al 2021). A relative gene dosage score was calculated for each genotype at each genomic bin by dividing the gene dosage at the bin by the background ploidy of the particular line. A Kendall's tau coefficient was calculated at each bin to test for statistical dependence between the relative dosage score and the phenotypic trait data (Schaeffer and Levitt 1956). Most indels encompassed more than one chromosomal bin, and contiguous bins were thus correlated, as previously described for this population (Bastiaanse et al., 2021). Consequently, the resulting P values were adjusted

through a modified Bonferroni correction for multiple testing in which P values were multiplied by the number of independent chromosomal bins (Bastiaanse et al. 2021). The number of independent bins was obtained through a dissimilarity matrix by calculating pairwise correlation coefficients between the relative dosage ratios of bins across all genotypes. These correlation coefficients were grouped using a hierarchical clustering method and individual branches were combined using a cutoff value of 0.7 (Bastiaanse et al. 2020). The original 469 genomic bins were merged into 40 independent bins through this method. Adjusted P values below a threshold of 0.05 were considered significant and signaled putative dQTL associated with a trait. The adjusted R-squared of the linear regression model fitting genomic bins was used to estimate the percentage of trait variance explained by dQTL.

## **RESULTS**

Here we used a subset of a previously described population of *P. deltoides* x *nigra* carrying genomically mapped indels to investigate the effect of gene dosage variation on stem anatomical and vessel traits. Of the 201 genotypes included in the analysis, 173 carried insertions and/or deletions, with the remaining lines included as non-indel controls. Genomic bins were defined by the breakpoints of indels across all lines included in this experiment (Materials and Methods), which represented 469 genomic bins covering 91.5% of the genome, as shown in Figure 2.1. Genomic bin size ranged from 0.01 to 5.2 Mb, with an average bin size of 0.78 Mb. Lesion coverage varied substantially between chromosomes, ranging from 1 to 16 indels per genomic bin, with a genome-wide average of 6 indels per bin.

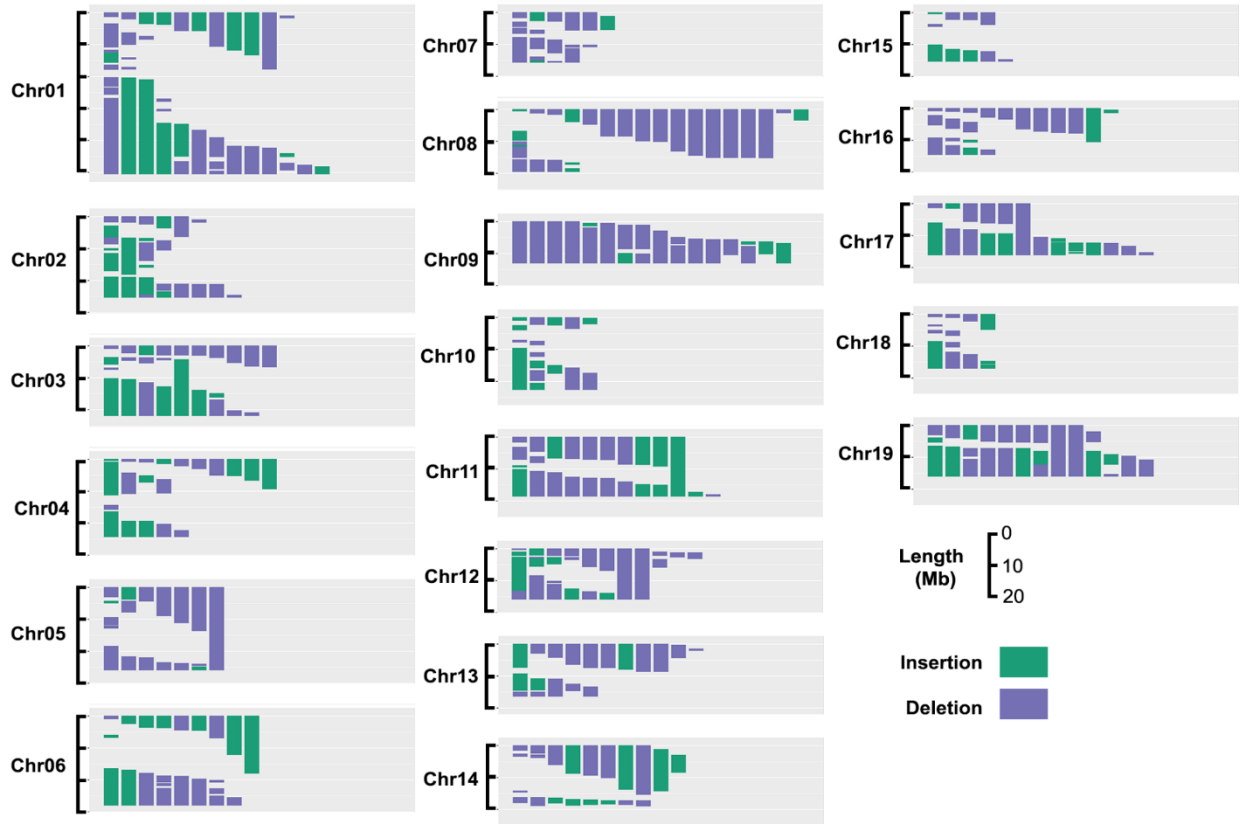


**FIGURE 2.1** | Insertion and deletion (indel) coverage across the poplar genome for genotypes included in this study. Based on the indel size and locations in the 201 genotypes chosen for this study, 95% percent of the genome is covered by at least one indel.

Clonal replicates of all genotypes were grown and measured under permissive greenhouse conditions, prior to destructive sampling and measuring wood anatomical and vessel traits (Materials and Methods). For each tree, a basal stem cross section was stained, digitally imaged, and analyzed to extract anatomical trait data as illustrated in Figure 2.2. Traits directly measured or calculated are summarized in Table 2.1 and include tree height (TH), mean vessel diameter (MVD), vessel frequency (VF), vessel grouping index (VGI), mean vessel circularity (MVC), non-lumen fraction (NF) and bark thickness (BT). Some hydraulic optimality models suggest that vessel width and quantity are a consequence of organ size (Olson and Rosell 2013). Both MVD and VF are known to be highly correlated to tree height, where larger trees have wider and less

numerous vessels compared to smaller trees at the same sampling height (Olson et al. 2014). To assess the portion of trait variation not explained by height, we evaluated correlations among raw anatomical and vessel trait data and tree height, and included height-corrected adjuncts for traits with significant correlations (Materials and Methods). Two traits were corrected this way: height-corrected mean vessel diameter (cMVD) and height-corrected vessel frequency (cVF) (Table 2.1).

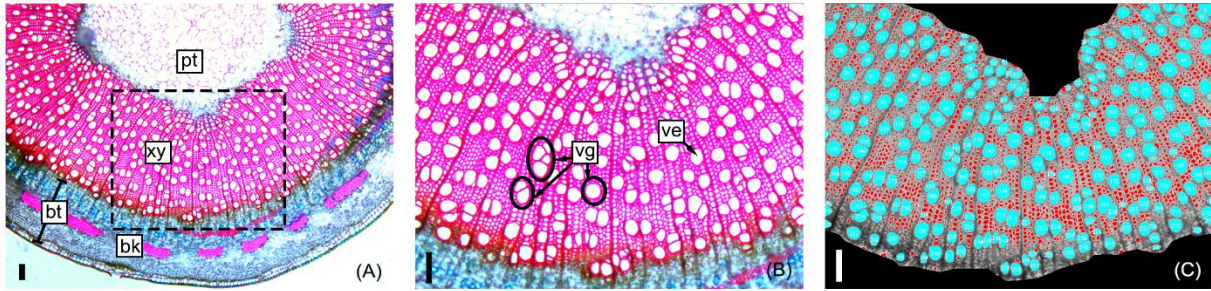


**FIGURE 2.2|** Representative sample of a poplar stem cross-section used to obtain stem and vessel anatomical trait data. Section micrographs include the pith (pt), secondary xylem (xy), and bark (bk); bark thickness (bt) is measured before image processing (A). Vessel elements (ve) and vessel group (vg) examples are shown within a close-up of the sampled section (B); vessel groups are single vessels or any number of clustered vessels with secondary cell walls that are in contact. Image J software (v2) was used to measure xylem area, automatically count vessels, and measure vessel areas and circularities (Materials and Methods).

**Table 2.1|** The means, standard deviations (SD) and ranges (R) of phenotypic traits measured in a 201 genotype poplar pedigree.

Trait	Abbr.	Units	Mean	SD	R
Tree height	TH	cm	64	32	5-168
Mean vessel diameter	MVD	$\mu\text{m}$	26	4.0	14.0-34.9
Height-corrected MVD	cMVD	unitless	0.0001	0.043	-0.136-0.123
Vessel frequency	VF	vessels/ $\text{mm}^2$	365	166	165-1000
Height-corrected VF	cVF	unitless	-0.0004	0.084	0.341-0.282
Vessel grouping index	VGI	vessel/vessel group	1.47	0.1	1.17-1.79
Mean vessel circularity	MVC	unitless	0.78	0.03	0.68-0.87
Non-lumen fraction	NF	unitless	0.8	0.04	0.66-0.91
Bark thickness	BT	$\mu\text{m}$	608	349	169-779

### *Pedigree trait distributions*

Distributions of raw trait data are shown in Figure 2.3; trait distribution means, standard deviations, and ranges are summarized in Table 1. All traits showed continuous variation, consistent with multigenic variation expected for classical quantitative traits. The final tree height at harvest varied substantially within the population, ranging from 5 to 168 cm, with a mean height of 64 and a standard deviation of 32 cm (Table 1; Figure 2.3A). MVD within the 201 genotype pedigree subset ranged from 14 to 36  $\mu\text{m}$  (Figure 2.3B), with an average of 26 and a standard deviation of 4  $\mu\text{m}$ . VF distribution was strongly skewed right (Figure 2.3D) and ranged from 165 to 1,000 vessels/ $\text{mm}^2$  of xylem, with an average of 365 and a standard deviation of 166 vessels/ $\text{mm}^2$ . VGI had a narrow distribution (Figure 2.3F) that ranged from 1.17 to 1.79 vessels/vessel group with a mean of 1.47 and a standard deviation of 0.1 vessels/vessel group. MVC had a narrow distribution (Figure 2.3G) that ranged from 0.68 to 0.87, with an average of 0.78 and a standard deviation of 0.03. NF distribution was narrow (Figure 2.3H) and ranged from 0.66 to 0.91 with a mean of 0.80 and a standard deviation of 0.04.

In comparison with non-indel control genotypes, indel genotypes extended the observed variation and defined the extremes of each phenotype as shown in Figure 2.3 and Table 2.2. Thus, indels generated phenotypic variation beyond the variation caused by allelic segregation. Consistent with previous findings (Bastiaanse et al., 2019), as a group lines with lesions had an overall negative effect on growth, as illustrated here by significantly lower tree heights for the lesion group (Table 2.2). Additional traits with significantly smaller means in the lesion line group included MVD and BT, while lesion lines had a larger mean for VF (Table 2.2). Thus, MVD, BT, and VF behave as growth-related traits with regards to response to lesion-induced dosage variation.

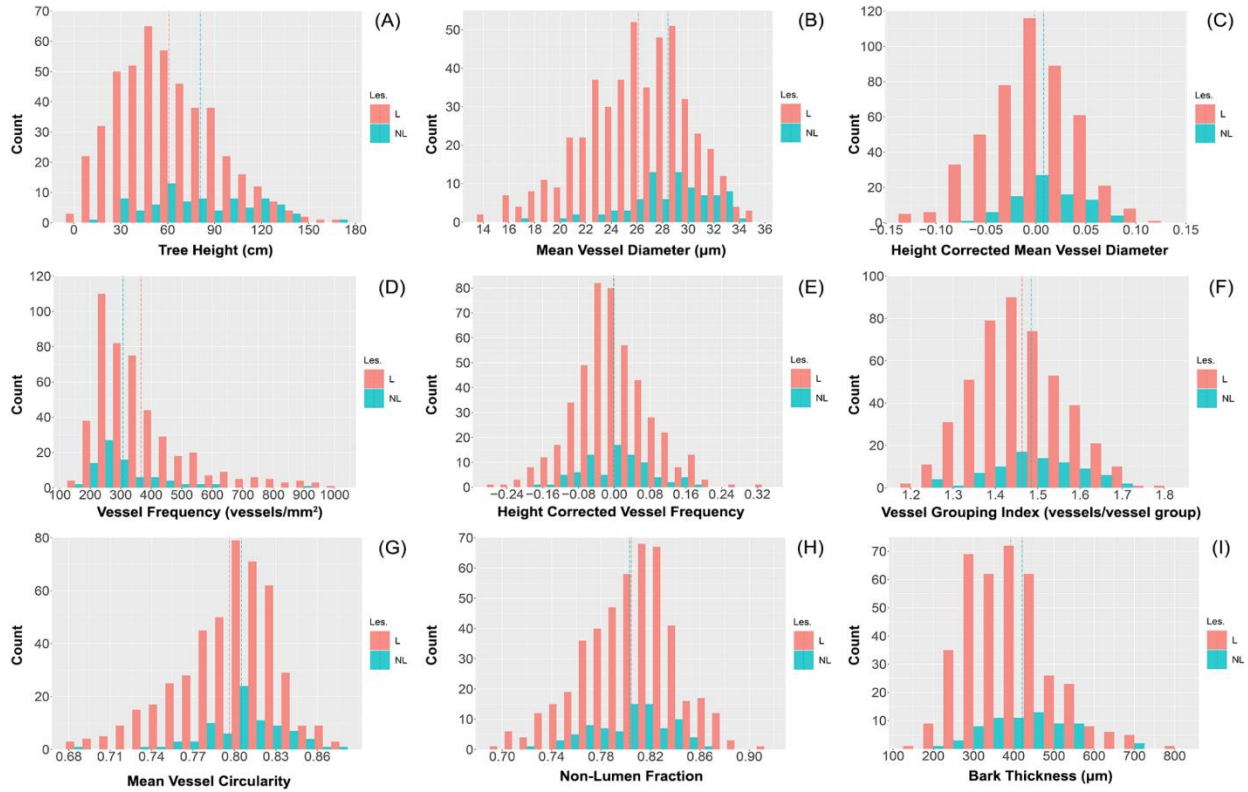


**FIGURE 2.3|** Untransformed wood anatomical trait and stem trait data distributions across the 201 genotypes included in the study. Values are for three clonal replicates per genotype. The red bars represent indel genotypes (173) and the blue bars represent non-lesion genotypes (28). Traits include tree height (A), mean vessel diameter (B), height-corrected mean vessel diameter (C), vessel frequency (D), height-corrected vessel frequency (E), vessel grouping index (F), mean vessel circularity (G), non-lumen fraction (H), and bark thickness (I). The red dotted lines represent the trait means of indel lines and the blue dotted lines represent the trait means of non-indel lines.

**Table 2.2|** The means, standard deviations (SD) and ranges (R) of phenotypic traits measured in a 201 genotype poplar pedigree across non-lesion (NL Lines) and lesion genotypes (L Lines).

Trait	(NL Lines)			(L Lines)		
	Mean	SD	R	Mean	SD	R
TH	80.9	34.6	9-166	60.8	30.8	5-168
MVD	28.4	3.3	16.6-34.3	26.1	4.0	14.0-34.9
cMVD	0.008	0.032	-0.064-0.082	-0.004	0.044	-0.136-0.123
VF	307	119	165-902	375	171	168-1000
cVF	0	0.074	-0.179-0.185	0	0.086	-0.282-0.341
VGI	1.48	0.1	1.25-1.69	1.46	0.1	1.18-1.79
MVC	0.81	0.030	0.69-0.87	0.80	0.035	0.68-0.87
NF	0.80	0.031	0.73-0.87	0.80	0.037	0.66-0.91
BT	421	99	221-690	392	105	169-779

### *Genotype effect and broad-sense heritability ( $H^2$ )*

ANOVA tests showed that genotype had a significant effect on all measured traits (Table 2.3). Both genotype ( $p < 0.0001$ ) and tree height ( $p < 0.0001$ ) had a statistically significant effect on MVD. There was a significant interaction between genotype and tree height ( $p < 0.0001$ ), indicating a departure from what would be expected if MVD was directly attributed simply to tree height. Genotype ( $p < 0.0001$ ) and tree height ( $p < 0.0001$ ) had significant effects on VF, but there was no significant interaction between genotype and tree height ( $p = 0.0597$ ). Genotype also had a significant effect on cMVD ( $p < 0.0001$ ) and cVF ( $p < 0.0001$ ), indicating significant genetic variance for these traits not directly attributable to tree size. An example of genotypes that significantly deviate from expected MVD based on tree height are shown in Figure 2.4. Genotype ( $p < 0.0001$ ), but not tree height ( $p = 0.193$ ), explained significant portions of VGI phenotypic variation. Genotype ( $p < 0.0001$ ), but not tree height ( $p = 0.186$ ), had a significant effect on MVC. Both genotype ( $p < 0.0001$ ) and tree height ( $p < 0.0001$ ) had a significant effect on NF.

Broad-sense heritabilities (repeatabilities) were calculated for all traits and are shown in Table 2.3. All wood and stem traits were moderately heritable. cVF had the lowest broad-sense heritability estimate among all traits ( $H^2 = 0.32$ ) with confidence intervals ranging from 0.22 to 0.41. MVC had the highest broad-sense heritability estimate ( $H^2 = 0.51$ ), with confidence intervals ranging from 0.42 to 0.59. As a reference to the estimation of vessel and stem anatomical trait heritabilities, tree height had a heritability of 0.45 in this study. All anatomical traits showed significant heritabilities suggest that the observed phenotypic variation for each trait has a substantial genetic basis. Together with the continuous phenotypic trait distributions, these results are consistent with the traits under study being quantitative traits influenced by multiple genes.

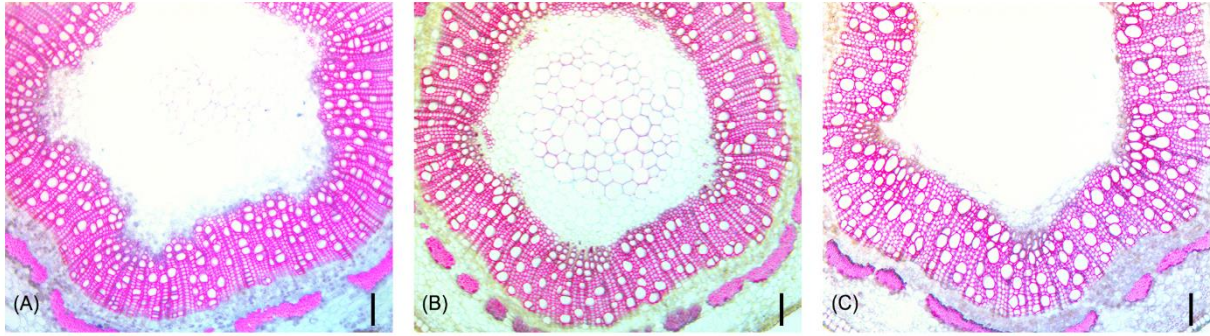


**FIGURE 2.4** | Representative stem cross-sections of 3 hybrid poplar genotypes that did not differ significantly in tree height (~30 cm) but show significant differences in vessel diameters. Genotype XXX\_100\_71 (A) had a mean vessel diameter of 20  $\mu\text{m}$ , XXX\_100\_70 (B) had a mean vessel diameter of 25  $\mu\text{m}$ , and XXX\_100\_93 (C) had a mean vessel diameter of 29  $\mu\text{m}$ . All scale bars are 100 microns.

**Table 2.3** | ANOVA test results and broad-sense heritabilities ( $H^2$ ) of phenotypic traits in a 201 genotype pedigree. P values (P) were obtained from two-way ANOVA tests for each trait, with genotype (Line) and tree height (TH) as independent factors. TH, cMVD and cVF were tested as dependent variables with line as the sole independent factor.  $H^2$  was estimated through intraclass correlation, with 95% confidence intervals for each heritability estimate shown.

Trait	Line (P)	TH (P)	Line*TH (P)	$H^2$	95% CI
TH	< 2e-16	-	-	0.45	$\pm 0.09$
MVD	< 2e-16	< 2e-16	1.16E-06	0.49	$\pm 0.09$
cMVD	< 2e-16	-	-	0.44	$\pm 0.09$
VF	< 2e-16	< 2e-16	0.0597	0.45	$\pm 0.09$
cVF	9.93E-12	-	-	0.32	$\pm 0.09$
VGI	1.38E-15	0.193	0.235	0.47	$\pm 0.09$
MVC	< 2e-16	0.186	0.393	0.51	$\pm 0.09$
NF	< 2e-16	4.70E-07	0.0799	0.5	$\pm 0.08$
BT	5.45E-11	< 2e-16	0.531	0.37	$\pm 0.09$

#### *Pearson's correlation tests between traits*

Correlations among all traits were calculated (Materials and Methods) and are summarized in Figure 2.5. The final tree height at harvest was strongly positively correlated with MVD ( $R=0.76$ ,  $P<0.01$ ) and strongly negatively correlated with VF ( $R= -0.78$ ,  $P<0.001$ ), similar to previous findings (Olson et al. 2014). Even after correcting for tree height, there was a negative

correlation between cMVD and cVF ( $R=-0.61$ ,  $P<0.05$ ), indicating potential interdependence of the size and frequency of vessel elements in wood that is independent of organ size. There was a weaker, but significant positive correlation between tree height and BT ( $R=0.52$ ,  $P<0.01$ ). VGI, MVC, and NF however, were not significantly correlated to tree height or to any other trait, suggesting that these traits might be independently regulated from each other. MVD and VF were strongly negatively correlated ( $R=-0.79$ ,  $P<0.001$ ), as previously reported (Olson et al. 2013; Olson et al., 2014) and suggesting either common regulation or direct influence of one trait on the other. BT was moderately but significantly positively correlated to MVD ( $R=0.48$ ,  $P<0.05$ ), and negatively correlated to VF ( $R=-0.46$ ,  $P<0.01$ ). BT could be considered a proxy for radial growth, and thus correlated with greater MVD and lower VF as expected for faster growing and larger trees.

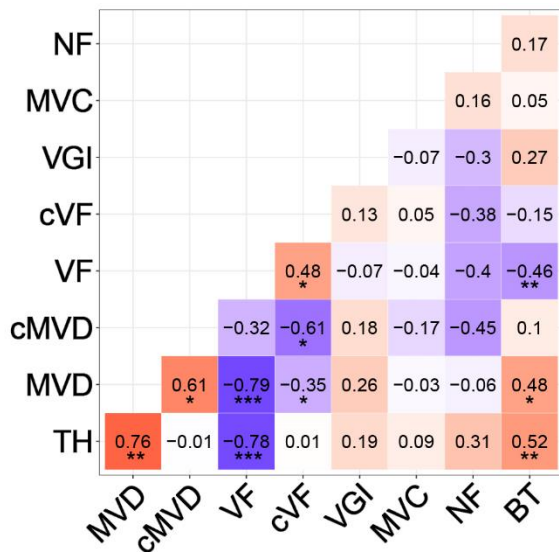


**FIGURE 2.5** | Pearson correlation coefficients between different wood and stem traits. Traits include tree height at harvest (TH), mean vessel diameter (MVD), height-corrected mean vessel diameter (cMVD), vessel frequency (VF), height-corrected vessel frequency (cVF), vessel grouping index (VGI), mean vessel circularity (MVC), non-lumen fraction (NF), and bark thickness (BT). Asterisks indicate significant correlations between traits ( $P\leq 0.05 = *$ ,  $P\leq 0.01 = **$ ,  $P\leq 0.001 = ***$ ).

### Dosage dependent QTL analyses

We used our previously described approach (Bastiaanse et al. 2019; Bastiaanse et al. 2020) for correlating gene dosage at genomic bins with phenotypes, and mapping dosage QTL for all stem and anatomical traits (Materials and Methods). Briefly, genomic bins were established based on indel breakpoints across all lines (genotypes). For each bin within each line, relative dosage

score (RDS) was defined as 0.5 for deletions, 1.5 for insertions, and 1 for normal diploid dosage. Correlations among relative dosage at each bin and each phenotype was then assessed across all lines genome-wide to identify dQTL. Adjacent bins were not independent and were frequently spanned by indels; thus P-values were adjusted for multiple testing based on the effective number of uncorrelated bins (Materials and Methods).

Correlations of dosage at genomic bins and each trait are shown in Figure 2.6 for TH, MVD, cMVD, cVF, VGI, and BT. There were no significant correlations between the remaining traits (VF, MVC and NF) and specific areas of the genome (not shown). Boxplots showing the relationship among dosage and trait values for each dQTL are shown in Figure 2.7. MVD and tree height were both significantly correlated with 3 contiguous genomic bins on chromosome 11, spanning 0.9 Mb. Lines with insertions in these regions did not significantly differ in MVDs or tree heights from lines lacking indels, while lines with deletions had significantly lower values for these traits (Figure 2.7A,B), potentially uncovering a maternal allele with unique function or lack of function. These dQTL explained 4.1% of MVD variance and 3.4% of tree height variance and contained 63 annotated genes. cMVD was significantly correlated to 7 genomic bins in chromosome 9, and 5 genomic bins on chromosome 16 (Figure 2.6). Together, these bins covered a length of 5.6 Mb and accounted for 14.9% of the total phenotypic variance of the trait. The dQTL within chromosome 9 included 380 annotated genes, while the dQTL within chromosome 16 included 370 annotated genes. Lines with deletions spanning either the chromosome 9 (Figure 2.7C) or chromosome 16 dQTL (Figure 2.7D) showed increased cMVDs, while lines with insertions showed the opposite phenotype, as might be expected for a dosage-sensitive negative regulator of growth. cVF was significantly correlated to five genomic bins in chromosome 9 and one genomic bin in chromosome 3 (Figure 2.6). These dQTL jointly covered 2.1 Mb that contained 246

annotated genes and explained 11.2% of the total phenotypic variance of the trait. Vessel frequency was not statistically significantly different in lines carrying deletions in the chromosome 3 cVF dQTL region compared to lines lacking indels (Figure 2.7E), while lines with deletions of the chromosome 9 cVF region did significantly differ from lines lacking indels (Figure 2.7F). Lines carrying insertions covering either the chromosome 3 or 9 cVF dQTL regions exhibited significantly higher cVF values (Figure 2.7E,F). The 5 dQTL bins on chromosome 9 associated with cVF overlapped with the 5 most significant bins correlated to cMVD, consistent with the idea of a common regulator affecting both traits. VGI was significantly correlated to 6 genomic bins spanning 4.2 Mb within chromosome 19 (Figure 2.6) that were not implicated in dQTL for any other trait. Along with the observation that VGI did not show significant correlations with other traits (Figure 2.5), these results suggest that this dQTL may identify a genetic factor specific to this trait. VGI for lines with deletions in the chromosome 19 VGI dQTL region did not statistically differ from lines lacking indels in this region, while lines with insertions had statistically greater VGI (Figure 2.7G). This dQTL explained 4.2% of the trait variance and contained 379 annotated genes. Finally, BT showed significant dQTL bins spanning a large region of Chromosome 1 (Figure 2.7H), which explained 7.2% of the trait variance. Gene dosage in this region was positively correlated with BT, and was not implicated in dQTL for other traits, despite correlations of BT phenotype with tree height, MVD and VF (Figure 2.5). The locations of all detected dQTL ( $P < 0.05$ ) and the percentage of trait variance explained by these regions are shown in Table 2.4.

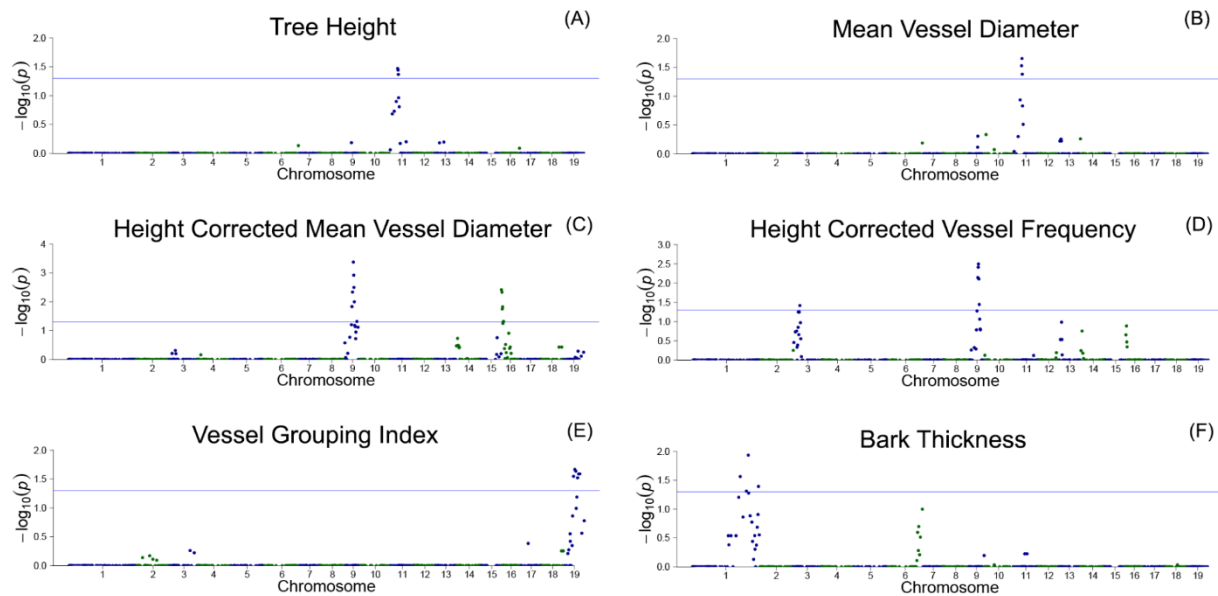


**FIGURE 2.6|** Dosage-dependent quantitative trait loci (dQTL) of traits. Traits with significant dQTL included tree height (A), mean vessel diameter (B), height-corrected mean vessel diameter (C), height-corrected vessel frequency (D), vessel grouping index (E), and bark thickness (F). Genomic bin position is plotted against the  $-\log_{10}$  of the P value for each correlation test. A significance threshold corresponding to a P value of 0.05 is depicted as a blue horizontal line. P values were adjusted using a relaxed Bonferroni correction (See Methods).

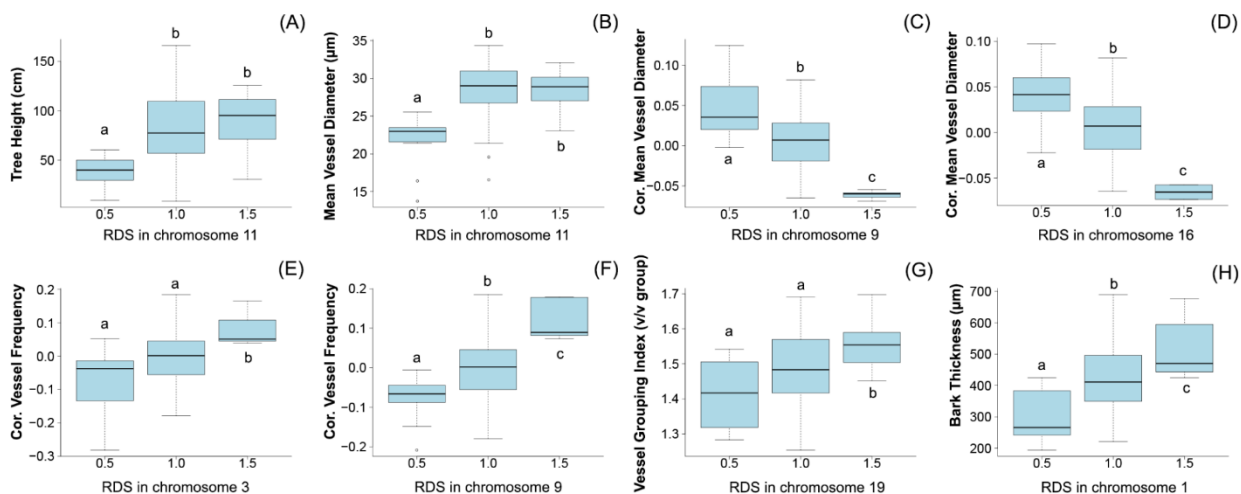


**FIGURE 2.7|** Relationship between trait value and relative dosage scores at genomic bins detected by dQTL analyses. Each boxplot shows all genotypes grouped by relative dosage score (RDS) at the most significant dQTL detected for each trait. Selected dQTLs were located on chromosome 11 for tree height (A) and mean vessel diameter (B), chromosome 9 (C) and chromosome 16 (D) for height-corrected mean vessel diameter, chromosome 3 (E) and chromosome 9 (F) for height-corrected vessel frequency, chromosome 19 for vessel grouping index (G), and chromosome 1 for bark thickness (H). Tukey pairwise comparisons were used to visualize significant differences in mean trait values between the groups; means that share a letter are not significantly different ( $p$ -value  $> 0.05$ ).

**Table 2.4|** Locations of all genomic bins with significant correlations ( $P < 0.05$ ) with stem or wood anatomical traits (dQTL). The adjusted R-squared of the linear regression model fitting the genomic bins was used to estimate the percentage of trait variance explained by dQTL.

<b>Trait</b>	<b>Chr</b>	<b>Location (MBP)</b>	<b>P</b>	<b>Variance explained (%)</b>	
TH	11	6.10-6.65	0.0338	3.4	
TH	11	6.60-6.75	0.0361		
TH	11	6.75-7.00	0.0429		
MVD	11	6.10-6.65	0.0297	4.1	
MVD	11	6.60-6.75	0.0222		
MVD	11	6.75-7.00	0.0416		
cMVD	09	5.40-5.60	0.0147	14.9	
cMVD	09	5.60-6.30	0.0046		
cMVD	09	6.30-6.80	0.0004		
cMVD	09	6.80-6.90	0.0012		
cMVD	09	6.90-7.10	0.0032		
cMVD	09	7.10-7.50	0.0100		
cMVD	09	8.50-9.90	0.0481		
cMVD	16	0-0.50	0.0038		
cMVD	16	0.50-0.80	0.0047		
cMVD	16	0.80-1.00	0.0178		
cMVD	16	1.00-1.30	0.0150	11.2	
cMVD	16	1.40-2.20	0.0478		
cVF	03	4.60-5.30	0.0383		
cVF	09	6.30-6.80	0.0072		
cVF	09	6.80-6.90	0.0039		
cVF	09	6.90-7.10	0.0032		
cVF	09	7.10-7.50	0.0078		
cVF	09	7.50-7.70	0.0358		
VGI	19	7.20-8.10	0.0283		4.2
VGI	19	8.10-9.10	0.0215		
VGI	19	9.10-9.60	0.0230		
VGI	19	10.6-10.8	0.0301		
VGI	19	10.8-12.2	0.0257		
VGI	19	12.2-12.4	0.0256	7.2	
BT	01	34.9-36.8	0.0273		
BT	01	39.1-41.8	0.0488		
BT	01	41.8-41.9	0.0116		
BT	01	49.3-49.6	0.0405		

## DISCUSSION

The regulation of vessel element morphological traits remains poorly understood, despite their key role in determining the hydraulic physiology of plants, and trees in particular. One fundamental feature of vessel elements that makes their study complex is their extreme developmental plasticity. Vessel elements show dramatic morphogenic variation, as seen by contrasting vessel elements with narrow lumens and spiral secondary cell wall thickenings produced during elongative growth, with vessels with wide lumens and extensive secondary cell walls produced during secondary growth. Vessel element diameter and frequency have also been shown to be positively correlated with tree size (Olson et al., 2014; Olson and Rosell, 2013). And vessel development and final morphology are highly responsive to environmental conditions and can be modified to produce morphologies better suited to fast growth under permissive conditions or mitigating the effects of unfavorable conditions such as drought (Rodriguez-Zaccaro and Groover, 2019). A fundamental question is then, to what extent are vessel traits such as final diameter under genetic control, versus non-genetic responses to environmental or physiological conditions?

Here we took advantage of a genomically characterized population of *P. deltooides x nigra* to provide new insights into the genetic control of vessel traits associated with water transport physiology. This study is unusual as it presents trait distributions, correlations, heritabilities, and dQTL for wood anatomical traits directly in a forest tree species within a pedigree carrying indels that create additional, dosage-based variation. All of the anatomical and vessel traits under study here showed significant heritabilities, indicating a significant degree of genetic control. As anticipated, some stem anatomical and vessel traits showed significant correlations with tree height. Specifically, significant positive correlations were found between tree height and MVD

(0.76) and BT (0.52), while VF showed a significant negative correlation (-0.76) with height. One goal was thus to determine the amount of phenotypic variation in the MVD and VF is attributed to genetic variation not associated with height. We analyzed this by removing the effect of tree height in ANOVA to calculate cMVD and cVF that were “corrected” for the effect of tree height. This approach was effective and showed that genetic variation independent of tree height had significant heritabilities for cMVD (0.44) and cVF (0.32). Thus, in addition to scaling by tree height, we observed additional significant variation among genotypes for MVD and VF, suggesting these are traits amenable to genetic manipulation and breeding independent of height or tree size.

Our irradiation hybrid germplasm also enabled analysis genome-wide scans for quantitative trait loci that are both responsive to gene dosage variation and that affect vessel traits. We found significant QTL for tree height, MVD, cMVD, cVF, VGI and BT. Other traits, VF, MVC, and NF did not reveal significant QTL, however. In each case, there are several types of genetic variation that would be transparent to our analysis here. These include genes that are involved in vessel trait regulation but that do not show dosage sensitivity (allelic variation), genes whose variation is masked by genetic redundancy or physiological compensation mechanisms, and genes with smaller effects. Regardless, some interesting conclusions can be reached about the genetic architecture and interplay of the traits under study here. For example, the correlation of tree height with MVD is reflected in a common dQTL on chromosome 11, perhaps representing a common regulator influencing each trait, or else a factor directly influencing one trait with indirect influence on the other. After correcting for tree height, significant genetic variation was still detected for cMVD, as reflected by a unique dQTL on chromosome 9. Interestingly, the cMVD trait was inversely proportional to dosage at this dQTL, predicting that a dosage-sensitive negative regulator of growth may be uncovered at this locus. Additionally, unique dQTL not shared by other

traits were identified for cVF, VGI and BT, suggesting potential trait-specific regulators at these loci. In addition to furthering our basic understanding of how these various wood anatomical traits are related to each other genetically, these results also provide insights into what traits may be independently targeted through breeding approaches. In this regard, identification of dQTL for vessel traits that are not shared by tree height is encouraging for the ability to select or breed for trees through selection on both height growth and vessel traits.

Previous studies point to challenges in genetic dissection of wood anatomy and vessel morphological traits. Quantitative genetic analyses of vessel traits in a *Populus deltoides* mapping population identified a single QTL, with the causative locus *ENLARGED VESSEL ELEMENT (EVE)* encoding a plasma membrane-localized protein affecting potassium uptake and presumably turgor in differentiating vessel elements (Ribeiro et al., 2020). Interestingly the EVE protein is not specific to vessel elements but also found in fibers, but nonetheless is supportive of the notion that potassium plays a key role in vessel expansion. A large genome-wide association study in *P. trichocarpa* identified a single QTL associated with intermediate wood vessel size, encoding a putative double-stranded RNA binding protein (Chhetri et al., 2020). Multi trait associations with vessel area phenotypes were identified for an additional six genes, including genes encoding a leucine-rich repeat containing protein and a serine-threonine protein kinase that might play signaling roles during vessel element differentiation. Interestingly, some vessel traits were correlated with latitude of the accessions included in the study, emphasizing that these adaptive traits are under genetic control and selection. Notably, there is no overlap among the QTL found in our study and any of these previous studies. Along with the modest number of QTL identified in these studies, it seems reasonable to speculate that the high responsiveness of vessel traits to

environmental variation make it especially challenging to measure genetic signal against a background of uncontrolled environmental variation.

Our results clearly demonstrate that vessel traits are under genetic control and that dosage-responsive QTL can be identified. While this is encouraging, we also see the opportunity to increase the power of detection and characterization of the genetic regulation of vessel traits. Notably, future studies could exploit automated phenotyping systems to minimize uncontrolled environmental variation, impose water stress treatments to examine vessel trait responses, and capture physiological data using image-based phenotyping to correlate with those responses. Similarly, high throughput histological phenotyping combined with machine learning-based approaches could provide more insightful and uniform means for analyzing wood anatomy and vessel features. A systems genomics strategy integrating vessel phenotypes, genomic locations in indels, and gene expression data could now be used to both summarize mechanisms and identify candidate genes for functional characterization, as we recently used for dissecting poplar leaf morphology (Bastiaanse et al, 2021).

The magnitude of problems associated with climate change effects on forests is large, with drought and increasing temperatures resulting in water stress that has already resulted in forest declines and associated wildfire in large areas of temperate and boreal forests. While vessel anatomy and hydraulics is only part of the picture, gaining new fundamental insights into how trees respond to environmental variation is a part of the needed information for producing solutions for managing and conserving forests in decades to come.

## **REFERENCES**

Baas, P., Werker, E., and Fahn, A. (1983). Some ecological trends in vessel characters. IAWA Bulletin 4, 141-159.

- Baastianse, H., Zinkgraff, M., Canning, C., Tsai, H., Lieberman, M., Comai, L., Henry, I., and Groover, A. (2019). A comprehensive genomic scan reveals gene dosage balance impacts on quantitative traits in *Populus* trees. *PNAS* 27, 13690-13699.
- Baastianse, H., Henry, I., Tsai, H., Lieberman, M., Canning, C., Comai, L., and Groover, A. (2020). A systems genetics approach to deciphering the effect of dosage variation of leaf morphology in *Populus*. *The Plant Cell* 0, 1-21.
- Barbour, M., and Whitehead, D. (2003). A demonstration of the theoretical prediction that sap velocity is related to wood density in the conifer *Dacrydium cupressinum*. *New Phytologist* 158, 477-488.
- Brodribb, T., and Feild, T. (2000). Stem hydraulic supply is linked to leaf photosynthetic capacity: evidence from New Caledonian and Tasmanian rainforests. *Plant, Cell and Environment* 23, 1381-1388.
- Carlquist, S. (2001). *Comparative Wood Anatomy - Systematic, Ecological, and Evolutionary Aspects of Dicotyledon wood*, 2nd Edn. Berlin: Springer Verlag.
- Carlquist, S. (1984). Vessel grouping of Dicotyledon wood. *Aliso* 10, 505-525.
- Chauhan, L., Raturi, R., and Gupta, S. (1999). Studies of anatomical variations in different clones of *Populus deltoides*. *Journal of Indian Forestry* 125, 526-532.
- Cheverud, J. (2001). A simple correction for multiple comparisons in interval mapping genome scans. *Heredity* 87, 52-58.
- Chhetri, H., Furches, A., Macaya-Sanz, D., Walker, A., Kainer, D., Jones, P., Harmand-Ware, A., Tschaplinski, T., Jacobson, D., Tuskan, G., and DiFazio, S. (2020). Genome-wide association study of wood anatomical and morphological traits in *Populus trichocarpa*. *Frontiers in Plant Science* 11, 545748.

- Cochard, H., Froux, F., Mayr, S., and Coutand, C. (2004). Xylem wall collapse in water-stressed pine needles. *Plant Physiology* 134, 401-408.
- Cutter, B. and Morphey, W. (1978). Effects of potassium on growth and wood anatomy of a populus hybrid. *Wood Fiber Science* 9, 282-288.
- Groover, A. and Jones, A. (1999). Tracheary element differentiation uses a novel mechanisms coordinating programmed cell death and secondary cell wall synthesis. *Plant Physiology* 119, 375-384.
- Hacke, U., Spicer, R., Schreiber, S., and Plavcova, L. (2016). An ecophysiological and developmental perspective on variation in vessel diameter. *Plant Cell and Environment* 40, 831-845.
- Hajek, P., Leuschner, C., Hertel, D., Delzon, S., and Schuldt, B. (2014). Trade-offs between xylem hydraulic properties, wood anatomy and yield in *Populus*. *Tree Physiology* 34, 744-756.
- Henry, I., Zinkgraf, M., Groover, A., and Comai, L. (2015). A system for dosage-based functional genomics in poplar. *The Plant Cell* 27, 2370-2383.
- Kruijer, W., Boer, M., Malosetti, M., Flood, P., Engel, B., Kooke, R., et al. (2015). Marker-based estimation of heritability in immortal populations. *Genetics* 199, 379-398.
- Larson, P. (1994). *The Vascular Cambium: Development and Structure*. Berlin, Heidelberg: Springer-Verlag.
- Lens, F., Sperry, J., Christman, M., Choat, B., Rabaey, D., and Jansen S. (2011). Testing hypotheses that link wood anatomy to cavitation resistance and hydraulic conductivity in the genus *Acer*. *New Phytologist* 90, 709-723.

- Loepfe, L., Martinez-Villalta, J., Pinol, J., and Mencuccini, M. (2007). The relevance of xylem network structure for plant hydraulic efficiency and safety. *Journal of Theoretical Biology* 247, 788-803.
- Olson, M., Tommaso, A., Rosell, J., Petit, G., Crivellaro, A., Isnard, S., Leon-Gomez, C., Alvarado-Cardenas, L., and Castorena, M. (2014). Universal hydraulics of the flowering plants: vessel diameter scales with stem length across angiosperm lineages, habits and climates. *Ecology Letters* 17, 988-997.
- Olson, M., and Rosell, J. (2013). Vessel diameter-stem diameter scaling across woody angiosperms and the ecological causes of xylem vessel diameter variation. *New Phytologist* 197, 1204-1213.
- Pinosio, S., Giacommo, S., Faivre-Rampant, P., Taylor, G., Jorge, V., Le Paslier, M., Zaina, G., Bastien, C., Cattonaro, F., Marroni, F., and Morgante, M. (2016). Characterization of the poplar pen-genome by genome-wide identification of structural variation. *Molecular Biology and Evolution* 33, 2707-2719.
- Ribeiro, C., Conde, D., Balmant, K., Dervinis, C., Johnson, M., McGrath, A. et al. (2020). The uncharacterized gene EVE contributes to vessel element dimensions in *Populus*. *PNAS* 117, 5059-5066.
- Rodriguez-Zaccaro, D., and Groover, A. (2019). Wood and water: How trees modify wood development to cope with drought. *Plants People and Planet* 1, 346-355.
- Schaeffer, M., and Levitt, E. (1956). Concerning Kendall's tau, a nonparametric correlation coefficient. *Psychology Buletin* 53, 338-346.
- Scholz, A., Klepsch, M., Karimi, Z., and Jansen, S. (2013). How to quantify conduits in wood? *Frontiers in Plant Science* 4, 56.

- Searson, M., Thomas, D., Montagu, K., and Conroy, J. (2004). Wood density and anatomy of water limited eucalypts. *Tree Physiology* 24, 1295-1302.
- Sellin, A., Rohej r, A., and Rahi, M. (2008). Distribution of vessel size, vessel density and xylem conducting efficiency within a crown of silver birch (*Betula pendula*). *Trees* 22, 205-216.
- Sperry, J. S., Hacke, U. G., & Pittermann, J. (2006). Size and function in conifer tracheids and angiosperm vessels. *American Journal of Botany* 93, 1490-1500.
- Sugiyama, Y., Nagashima, Y., Wakazaki, M., Sato, M., Toyooka, K., Fukuda, F., and Oda, Y. (2019). A Rho-actin signalling pathway shapes cell wall boundaries in Arabidopsis xylem vessels. *Nature Communications* 10, 468.
- Tyree, M. (1989). Cavitation in trees and the hydraulic sufficiency of woody stems. *Annals of Forest Science* 46, 330-337.
- Tyree, M. T., & Sperry, J. S. (1989). Vulnerability of xylem to cavitation and embolism. *Annual Reviews in Plant Physiology* 40, 19-36.
- Tyree, M., & Zimmermann, M. H. (2002). *Xylem structure and the ascent of sap*. Heidelberg, Berlin: Springer-Verlag.
- Turner, S., Gallois, P., and Brown, D. (2007). Tracheary element differentiation. *Annual Review of Plant Biology* 58, 407-433.
- Turner, S., and Somerville, C. (1997). Collapsed xylem phenotype of Arabidopsis identifies mutants deficient in cellulose deposition in the secondary cell wall. *The Plant Cell* 9, 689-701.
- Venturas, M., Sperry, J., and Hacke, U. (2017). Plant xylem hydraulics: what we understand, current research and future challenges. *Journal of Integrative Plant Biology* 59, 356-389.

- Villar-Salvador, P., Castro-Diez, P., Perez-Rontome, C., and Montserrat-Marti, G. (1997). Stem xylem features in three *Quercus* (Fagaceae) species along a climate gradient in NE Spain. *Trees* 12, 90-96.
- von Arx, G., Kueffer, C., and Fonti, P. (2013) Quantifying plasticity in vessel grouping-added value from the image analysis tool RoXAS. *IAWA J.* 34, 433–445.
- Wagner, K., Ewers, F., and Davis, S. (1998). Tradeoffs between hydraulic efficiency and mechanical strength in the stems of four co-occurring species of chaparral shrubs. *Oecologia* 117, 53-62.
- White, F. M. (2011). *Fluid mechanics*. New York: McGraw-Hill Higher Education.
- Zanne, A., Westoby, M., Falster, D., Ackerly, D., Loarie, L., Arnold, S., et al. (2010). Angiosperm wood structure: global patterns in vessel anatomy and their relation to wood density and potential conductivity. *American Journal of Botany* 97, 207-215.
- Zhang, B., Zhu, W., Diao, S., Wu, X., Lu, K., Ding, C, and Su, X. (2019). The poplar pangenome provides insights into the evolutionary history of the genus. *Nature Communications in Biology* 2, 215.

## **Chapter 3. A systems genetic analysis of vessel traits in poplar**

**F. Daniela Rodriguez-Zaccaro, Meric Lieberman, Isabelle Henry, Andrew Groover**

### **Abstract**

Wood is the water conducting tissue of tree stems. Like most angiosperm trees, poplar wood contains water conducting vessel elements whose functional properties affect water transport and growth rates, as well as susceptibility to cavitation and hydraulic failure during water stress and drought. Here we used a large population of poplar carrying genomically characterized chromosomal insertions and deletions to undertake a systems genomics analysis of vessel traits. In a previous study we measured vessel trait phenotypes within this poplar pedigree and used information about the location of indels in each line to locate regions of the genome harboring dosage quantitative trait loci (dQTL) associated with each vessel trait. Here we used a subset of that population to capture gene expression for wood forming tissues and integrate that with previous trait and dQTL information to describe putative mechanisms and individual candidate genes underlying traits.

### **INTRODUCTION**

The vascular cambium is a secondary meristem composed of ray and fusiform initials that give rise to both wood and inner bark tissues. In the developing wood of the model tree genus *Populus*, ray cambial initials differentiate into parenchyma ray cells, which store and transport starches, sugars, proteins, and fats (Sauter and Neumann 1994). Fusiform initials, which are elongated along the axis of the stem, give rise to the wood axial cell system consisting of fiber cells and vessel elements. Fiber cells provide mechanical support to sustain tree growth and are characterized by their libriform shape, thick lignified secondary cell walls and often by programmed cell death at functional maturity (Esau 1977). Vessel elements, the water conducting cells in wood, develop through rapid and dramatic radial cell expansion involving

both symplastic and intrusive growth (Wilczek et al. 2011). Dead at functional maturity, highly lignified individual vessel elements connect end-to-end to form longer conduits called vessels, allowing for the upward flow of water under tension. The dimensions and distribution of vessels in wood help determine tissue hydraulic and mechanical function.

In particular, the width, number, and clustering of vessels affect water transport efficiency and vulnerability to hydraulic failure under stressful conditions. Small variations in vessel diameter can have a large impact on water transport efficiency, with wider vessels allowing for greater volumetric flow rates (Baas et al. 2004; Venturas et al. 2017). Vessels that are in direct contact share pit pairs through which water can flow laterally. Consequently, increased vessel clustering (measured through vessel grouping indices) allows for greater vessel network interconnectivity and greater stem-specific hydraulic conductivities (Lens et al. 2011; Hajek et al. 2014). The ability of trees to transport water efficiently is tied to their photosynthetic capacity and growth rate (Brodribb and Field, 2000; Tyree et al. 1998). Greater water transport efficiency, however, can lead to increased vulnerability to hydraulic failure through freeze-thaw and drought-induced cavitation (Feng et al. 2015; Gleason et al. 2016). The number of vessels within a cross-sectional area of wood (termed vessel frequency) is often strongly negatively correlated to vessel diameter (Sperry et al. 2008). Greater vessel frequencies can buffer trees from hydraulic failure by decreasing the impact of cavitation of a single vessel on the overall conductivity of a stem (Baas et al. 1983; Ewers et al. 2007). Some studies have linked greater vessel grouping to increased vulnerability to cavitation (Scholz et al. 2013; Guet et al. 2015), possibly due to an increased probability of embolism spread throughout a more interconnected xylem network (Loepfe et al. 2007). However, greater vessel grouping indices have also been related to decreased vulnerability to cavitation (Lens et al. 2010; Smith et al. 2014), likely due to

the presence of alternate sap pathways that can bypass embolism blockage (Carlquist 1984). The cross-sectional shape of vessels (termed vessel circularity) can also affect transport efficiency, as increasing deviations from perfect circularity can significantly decrease the volumetric flow rate of water through a conduit (Zhao et al. 2019). Vessel width and frequency scale with tree height and diameter; taller and thicker trees have wider and less numerous vessels than shorter and thinner trees at the same sampling height. Accordingly, taller trees, while more conductive, are more vulnerable to drought and freeze-thaw cycles (Olson et al. 2018).

Auxin transport and biosynthesis disturbances have been shown to alter vessel width, frequency and grouping resulting from changes in cell differentiation patterns (Tuominen et al. 1997; Junghans et al. 2004; Johnson et al. 2018). Stressful environmental conditions including drought, extreme heat and high salinity have also been known to reduce cambial activity and result in wood with smaller and more numerous vessels (Arend and Fromm 2007; Fonti et al. 2013). Recent evidence points towards the significant role of abscisic acid in the mediation of stress response signals in poplar wood (Yu et al. 2021). Recent application of genomic approaches has provided some insights into specific regulatory pathways, including identification of AREB1 and NAC transcription factors affecting vessel size in response to ABA (Li et al, 2019; Yu et al. 2019). However, a general limitation of genetic analysis of vessel traits has been the lack of suitable germplasm for robust functional genomic dissection of traits. We previously established a poplar population for functional genomics based on gene dosage. A large population of *Populus deltoides* x *P. nigra* hybrids was created, using gamma irradiation of pollen to create chromosomal deletions and additions in the resulting F1 progeny. The full genome of each F1 line was sequenced to precisely locate the chromosomal positions of deletions and insertions. Genetic analyses have been used in this population to locate regions of

the poplar genome that affect phenotype trait values when relative gene dosage is modulated (Bastiaanse et al. 2020). Using this approach for vessel traits, our previous study demonstrated significant heritabilities as well as dosage quantitative trait loci (dQTL) affecting multiple vessel traits (see “Chapter 2”). The traits examined in both our previous and present study include mean vessel diameter (MVD), vessel frequency (VF), vessel grouping index (VGI), mean vessel circularity (MVC) and non-lumen fraction (NF). Tree height at harvest, although not a wood anatomical trait, was included as it is highly correlated to vessel traits. A list of all examined traits can be found in Table 3.1.

Here we extend our previous study by producing gene expression data from wood forming tissues from genotypes sampled from the previous dQTL study. We use a systems genetics approach similar to that recently described for this same poplar population (Bastiaanse et al. 2021). Our aim is to provide overviews of putative mechanisms, gene modules, and individual candidate genes underlying vessel traits through systems genetic analyses integrating gene expression, dQTL, and phenotype data.

## **MATERIALS AND METHODS**

### **Plant Materials**

A subset of 33 poplar hybrid genotypes was selected from a larger group of 201 lines included in a previous study (see “Chapter 2”). These lines belong to a pedigree produced by crossing two female *P. deltoides* with gamma-irradiated pollen of a male *P. nigra*. The resulting F1 hybrids were completely sequenced using Illumina short reads and analyzed to detect insertions and deletions (indel mutations) using relative sequencing read coverage values (Henry et al. 2015). These hybrids were found to have mostly paternally derived large-scale indel mutations throughout their genomes. The full pedigree consists of nearly 800 replicated lines maintained at the US Forest

Service Institute of Forest Genetics (IFG) in Placerville, CA. All 201 lines included in the previous study were propagated as multiple clonal replicates through stem cuttings from the field during the spring of 2018. Cuttings were planted in individual 2.83-L pots inside a greenhouse at the IFG and were allowed to become established during a 2-month growth period. Three clonal replicates per line were then selected to include in a randomized complete block design across three benches. Trees were watered using a drip irrigation system and kept at a near constant temperature of 23°C. All trees were harvested for woody stem segments and coppiced in the late fall of 2018. These stems were processed to obtain stem and wood anatomical trait data used in our previous study (see “Chapter 2, Materials and Methods”). A summary of all examined traits can be found in Table 3.1. Trees were then allowed to regrow a main stem from the original cutting during the spring and early summer of 2019 under the same greenhouse conditions established in the previous growth season.

### **RNA-seq**

The stems of 33 genotypes (2-3 replicates per genotype) were harvested in July of 2019. Genotypes were selected based on results from a previous wood phenotype screen and dQTL analyses (see “Chapter 2, Results”). Specifically, 11 genotypes were selected due to the presence of indel mutations spanning contiguous dQTL regions associated with both cMVD and cVF in chromosome 9. Six more genotypes were selected based on the presence of indels spanning adjoining dQTL regions associated to cMVD in chromosome 16. Nine genotypes were selected for their extreme cMVD and cVF phenotypes, regardless of indel mutation locations. Lastly, 7 genotypes were randomly selected as non-lesion controls. The final height before harvest was obtained for each of these trees, measuring from the point of emergence of the current year stem to the shoot apex. Stems were then harvested 5 to 10 cm from the point of emergence from the

original cutting. Wood forming tissues were collected from harvested stems by gently peeling off the bark and scraping the uncovered tissue with double-edged razorblades. The phloem and vascular cambium were removed with the bark, while the wood forming tissues remained on the debarked stem before collecting (Lin et al., 2014). Tissues from each stem were placed in individual aluminum foil envelopes and quickly submerged in liquid nitrogen before being stored at -80°C.

Frozen tissue samples were ground to a fine powder using ceramic mortar and pestles containing liquid nitrogen. Total RNA was extracted from each sample and then purified through a protocol adapted from the TRIzol reagent user guide (Life Technologies) and the RNeasy handbook (QIAGEN). RNA samples were assessed for quantity and quality using a Qubit fluorometer (Invitrogen) and a Bioanalyzer (Agilent Technologies), respectively. A 3' Tag-Seq mRNA library preparation kit (Lexogen QuantSeq) was used to construct cDNA libraries for each sample. Ninety-one libraries were multiplexed across three flow cell lanes of an Illumina HiSeq 4000 run generating 90 bp single end reads.

### **Preprocessing and Read Counts Table Generation**

FASTQ files were processed by removing unique molecular identifier (UMI) barcodes from sequences and adding them to sequence read names using the “extract” command in the “UMI-Tools” (v1.1.2) Python package (Smith et al., 2017). Files were then demultiplexed using 6 nucleotide long single indices through the Python tool “Allprep” (scripts available at: <https://github.com/Comai-Lab/allprep>). Reads were mapped to the *Populus trichocarpa* reference genome (v3.1) using STAR software (v2.6) (Dobin and Gingeras, 2015). The produced SAM files were then sorted using the package “SAMtools” (Li et al., 2009) and deduplicated to correct for amplification bias using UMIs in the sequence read names through the “dedup”

command in “UMI-Tools” (Smith et al., 2017). The “htseq-count” Python script (from the HTSeq package v0.13.5) was used to calculate the number of read counts mapped to each gene in the deduplicated SAM files (Anders et al., 2015). Normalization factors were calculated using the “calcNormFactors” function (TMM method) in the R package “edgeR” (v2.7) to correct for raw library sizes (Robinson et al., 2010). Genes with a maximum expression of less than 10 counts across all samples were filtered out as low-expressed or unexpressed genes. The “voom” function in the R package “limma” was used to transform counts into log<sub>2</sub> CPM by implementing the previously calculated normalization factors. This function was also used to obtain weights to correct for differences in expression variance across genes (Law et al., 2014; Liu et al., 2015). A linear model using weighted least squares for each gene was then fitted using the “lmFit” function in “limma” (Ritchie et al., 2015). Model coefficients were extracted to produce a final gene expression dataset.

### **Pearson Correlations Among Traits**

Trait data obtained from trees harvested in 2018 for our previous study (see “Chapter 2”) were used to find correlations between all trait combinations within the 33-genotype subset selected for our current project. Pearson correlations and their corresponding P values were obtained using base R (v4.1.0), with significant correlations declared for P values of less than 0.05. Trait data include tree height at harvest (TH), mean vessel diameter (MVD), height-corrected mean vessel diameter (cMVD), vessel frequency (VF), height-corrected vessel frequency (cVF), vessel grouping index (VGI), mean vessel circularity (MVC), non-lumen fraction (NF), and bark thickness (BT). A description of all examined traits can be found in Table 3.1.

## Differential Expression and GO Enrichment Analysis

Stem and wood anatomical data previously collected for Chapter 2 analyses were used to identify the lines with the highest and lowest values for each trait within the 33-genotype subset sampled for this study. Together, the 8 lines with the highest trait values were compared to the 8 lines with the lowest trait values (16 lines for each trait, 2-3 replicates per line) in a differential expression analysis. Lines with high and low TH, VF, MVD, cMVD, cVF, VGI, MVC, NF and BT were contrasted. Using the previously fitted linear model, the “makeContrasts” and “contrasts.fit” functions in “limma” were used to calculate log fold changes in expression between high and low value trait groups. Differentially expressed genes were then identified using the “eBayes” function, which calculates moderated t-statistics from which P values can be obtained. P values were adjusted for multiple testing through the Benjamini-Hochberg false discovery rate correction method (Ritchie et al., 2015). Differentially expressed genes (adjusted  $P < 0.05$ ) were classified into two different sets: genes that were more highly expressed in lines with greater trait values and genes that were more highly expressed in lines with lower trait values.

The functional characterization of these gene sets was assessed through a GO enrichment analysis performed with *Arabidopsis thaliana* best BLAST hits of *P. trichocarpa* genes. *Populus* GO annotations are incomplete within many important biological categories and were consequently not used. The “atGOanalysis” function in the “treeGO” R package was used to run hypergeometric tests to determine what GO terms within the biological process ontology (BP) are significantly overrepresented in each gene set ( $P < 0.05$ ). Scripts are available at: <https://github.com/mzinkgraf/treeGO>. Annotations for *P. trichocarpa* (v3.1) including *A. thaliana* best BLAST hits were downloaded from Phytozome

(<http://www.phytozome.net/poplar.php>). The Arabidopsis GO genome annotations were downloaded from TAIR (<https://www.arabidopsis.org/download/>).

### **Weighted Gene Correlation Network Analysis**

To identify candidate genes related to stem and wood anatomical traits, gene coexpression networks were constructed using the weighted gene correlation network analysis R package (WGCNA, v1.70-3; Langfelder and Horvath, 2008). All 33 sampled genotypes were included in the analysis, with 2-3 replicates per genotype. Twenty-six of these lines had large-scale indels throughout their genome, including 17 selected for the presence of indels in specific areas of chromosomes 9 and 16. A previous WGCNA study involving 164 dosage mutant lines from this pedigree found that half of all gene modules were localized within individual chromosomes, suggesting the creation of artificial indel-induced modules (Bastiaanse et al., 2021). To account for this effect, TMM and variance normalized log<sub>2</sub> CPM gene expression data (described above) were processed into an indel-normalized data set. In indel lines, the expression of genes located within indel regions was replaced with the average expression of these genes in all other lines, eliminating the cis-effects of indels on expression (Bastiaanse et al., 2021). However, this approach can potentially compromise the ability to detect real biological correlations. Gene network construction and downstream analyses were thus run using both indel-normalized and non indel-normalized datasets to determine if normalization is necessary.

Coexpression networks were built by obtaining Pearson's correlation coefficients for every expressed gene pair combination across all samples. Weighted adjacencies were then calculated through a transformation of coefficients involving a soft thresholding power of 12. This soft thresholding power was chosen for both networks to produce an 82% model fit to a scale-free topology. Topological overlap matrices (TOM) produced from the adjacencies were

then used to calculate measures of topological overlap dissimilarities. Color-labeled modules of highly coexpressed genes were identified through the hierarchical clustering of these dissimilarities using a dynamic tree cutting height of 0.99. Eigengenes, or the weighted average of the expression of all genes within a module, were calculated and used to merge modules showing correlations of 0.75 or higher (Figure 3.4). WGCNA scripts are available at: <https://horvath.genetics.ucla.edu/html/CoexpressionNetwork/Rpackages/WGCNA/Tutorials/>. Module stability was assessed for both networks through repeated resampling of 63% of all libraries, producing 49 coexpression network iterations (Figure 3.5) Module stability scripts are available at: <https://horvath.genetics.ucla.edu/html/CoexpressionNetwork/FastCalculations/RExamples/resamplingStudy-large.pdf>. The physical locations of all coexpression modules across the Poplar genome were visualized using the R package “chromoMap” v0.3.1 (Anand and Rodriguez Lopez, 2020).

Stem and wood anatomical traits were tested for significant Pearson correlations with module eigengene values ( $P < 0.05$ ). Specifically, trait data obtained from trees harvested in 2018 for our previous study (see “Chapter 2”) were used to test for correlations with the gene expression of trees harvested in 2019 belonging to the same 33 genotypes. Trait data include tree height at harvest (TH), mean vessel diameter (MVD), height-corrected mean vessel diameter (cMVD), vessel frequency (VF), height-corrected vessel frequency (cVF), vessel grouping index (VGI), mean vessel circularity (MVC), non-lumen fraction (NF), and bark thickness (BT). Two TH datasets were included in the analysis, TH collected from 2018 plants, and TH collected from the 2019 plants harvested for RNA. Gene coexpression modules were examined for functional enrichment through a GO enrichment analysis using *Arabidopsis thaliana* best BLAST hits of *P. trichocarpa* genes. Populus GO terms were not used due to limited annotations within many

relevant biological categories. The “treeGO” R package was used to perform hypergeometric tests to identify GO terms that are significantly overrepresented ( $P < 0.05$ ) within each module. See the “Differential Expression and GO Enrichment Analysis” section above for links to publicly available scripts. Gene significance (GS) vs. module membership (MM) plots were obtained for biologically interesting modules. GS is the correlation between the expression of a particular gene and a trait of interest, while MM is the correlation between the expression of a gene and the eigengene value of the module.

### **Dosage Sensitivity Analysis**

We tested for the presence of dosage sensitive genes within two previously identified cMVD and cVF dQTL regions. One dQTL region is located on chromosome 9 (from 6.3 to 6.8 Mbp) and was highly correlated to both cMVD and cVF. The other dQTL region was located on chromosome 16 (from 0 to 0.5 Mbp) and was highly correlated to cMVD. Genotypes were grouped into relative dosage score (RDS) categories determined by the presence of insertions or deletions at each dQTL region. Lines with deletions have an RDS of 0.5, lines without indels have an RDS of 1.0 and lines with insertions have an RDS of 1.5. All genes expressed within a dQTL region were then tested for significant differences in gene expression across RDS categories through ANOVAs ( $P < 0.05$ ). Three lines with deletions, 4 lines without lesions and 2 lines with insertions covering the chromosome 9 region were included in an ANOVA. Four lines with deletions, 4 lines without lesions and 2 lines with insertions spanning the chromosome 16 region were included in a separate ANOVA. The 4 non-lesion lines were randomly selected. Each analysis was followed by a Tukey’s honest significance post hoc test. Analyses were performed using base R (v4.1.0).

## RESULTS

Here we produced gene expression data for wood forming tissues from 33 previously identified genotypes of our poplar indel population selected based on vessel trait phenotypes and associated dQTL. Genotypes in the study were selected based on results from our previous dQTL analyses (see “Chapter 2, Results”). Specifically, 11 genotypes were selected due to the presence of indel mutations spanning contiguous dQTL regions associated with both cMVD and cVF in chromosome 9. Six more genotypes were selected based on the presence of indels spanning adjoining dQTL regions associated to cMVD in chromosome 16. Nine genotypes were selected for their extreme cMVD and cVF phenotypes, regardless of indel mutation locations. Lastly, 7 genotypes were randomly selected as non-lesion controls. Wood forming tissues were harvested from clonal replicates of each line grown under uniform greenhouse conditions, and total RNA isolated and used to generate RNAseq libraries for Illumina sequencing (Materials and Methods). After sequencing, resulting reads were filtered, mapped, and used to generate read counts for each expressed gene within each sample (Materials and Methods).

We implemented three different approaches to identify broad biological pathways and candidate genes related to wood anatomical traits in poplar. All examined traits are described in Table 3.1. First, we conducted differential expression analyses contrasting the 8 lines with the highest and 8 lines with lowest values for each trait. Sets of differentially expressed genes were then examined for functional enrichment through GO enrichment analyses. A second approach involved constructing weighted networks of coexpressed genes (through WGCNA) including all 33 sampled genotypes. This approach involved testing for correlations between traits and gene modules and testing for gene module enrichment of biological process GO terms. Lastly, a dosage sensitivity analysis was performed on genes within previously identified cVF and cMVD dosage QTL with the purpose of finding candidate genes related to these traits.

## Pearson’s Correlation Tests Between Traits

Pearson correlation coefficients were calculated for all stem and wood anatomical trait combinations across 33 hybrid poplar genotypes (Figure 3.1). Trait data used in these analyses were obtained from trees harvested in 2018 for our previous study (see “Chapter 2”), with a total of 10 trait combinations producing statistically significant correlations ( $P < 0.05$ ). As expected, TH was positively correlated to both MVD ( $R = 0.66$ ,  $P < 0.01$ ) and BT ( $R = 0.70$ ,  $P < 0.001$ ), and strongly negatively correlated to VF ( $R = -0.85$ ,  $P < 0.001$ ). Previous studies have shown that MVD, VF and BT predictably scale with tree height (Olson et al., 2014; Cellini et al., 2012). Vessel frequency in turn showed a strong negative correlation to MVD ( $R = -0.82$ ,  $P < 0.001$ ) and BT ( $R = -0.67$ ,  $P < 0.001$ ). Height corrected MVD (cMVD) and cVF were also negatively related ( $R = -0.67$ ,  $P < 0.05$ ). VGI, MVC and NF showed no significant correlations to any trait. These results indicate that the 33 lines selected for the current study show the expected trait-trait relationships seen in the full 201-line dataset examined in our previous study. These trait correlations were obtained to provide context for the design and interpretation of gene expression analyses that involve phenotypic data in our current study.

**TABLE 3.1** | Stem and wood anatomical traits examined across 33 hybrid poplar lines (*Populus deltoides* × *nigra*).

Trait	Abbr.	Units
Tree height	TH	cm
Vessel frequency	VF	vessels/mm <sup>2</sup> xylem
Height-corrected VF	cVF	unitless
Mean vessel diameter	MVD	µm
Height-corrected mean vessel diameter	cMVD	unitless
Mean vessel circularity	MVC	unitless
Vessel grouping index	VGI	vessels/vessel group
Non-lumen fraction	NF	unitless
Bark thickness	BT	µm

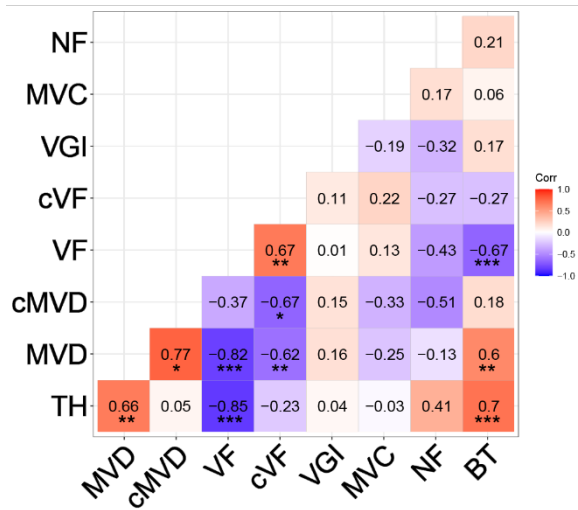


**FIGURE 3.1** Pearson correlation coefficients between different wood and stem traits across 33 hybrid poplar genotypes. Traits include tree height at harvest (TH), mean vessel diameter (MVD), height-corrected mean vessel diameter (cMVD), vessel frequency (VF), height-corrected vessel frequency (cVF), vessel grouping index (VGI), mean vessel circularity (MVC), non-lumen fraction (NF), and bark thickness (BT). Asterisks indicate significant correlations between traits (\* $p \leq 0.05$ ; \*\* $p \leq 0.01$ ; \*\*\* $p \leq 0.001$ ).

### Differential Expression and GO Enrichment Analyses

Mapped read counts from RNAseq data were used in differential expression and subsequent GO enrichment analyses to find broad biological pathways associated with stem and wood anatomical traits (Materials and Methods). The lines with the highest and lowest trait values within the 33-genotype subset sampled for this study were chosen for contrast based on data previously collected for Chapter 2 analyses. Specifically, the 8 lines with the highest trait values and the 8 lines with the lowest trait values were contrasted through differential expression analyses run with the R package “limma”. Examined traits are described in Table 3.1. Out of the 42,950 genes annotated in the *P. trichocarpa* genome (v3.1) 16,100 were found to be expressed in wood forming tissues. Differentially expressed genes were found across high and low TH, VF, MVD, MVC, NF and BT lines ( $P \text{ adj.} < 0.05$ ; Table 3.2). High and low TH lines showed the largest number of differentially expressed genes across all examined traits (8,945 genes). Fifty-two percent of these genes were upregulated in lines with greater THs (4,660 genes, termed high TH set), and 48% were upregulated in lines with lower THs (4,285 genes, termed low TH set).

Like TH, all groups of differentially expressed genes were divided into two sets: a set of genes upregulated in high trait value lines and a set of genes upregulated in low trait value lines (Table 3.2). High and low VF lines showed the second largest number of differentially expressed genes across examined traits (5,075 genes), followed by MVD (3,562 genes). High and low BT lines showed a much smaller number of differentially expressed genes (Table 3.2). TH, VF, MVD and BT were all significantly correlated (Figure 3.1), and thus differential expression analyses for these traits involved similar, but not identical, top and bottom lines. MVD and VF shared the largest number of lines in their analyses, with 11 out of 16 lines in common. VF and BT shared the lowest number of lines, with 6 out of 16 lines in common. Inclusion of shared top and bottom lines resulted in similar sets of differentially expressed genes across these four traits.

Functional enrichment analyses found significant overrepresentation of 360 biological process GO terms within the high TH set and 358 within the low TH set ( $P < 0.05$ ). High and low VF and MVD sets were highly enriched in many of the same top annotations found in the TH sets. The low TH, high VF and low MVD gene sets were the most significantly enriched in stress response, transcription regulation and hormone related terms, among others (Figure 3.2). Stress response related genes were the most numerous and significantly overrepresented within these gene sets. Response to cold, water deprivation and oxidative stress were some of the most significant specific stress response terms. Transcription regulation related genes were the second most numerous and overrepresented in the three sets. In addition, the three sets were highly enriched in hormone related genes and included abscisic acid, jasmonic acid and cytokinin response annotations. Genes related to abscisic acid response represented the majority of genes with specific hormone related terms. The high TH, low VF and high MVD sets were the most significantly enriched for genes associated with Golgi, vesicle, cell wall, cell growth and xylem

related terms, among others (Figure 3.2). Cell wall biogenesis and organization related terms were the most significantly overrepresented in these three sets. Within this category, hemicellulose and xylan related annotations were the most significantly overrepresented, followed by pectin and cellulose. In addition, these sets were highly enriched in vesicle mediated transport genes, with most of these genes involved specifically in Golgi vesicle transport. Genes related to Golgi apparatus organization were overrepresented as well. High TH, low VF and high MVD sets were also highly enriched in cell growth and xylem related terms. Specific multidimensional cell growth and xylem vessel member cell differentiation terms were overrepresented within these categories, respectively. Although BT was significantly correlated to TH, VF and MVD (Figure 3.1), the high and low BT gene sets did not show all of the same GO enrichment patterns present in the previous sets. The high BT set was the most highly enriched in cell differentiation, xylem and phloem histogenesis and xylem development related terms. Cell wall, Golgi organization and cell growth related terms were also overrepresented in the set, but to a lesser degree than in the TH, VF and MVD sets. The low BT was the most highly enriched in transcription regulation related terms. Auxin, abscisic acid, jasmonic acid and cytokinin related genes were also overrepresented (Figure 3.2).

There were no differentially expressed genes across high and low cVF, cMVD and VGI lines ( $P_{adj} > 0.05$ ). In contrast, 62 genes were differentially expressed between high and low MVC genotypes, with 48 of these genes showing a greater expression in high MVC lines (high MVC set) and 14 showing a greater expression in low MVC lines (low MVC set). However, a GO enrichment analysis found no significantly overrepresented terms in either gene set ( $P_{adj} > 0.05$ ). Lastly, 761 genes were differentially expressed between high and low NF lines, with 61% upregulated in high NF lines (466 genes, high NF set) and 39% upregulated in low NF lines

(295 genes, termed low NF set). Only the high NF set showed functional enrichment, with significant overrepresentation of Golgi vesicle transport and polysaccharide biosynthetic process related terms. Although not statistically significant, NF showed moderate correlations to TH and VF (Figure 3.2), suggesting similar sets of differentially expressed genes. Hypergeometric tests confirmed this by showing significant overrepresentation of VF set genes in NF gene sets ( $P < 0.00001$ ).

**TABLE 3.2** | Differential expression analysis results between the 8 lines with the highest values and the 8 lines with the lowest values for each trait across 33 hybrid poplar genotypes. Genes are differentially expressed across contrasted groups when the  $P_{adj.} < 0.05$ .

<b>Contrasted Groups</b>	<b>Number of DE genes</b>	<b>Number of genes upregulated in each group</b>
High TH lines	8945	4660
Low TH lines		4285
High VF lines	5079	2359
Low VF lines		2720
High cVF lines	0	-
Low cVF lines		-
High MVD lines	3562	1721
Low MVD lines		1841
High cMVD lines	0	-
Low cMVD lines		-
High MVC lines	62	48
Low MVC lines		14
High VGI lines	0	-
Low VGI lines		-
High NF lines	761	466
Low NF lines		295
High BT lines	602	364
Low BT lines		238

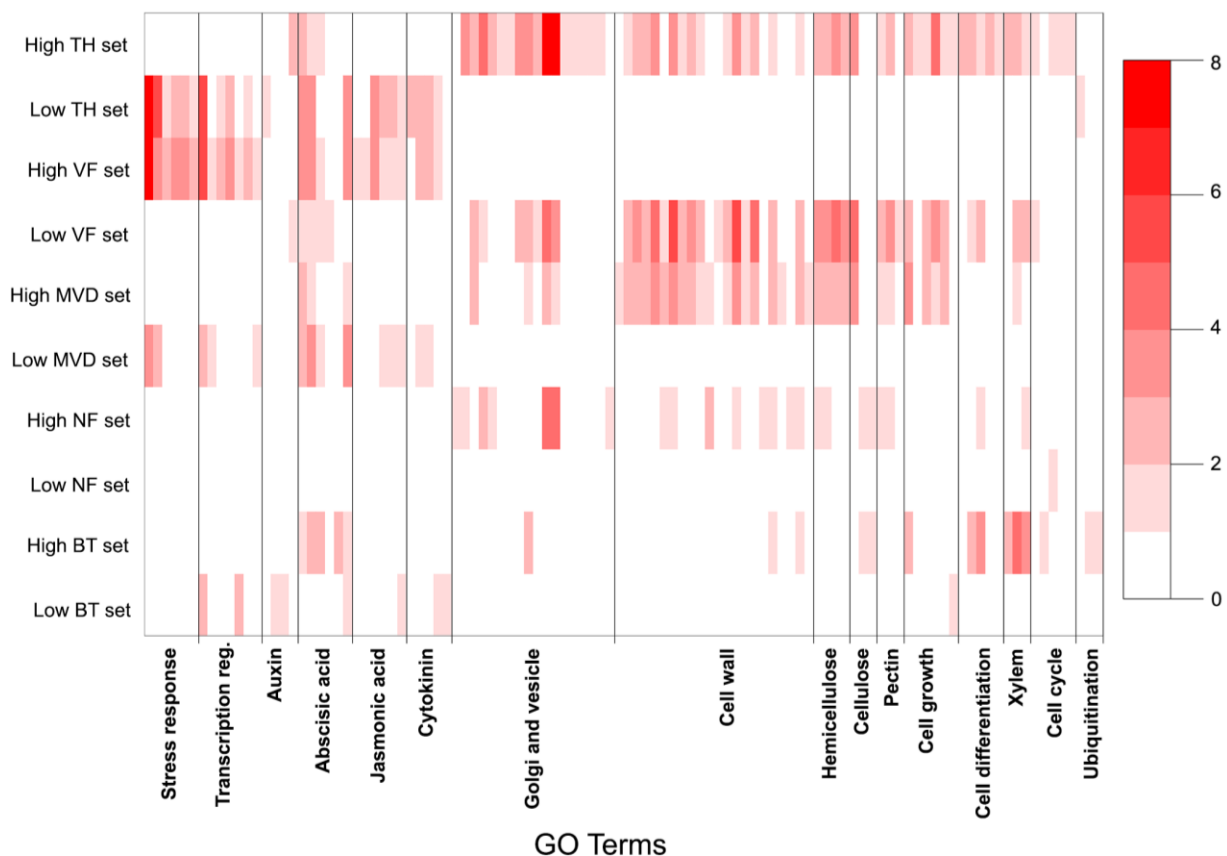


**FIGURE 3.2** | GO enrichment analysis heatmap showing significant overrepresentation ( $P < 0.05$ ) of GO terms (BP) within gene sets obtained from differential expression analyses between lines with high and low values for tree height at harvest (TH), vessel frequency (VF), mean vessel diameter (MVD), non-lumen fraction (NF) and bark thickness (BT). High trait sets contain genes that were upregulated in lines with high trait values, while low trait sets contain genes that were upregulated in lines with low trait values. The color bars show the  $-\log_{10}$  of P values generated from hypergeometric tests.

## Weighted Gene Correlation Network Analysis

### *Network Construction and Characterization*

Gene coexpression networks were constructed to identify broad biological pathways and candidate genes related to stem and wood anatomical traits using Weighted Gene Correlation Network Analysis (WGCNA) (Langfelder and Horvath, 2008). All 33 sampled lines were included in the analysis, with 2-3 replicates per line. Twenty-six of these genotypes have large-scale indel mutations that could potentially induce the production of artificial modules (Baastianse et al., 2020). Consequently, network construction and subsequent analyses involved

both a non indel-normalized and an indel-normalized gene expression dataset (Materials and Methods). Nineteen color-labeled modules consisting of highly coexpressed genes were identified within each network (Figure 3.3). Module sizes were similar across non-normalized and indel normalized networks and ranged from 46 to 4711 genes per module. The two largest gene sets within both networks were the turquoise and blue modules (Table 3.3). Modules that share the same color label across networks are not necessarily equivalent. However, the turquoise and the blue modules appeared to be analogous across networks based on large numbers of shared genes. The turquoise module produced from the indel-normalized dataset shared 95% of its genes with the non indel-normalized turquoise module. Likewise, the blue module generated from the indel-normalized dataset shared 85% of its genes with its non indel-normalized counterpart. Hypergeometric tests confirmed the highly significant overrepresentation of genes of the non-normalized modules in each normalized module ( $P < 0.00001$ ).

A module stability analysis showed that individual modules within each network persist across many network construction subsampling iterations, suggesting that these modules are robust. Some modules were more stable than others, with the turquoise and blue modules showing the greatest stability within both networks (Figure 3.4). The broad physical locations of modules throughout the Poplar genome were visualized using the ChromoMap R package (Anand and Rodriguez Lopez, 2020). Non indel-normalized dataset modules were widespread throughout the genome, with genes from every module represented across most chromosomes (Figure 3.5, 3.6). The light-yellow and orange modules were the least widely distributed, with most of their genes located on chromosome 9 (Figure 3.6). The high number of lines with large-scale indel mutations on this chromosome suggests that these modules could be indel-induced.

However, regions in chromosome 9 with high indel coverage depth also included many genes that were assigned to other modules. For example, a 0.5 Mbp genomic bin with a high indel coverage depth contained 41 expressed genes, with only 13 belonging to the light-yellow module (Figure 3.7). In contrast, no modules were predominantly located on chromosome 16, even with the inclusion of many lines with indels in this chromosome (Figure 3.5, 3.6). There was a heterogenous distribution of modules in high indel coverage depth regions in chromosome 16, as shown in a 0.5 Mbp bin located on said chromosome (Figure 3.8). Modules produced from the indel-normalized dataset were also widely distributed across the Poplar genome, with genes from each module found across nearly every chromosome (Figure 3.9). No individual module was primarily located in any single chromosome.

Non indel normalized		Indel normalized	
Module*	Gene number	Module*	Gene number
Turquoise	4711	Turquoise	4289
Blue	4630	Blue	4267
Brown	2033	Lightyellow	2088
Tan	1534	Green	1488
Darkgreen	947	Lightcyan	1156
Black	904	Greenyellow	997
Pink	467	Grey60	605
Purple	358	Darkorange	542
Lightgreen	311	Lightgreen	534
Greenyellow	286	Tan	239
Darkturquoise	285	Darkred	239
Cyan	175	Salmon	193
Lightcyan	147	Cyan	188
Grey60	144	Midnightblue	182
Lightyellow	137	Darkgreen	123
Darkred	126	Darkgrey	97
Darkgrey	80	White	79
Orange	69	Steelblue	54
Darkorange	60	Paleturquoise	46

**Table 3.3|** List of WGCNA gene modules obtained from a non indel and an indel normalized dataset. Each dataset produced 19 modules. *\*Modules with the same color labels are not necessarily equivalent.*

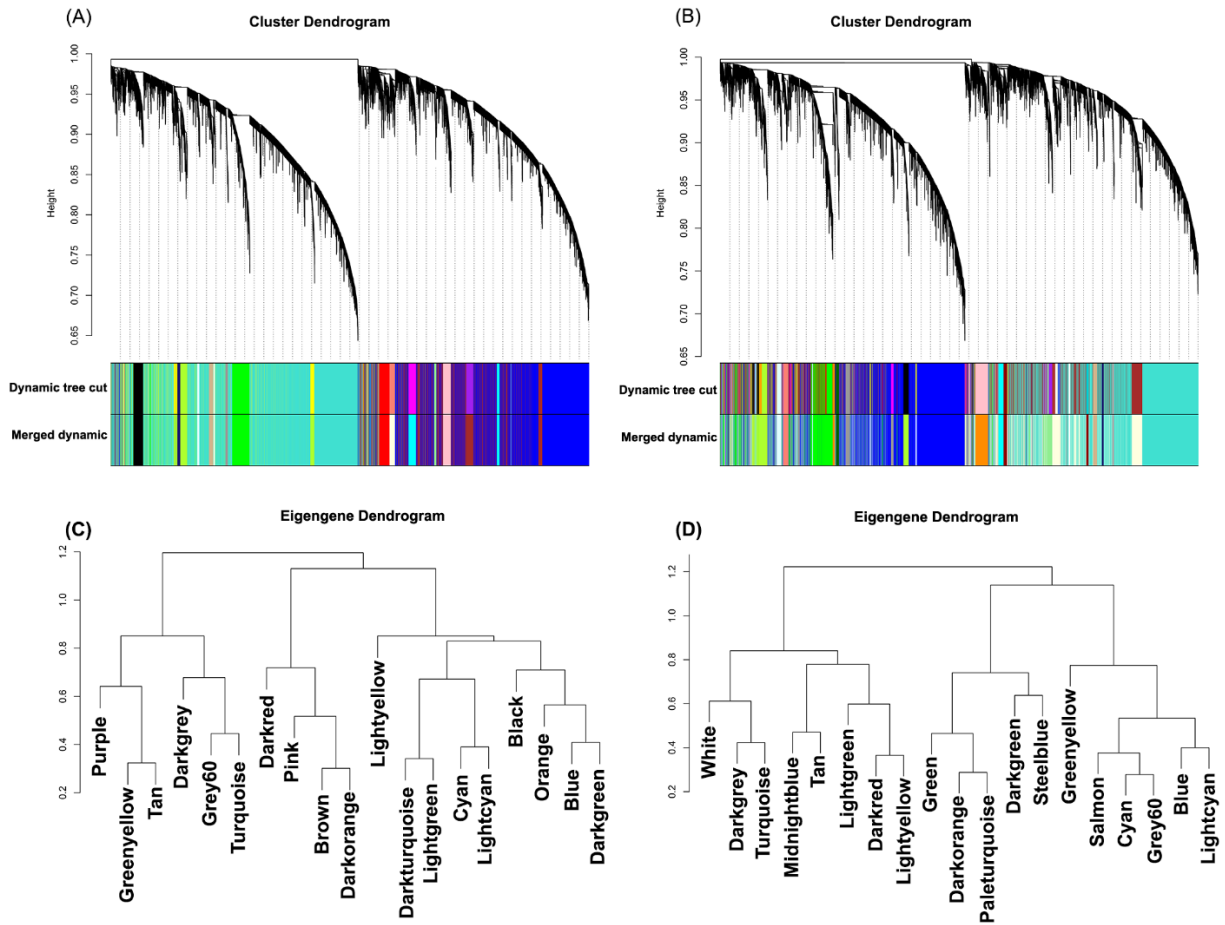


**FIGURE 3.3** | Gene network construction through weighted gene correlation network analysis (WGCNA) using a non indel normalized (A, C) and an indel normalized (B, C) gene counts dataset. Average linkage hierarchical clustering of adjacency-based dissimilarity is represented through dendrograms (A, B), with branches representing groups of highly coexpressed genes. These branches are cut into color-labeled modules based on a fixed height method. Module eigengenes are calculated and used to merge highly correlated modules. Both datasets produced 19 gene modules (C, D).

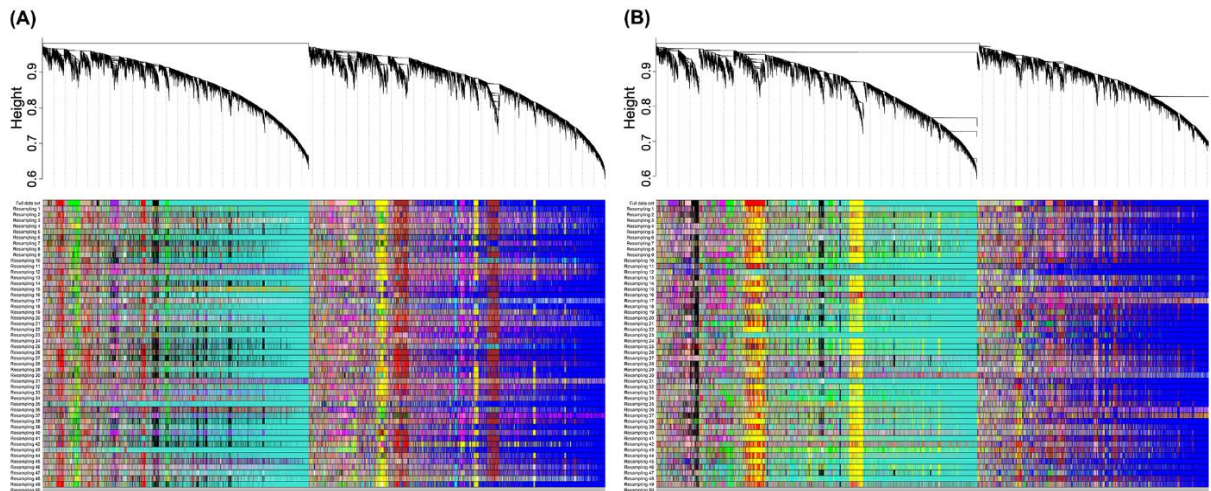


**FIGURE 3.4** | Stability analyses of gene modules derived from a non indel normalized (A) and an indel normalized (B) gene expression dataset. Dendrogram branches correspond to modules that are represented by color blocks in the row labeled “Full data set”. The color blocks below the first row represent module assignments obtained through repeated resampling of 63% of all sample libraries (49 network iterations constructed). Modules that persist across network construction iterations are considered more stable, or robust.

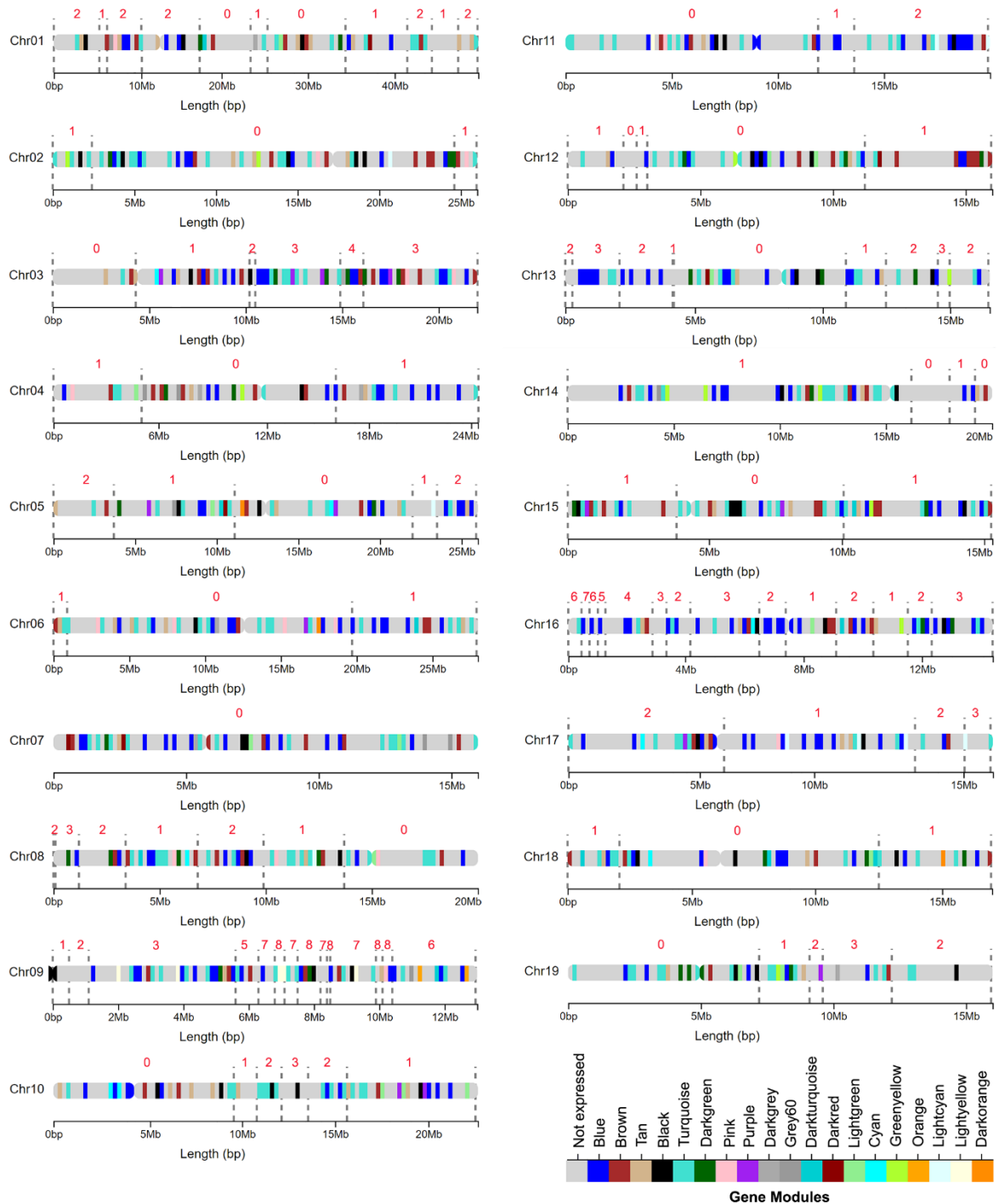


**FIGURE 3.5** | Broad genomic locations of gene modules identified through a weighted gene coexpression network analysis (WGCNA) using a non indel normalized dataset. Colored regions along chromosomes represent areas with a high density of genes in a particular module. The grey dotted lines mark the edges of indel regions. The number above each region represents the number of genotypes with indels in said region.

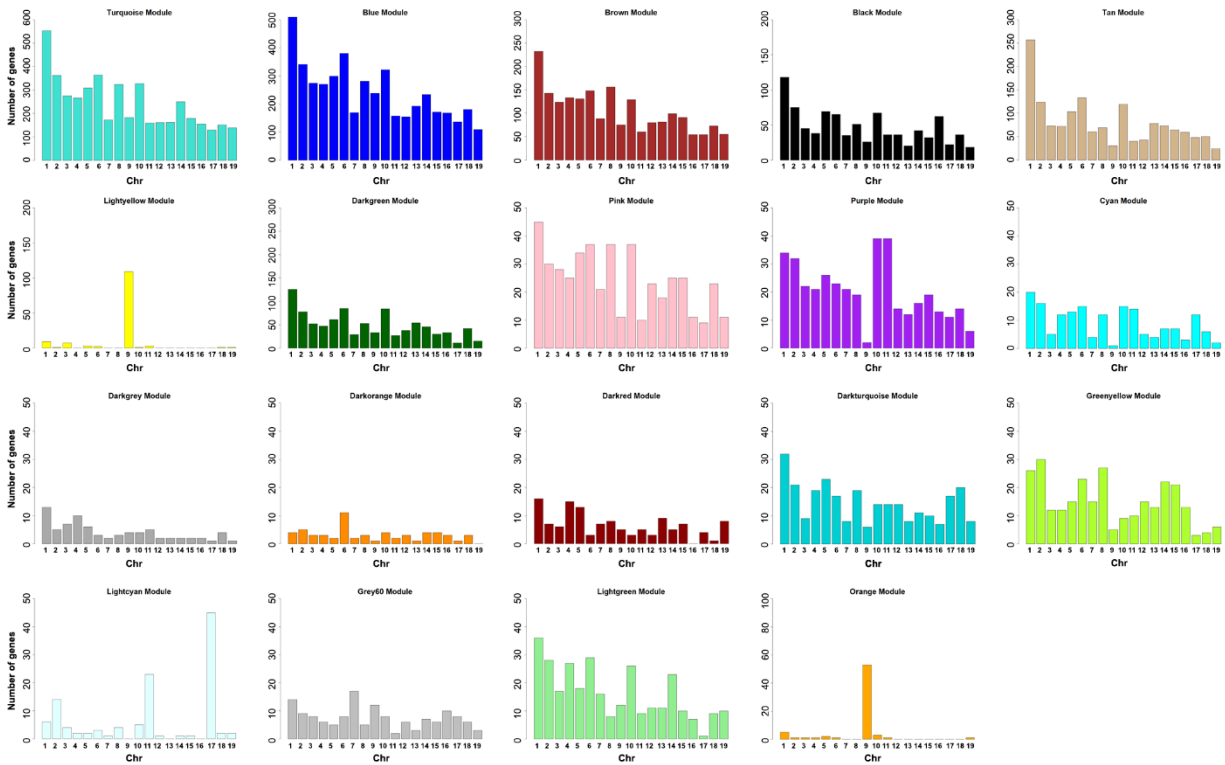


**FIGURE 3.6** | Module gene distributions across 19 Poplar chromosomes. Nineteen modules were generated from a non indel-normalized dataset.

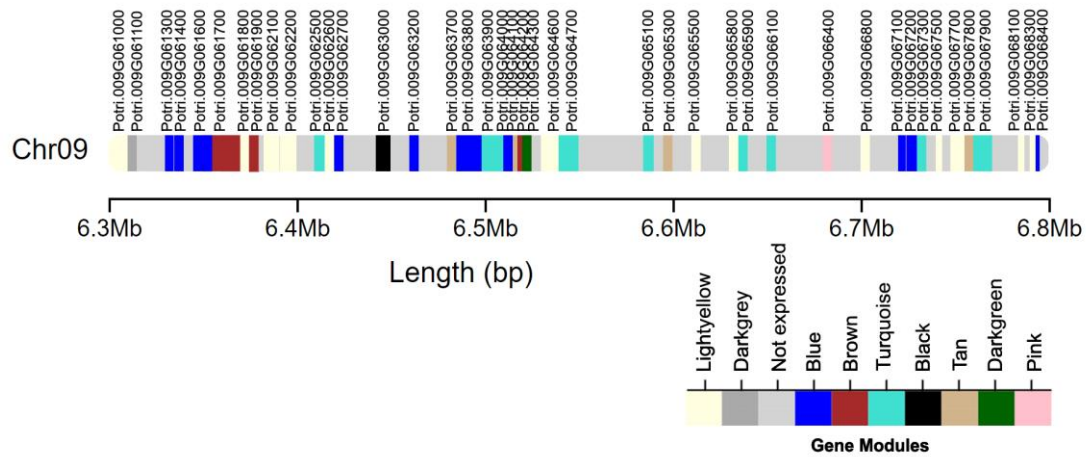


**FIGURE 3.7** | Locations and module identities of expressed genes within a previously identified dQTL region in chromosome 9. Each expressed gene belongs to a particular gene module determined through a WGCNA using a non indel normalized dataset. Seven lines included in the analysis had indel mutations spanning this genomic bin.

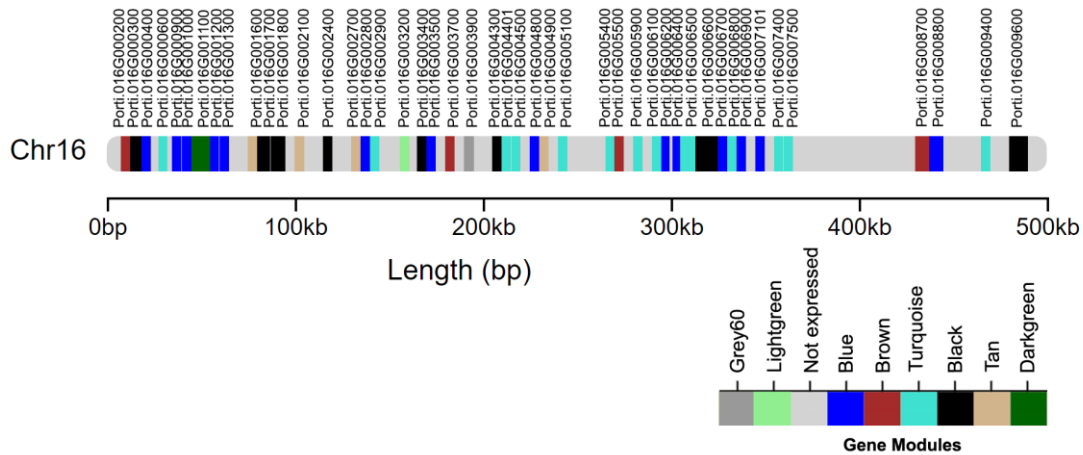


**FIGURE 3.8** | Locations and module identities of expressed genes within a previously identified dQTL region in chromosome 16. Each expressed gene belongs to a particular gene module determined through a WGCNA using a non indel normalized dataset. Six lines included in the analysis had indel mutations spanning this genomic bin.

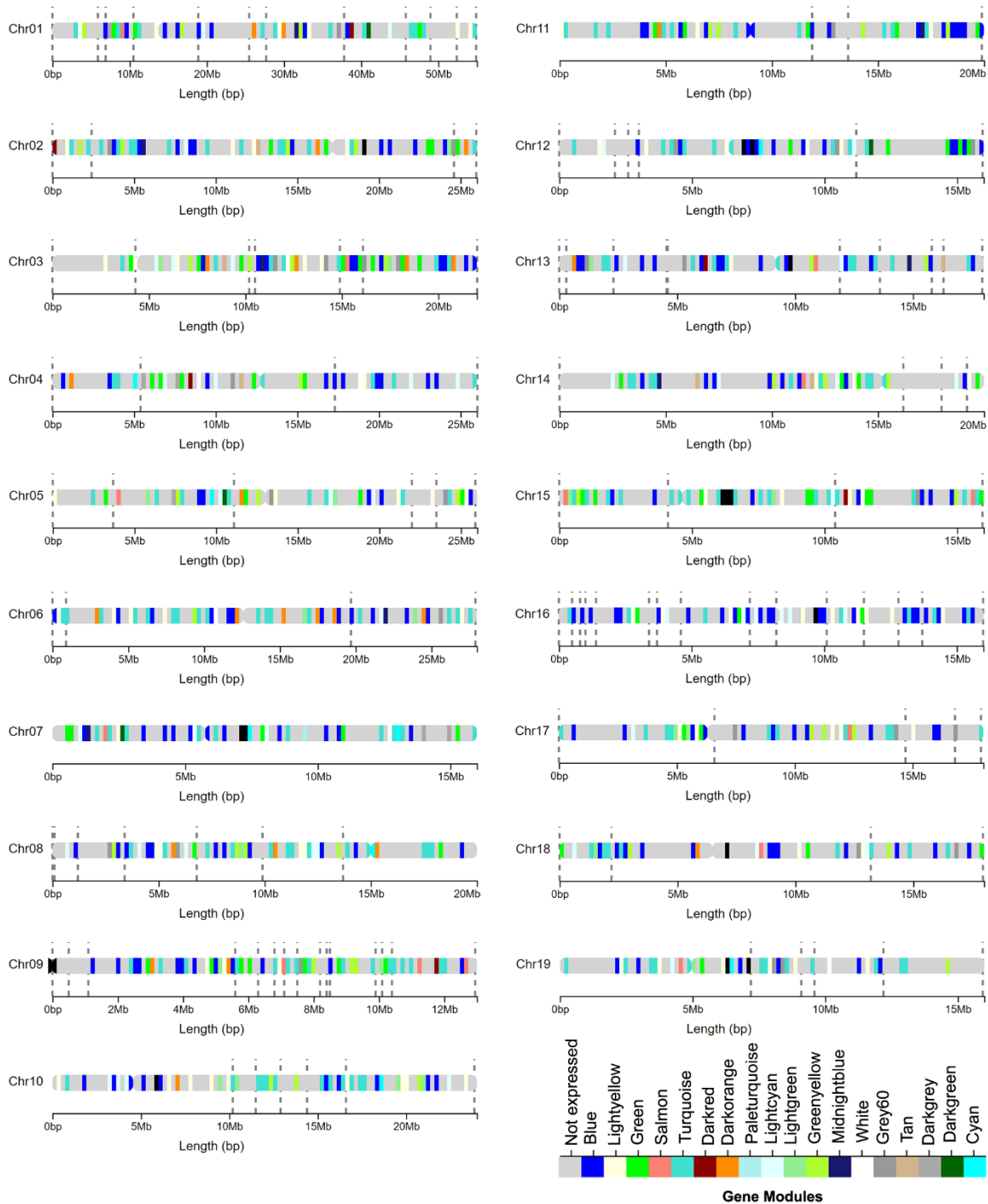


**FIGURE 3.9** | Broad genomic locations of gene modules identified through a weighted gene coexpression network analysis (WGCNA) using an indel normalized dataset. Colored regions along chromosomes represent areas with a high density of genes in a particular module. Gene expression in indel lines at each indel region was replaced by the average expression of all lines at that region. The grey dotted lines mark the edges of indel regions. \*The Steelblue module is not shown as it is made up exclusively of genes in unassigned contig scaffolds.

### *Gene Module and Trait Correlations*

The weighted average of gene expression (or the eigengene value) in each module was tested for significant correlations with stem and wood anatomical trait data. Most trait data were obtained from a subset of 33 lines harvested in 2018 for our previous study (Materials and Methods). Final tree height before harvest was measured in both 2018 (TH\_18) and 2019 (TH\_19), with 2019 tree heights as the only trait measured on the same individual plants that RNA was collected from. The majority of gene modules were significantly correlated to at least one stem or wood anatomical trait across both non indel-normalized and indel normalized networks. A smaller number of modules were significantly associated with only wood anatomical traits, with 8 modules in the non-normalized and 6 in the indel-normalized network ( $P < 0.05$ ; Figure 3.10). Tree heights in both years were the most strongly correlated to the turquoise, blue, dark-grey and dark-green modules in the non indel-normalized network, which together comprised about 64% of all expressed genes. Similarly, 6 modules in the indel-normalized network were the most strongly correlated to both TH\_18 and TH\_19 and together made up about 65% of all expressed genes (Figure 3.10b, Table 3.3). These findings suggest that gene expression patterns are closely tied to genotype across growing seasons for this trait.

Among wood anatomical traits, VF was the most highly correlated to any gene module across both networks and had the greatest number of significant correlations to modules ( $P < 0.05$ ; Figure 3.10). VF was the most strongly correlated to the blue and turquoise modules in both non normalized and indel normalized networks, showing moderate positive correlations to the turquoise modules ( $R = 0.54$  and  $0.56$ ) and moderate negative correlations to the blue modules ( $R = -0.54$  and  $-0.56$ ). Similarly, MVD was significantly correlated to 3 modules in both networks including the blue ( $R = 0.41$ ,  $0.38$ ) and turquoise modules ( $R = -0.40$ ,  $-0.40$ ). Height corrected VF

was positively related to the light-yellow ( $R=0.51$ ) and the grey60 ( $R=0.36$ ) modules within the non indel-normalized network. In contrast, cVF was only correlated to the dark-grey module ( $R=0.35$ ) in the normalized network, which was similar to the grey60 module in the non-normalized network. The light-yellow module had no analogous counterpart after indel normalization. Height corrected MVD was not significantly related to any module in either network, despite its strong relationship to cVF (Figure 3.1).

VGI was significantly related to the cyan module in the non-indel normalized network ( $R=-0.39$ ). However, there were no significant VGI-module relationships after indel normalization. NF was the most strongly related to the cyan ( $R=0.41$ ) and the light-cyan ( $R=0.39$ ) modules in the non indel-normalized network. These significant correlations disappeared after indel normalization. BT was positively correlated to TH and MVD and negatively correlated to VF. Interestingly, BT was uncorrelated to the turquoise and blue modules in both networks, which represent the biological pathways and genes most strongly related to TH, MVD and VF (Figure 3.1). BT was the most strongly related to the cyan module in the non-normalized network ( $R=0.47$ ), and to the light-cyan module in the normalized network ( $R=0.48$ ). MVC was uncorrelated to all non indel-normalized network modules. Unexpectedly, this trait was significantly related to the steel-blue module in the indel-normalized network ( $R=0.34$ ; Figure 3.10).

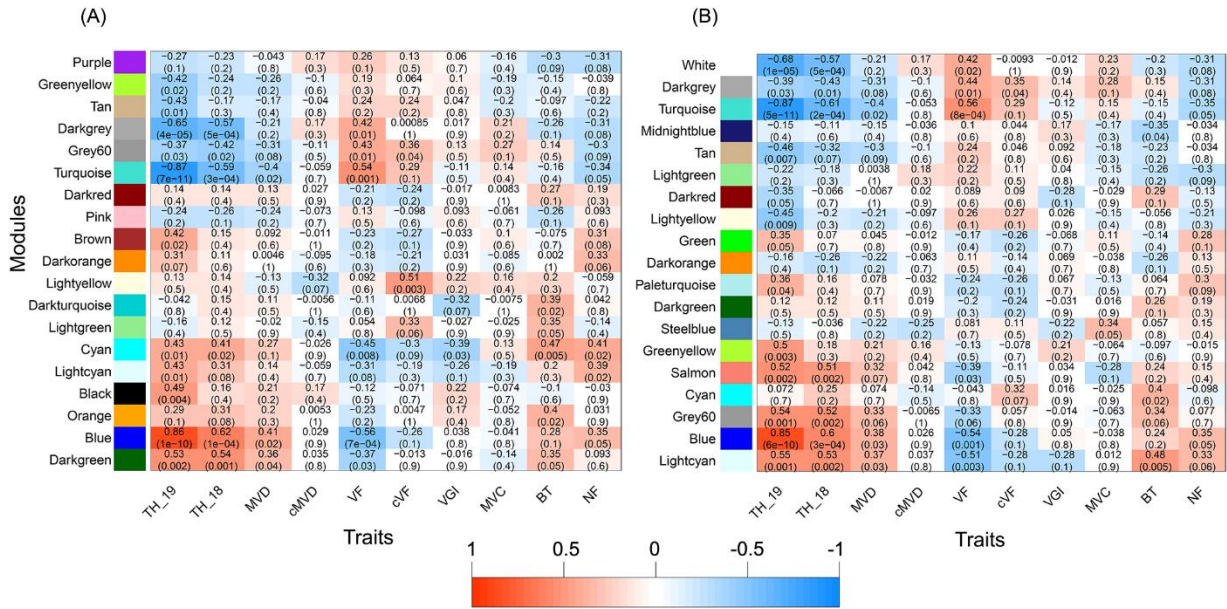


**FIGURE 3.10** | Module eigengene and trait correlations across 33 hybrid poplar genotypes. Non indel normalized (A) and indel normalized (B) datasets were analyzed. Wood anatomical traits include mean vessel diameter (MVD), height-corrected mean vessel diameter (cMVD), vessel frequency (VF), height-corrected vessel frequency (cVF), vessel grouping index (VGI), mean vessel circularity (MVC), and non-lumen fraction (NF). Stem traits include tree height (TH) and bark thickness (BT). Each box includes a Pearson’s correlation coefficient (represented by a color bar) and a P value to help identify statistically significant correlations ( $P < 0.05$ ). Modules with the same color labels across datasets are not necessarily equivalent.

### Gene Module GO Enrichment Analyses

Gene coexpression modules were related to broad biological functions through GO enrichment analyses. The turquoise modules showed nearly identical functional enrichment results across non indel-normalized and indel-normalized networks (Figure 3.11). Consequently, here we only report our findings for the turquoise module in the non indel-normalized network. The turquoise module was significantly enriched in stress response, transcription regulation and hormone related terms, among others ( $P < 0.05$ ). Response to stress was one of the most significantly overrepresented terms, with 107 genes with this annotation included in the module. Response to cold and water deprivation were the most significantly overrepresented specific

stress response terms. Twenty-seven genes had response to cold annotations, while 17 were related to response to response to water deprivation. Response to oxidative stress and water deprivation terms were also overrepresented in the module. After stress response, transcription regulation related terms were among the most numerous and significantly overrepresented, with 76 genes in the turquoise module. The majority of these genes were related to regulation of DNA-templated transcription. Lastly, this module was highly enriched in response to hormone terms, which together encompassed 45 genes. In particular, genes annotated with response to abscisic acid terms were the most numerous and overrepresented within this category, with 24 genes included in the turquoise module. Response to jasmonic acid and cytokinin related terms were also significantly overrepresented.

Much like the turquoise modules, the blue modules showed very similar functional enrichment patterns across non indel and indel-normalized gene coexpression networks (Figure 3.11). Here we report results for the blue module from the non indel-normalized network. The blue module was significantly enriched in vesicle transport, Golgi, cell wall, cell growth and cell differentiation related terms, among others ( $P < 0.05$ ). Vesicle mediated transport related terms were the most significantly overrepresented, with 39 annotated genes within the module. Twenty-three of these genes were annotated with Golgi vesicle transport and organization terms, which were also overrepresented. In addition, the blue module was highly enriched in cell wall organization and biogenesis terms, with 20 genes with these annotations included in the module. Hemicellulose was the most overrepresented among specific cell wall component related terms, followed by pectin and cellulose. Lastly, cell growth and differentiation associated terms were greatly overrepresented in the blue module. Eighteen genes were annotated with cell growth related terms, including those associated with multidimensional cell growth. Twenty-four genes

were annotated with cell differentiation terms, including those related to vessel element cell differentiation.

The dark-green module was the third largest gene set in the non indel-normalized network that was significantly correlated to any wood anatomical trait (Table 3.3; Figure 3.10a). Based on hypergeometric test results and shared trait correlations, this module was related but not analogous to the light-cyan module in the indel-normalized network. Both modules were highly enriched in proteolysis and endoplasmic reticulum stress related terms. Ubiquitin catabolic process and ERAD pathway related terms were particularly overrepresented within both modules. The cyan module showed the strongest correlation to BT and the third strongest correlation to VF in the non indel-normalized network, after the turquoise and blue modules. This module shared 82% of its genes with the light-cyan module in the normalized network and was highly enriched in xylem and phloem pattern formation related annotations. The light-yellow and grey60 modules in the non indel-normalized network were correlated to cVF and were enriched in cell cycle and lipid biosynthesis related terms, respectively. The light-yellow module, which showed the strongest relationship to cVF, had no equivalent module in the indel normalized network. The grey60 module was closely related to the dark-grey module in the indel normalized network and was likewise enriched in lipid biosynthesis related genes (Figure 3.11).

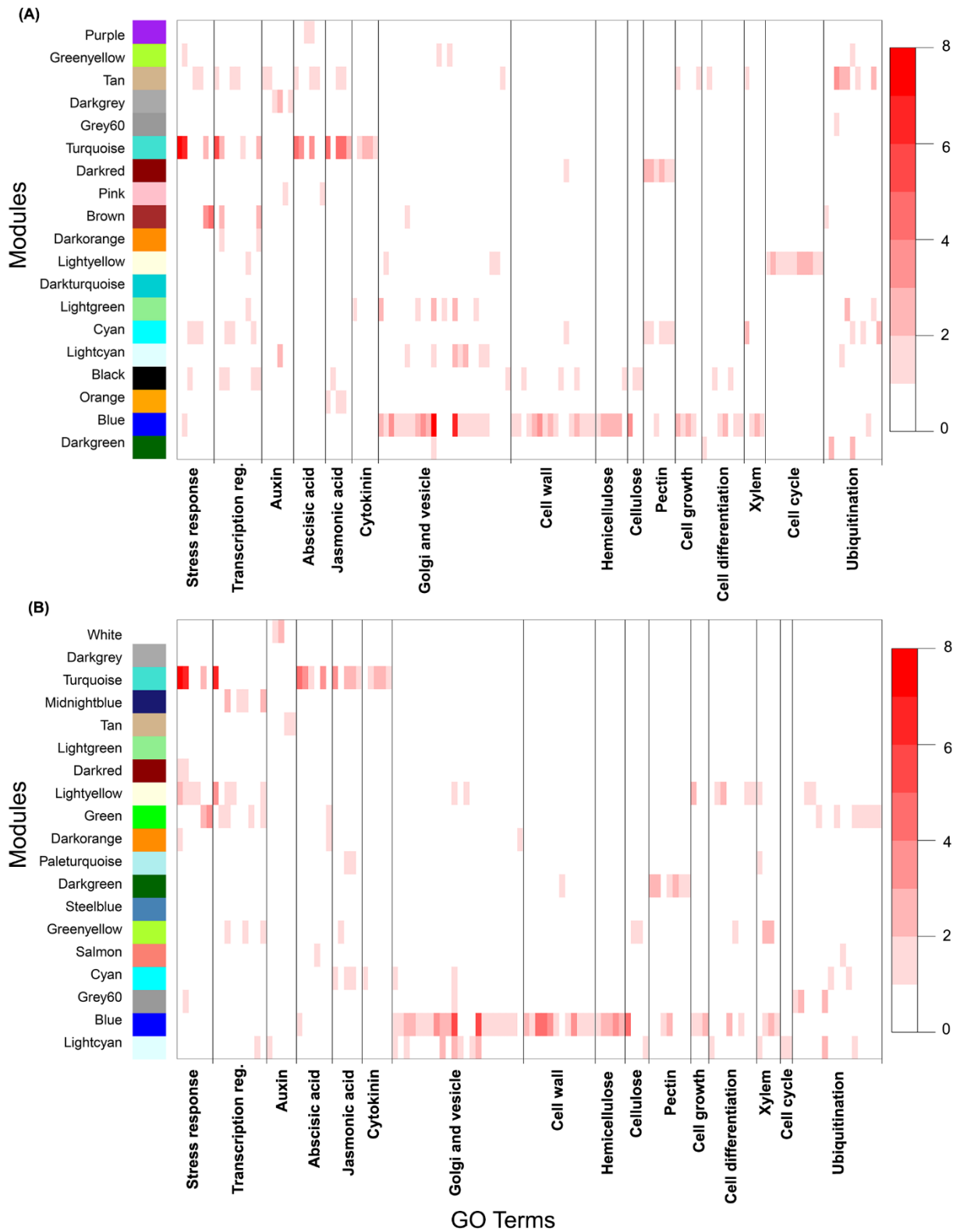


**FIGURE 3.11** | Enrichment analysis heatmaps showing significant overrepresentation ( $P < 0.05$ ) of GO terms within gene modules. Non indel normalized (A) and indel normalized (B) gene expression datasets were analyzed. The color bars represent the  $-\log_{10}$  of P values generated from hypergeometric tests. Modules with the same color labels across datasets are not necessarily equivalent.

### *Gene Significance vs Module Membership Plots*

Biologically relevant modules were next examined for candidate genes related to wood anatomical traits through gene significance (GS – a measure of correlation between a gene’s expression and a phenotype) vs module membership (MM – a measure of correlation between a gene’s expression and the eigengene of the module) plots. Trait correlation and GO enrichment analysis results were largely similar across networks, thus candidate gene selection was limited to non indel-normalized network modules. Here we focus on VF related candidate genes, as this trait showed the strongest and most numerous correlations to modules among the examined wood anatomical traits. Height corrected VF candidate genes were also selected. Genes with the greatest GS and MM values within overrepresented GO categories were identified as candidate genes within each selected module (Figure 3.12, Table 3.4).

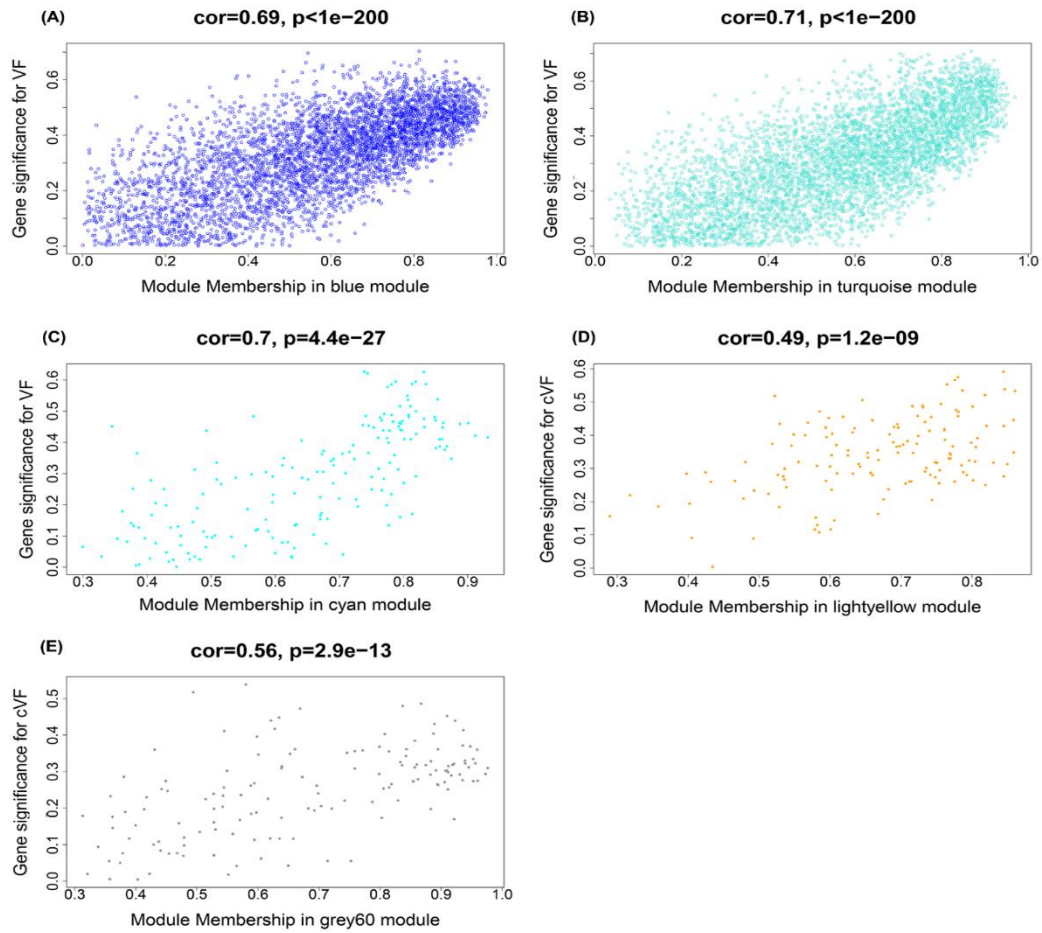


**FIGURE 3.12** | Gene significance (GS) vs module membership (MM) scatterplots of selected modules identified from a non indel normalized dataset. The Blue, Turquoise and Cyan module plots (A-C) show GS for vessel frequency (VF), while the Lightyellow and Grey60 plots (D,E) show GS for height-corrected vessel frequency (cVF). These modules showed highly significant correlations between GS and MM.

**TABLE 3.4|** Candidate genes related to vessel frequency (VF) and height corrected vessel frequency (cVF) across four gene modules. Gene modules were selected based on significant correlations to VF and cVF and GO enrichment analysis results. Candidate genes with the greatest module membership (MM) and gene significance (GS) within overrepresented GO categories were selected from each module. *P. trichocarpa genome v3.1*.

Gene	Module	Trait	GS	MM	Symbol	GO Terms (BP)
Potri.007G122100	turquoise	VF	0.60	0.76	RCI3	Response. to cold, desiccation, oxidative stress
Potri.004G149100	turquoise	VF	0.58	0.84	COR413	Response to water deprivation
Potri.002G013200	turquoise	VF	0.52	0.90	ERD10	Response to cold, water deprivation
Potri.014G104200	turquoise	VF	0.50	0.78	CIPK9	Response to cold, salt stress
Potri.012G044300	turquoise	VF	0.48	0.95	NUDT4	Response to water deprivation, salt stress
Potri.004G056900	turquoise	VF	0.64	0.91	DOF2	Regulation of transcription
Potri.012G100200	turquoise	VF	0.60	0.79	CAL	Regulation of transcription
Potri.005G073100	turquoise	VF	0.63	0.92	DSO	Response to abscisic acid
Potri.014G030700	turquoise	VF	0.59	0.93	CDPK1	ABA activated signaling pathway
Potri.014G095500	turquoise	VF	0.42	0.69	JAR1	JA metabolic process
Potri.010G108200	turquoise	VF	0.32	0.80	JAI3	JA metabolic process
Potri.010G102900	turquoise	VF	0.52	0.77	CRE1	CK activated signaling pathway
Potri.003G136300	turquoise	VF	0.50	0.80	CRF2	CK activated signaling pathway
Potri.010G177200	blue	VF	-0.60	0.82	COG1	Golgi vesicle-mediated transport
Potri.014G066800	blue	VF	-0.54	0.84	GOS12	Golgi vesicle-mediated transport
Potri.018G086600	blue	VF	-0.50	0.85	GC1	Golgi organization
Potri.019G076300	blue	VF	-0.59	0.73	GXM	Xylan metabolic process
Potri.013G102200	blue	VF	-0.55	0.80	GXM	Xylan metabolic process
Potri.007G107200	blue	VF	-0.51	0.95	GUX1	Xylan biosynthetic process
Potri.002G257900	blue	VF	-0.54	0.91	IRX5	Cellulose biosynthetic process
Potri.011G069600	blue	VF	-0.48	0.96	IRX1	Cellulose biosynthetic process
Potri.018G062700	blue	VF	-0.53	0.95	Pectin lyase	Carbohydrate metabolic process
Potri.008G182700	blue	VF	-0.67	0.90	ARP3	Cell growth
Potri.014G115000	blue	VF	-0.50	0.75	XET33	Cell growth
Potri.013G001000	blue	VF	-0.52	0.84	MYB61	Cell differentiation

Potri.012G126500	blue	VF	-0.45	0.78	VND4	Xylem vessel differentiation
Potri.005G148000	cyan	VF	-0.63	0.83	COV1	Stem vascular tissue pattern formation
Potri.009G062100	lightyellow	cVF	0.53	0.79	BB	Negative regulation of cell proliferation
Potri.009G020600	lightyellow	cVF	0.37	0.77	RINT1	Cell cycle progression
Potri.009G075700	lightyellow	cVF	0.35	0.86	UBA1	Cell aging
Potri.009G062600	lightyellow	cVF	0.32	0.75	MKRN	Cell aging

---

## Dosage Sensitivity Analysis

One prediction is that the causative gene(s) underlying dQTL should be expressed in wood forming tissues and should themselves respond to dosage in terms of expression. We thus tested for the presence of dosage sensitive genes within two cMVD and cVF dosage QTL regions (dQTL) identified in a previous study (see “Chapter 2, Results”). Genes with expression that is uncorrelated to dosage at these regions are unlikely to be related to cMVD and cVF and can be ruled out as candidate genes. These regions were selected because they were the most significantly correlated to any examined stem or wood anatomical trait. One dQTL region was located on chromosome 9 (from 6.3 to 6.8 Mbp) and was significantly correlated to both cMVD and cVF. The second region was located on chromosome 16 (from 0 to 0.5 Mbp) and was significantly related to cMVD (see “Chapter 2, Results”). Lines were placed in relative dosage score (RDS) groups determined by the presence of insertions or deletions spanning each dQTL region. Forty-two genes were expressed out of a total of 75 annotated genes within the chromosome 9 region. Eighteen of these genes showed significantly different expression across lines with different RDS values, suggesting dosage sensitivity ( $P < 0.05$ ). The expression of most of the 18 genes showed a positive relationship to their dosage in the region, with more copies of a gene leading to greater expression (Figure 3.13). Slopes obtained from linear regressions of gene expression data across different RDS lines ranged from 0.70 to 2.04, showing a wide variation in the effect of dosage on expression (Table 3.5). Within the chromosome 16 region, 46 out of 103 annotated genes were expressed in wood forming tissues. Seventeen of these genes showed significantly different expression across different RDS line categories ( $P < 0.05$ ; Figure 3.14). As expected, the expression of these genes was positively related to their gene dosage, with lines with greater RDS values showing greater expression (Figure 3.14). Slopes obtained

from linear regressions of gene expression data across RDS categories ranged from 0.83 to 2.12, showing a large variation in the effect of dosage on expression (Table 3.6).

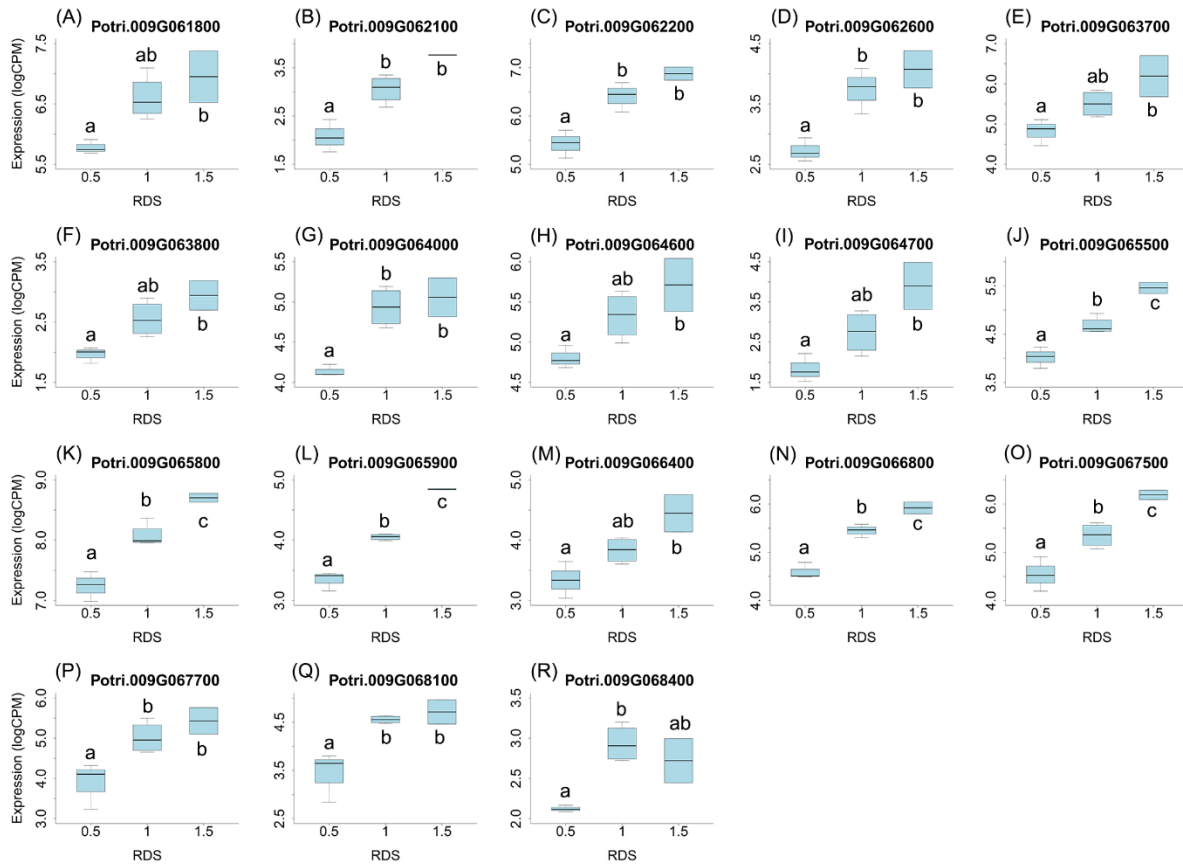


**FIGURE 3.13** | Putative dosage-sensitive genes within a previously identified dosage dependent QTL (dQTL) in chromosome 9. Each boxplot shows genotypes grouped by RDS at each gene locus within the dQTL region (6.3-6.8 Mbp). Only genes that had significantly different expression levels across RDS categories were included (determined by ANOVAs). Tukey pairwise comparisons were used to show significant differences in gene expression values between RDS groups; means that share a letter are not significantly different ( $p > 0.05$ ). *P. trichocarpa* genome v3.1.

**Table 3.5** Putative dosage-sensitive genes within a previously identified dosage dependent QTL (dQTL) region in chromosome 9 (6.3-6.8 Mbp). Genotypes were grouped by RDS at each gene locus within the dQTL region. An ANOVA was performed using gene expression data across different RDS groups. Only genes that had significantly different expression levels across RDS categories were included ( $P < 0.05$ ). The slope obtained from the linear regression of gene expression data across RDS groups is included to show the magnitude of the effect of dosage on expression. *P. trichocarpa* genome v3.1.

Gene	P	Slope	Symbol	GO Term (BP)
Potri.009G061800	2.4E-2	1.22	DIS3	Nucleic acid bond hydrolysis
Potri.009G062100	1.6E-3	1.71	BB	Regulation of cell proliferation
Potri.009G062200	1.7E-3	1.50	AAC2	Transmembrane transport
Potri.009G062600	5.0E-3	1.41	MKRN	Protein ubiquitination
Potri.009G063700	3.1E-2	1.37	Transmembrane	-
Potri.009G063800	1.6E-2	1.00	RNA-binding	mRNA processing
Potri.009G064000	5.6E-3	0.98	LSM7	Nuclear mRNA degradation
Potri.009G064600	3.6E-2	0.92	SWAP	RNA splicing
Potri.009G064700	1.7E-2	2.04	Basic HLH	Regulation of transcription
Potri.009G065500	5.0E-4	1.42	GFA2	Response to heat
Potri.009G065800	5.7E-4	1.48	Ribosomal L6	Translation
Potri.009G065900	8.5E-6	1.50	RNA-binding	Nucleic acid binding
Potri.009G066400	1.7E-2	1.09	Trans. initiation	Translation initiation
Potri.009G066800	1.3E-4	1.36	SCAB1	Actin filament organization
Potri.009G067500	1.8E-3	1.64	RNA-binding	mRNA splicing
Potri.009G067700	2.2E-2	1.61	PYD2	Pyrimidine catabolic process
Potri.009G068100	7.3E-3	1.37	SKIP2	Protein ubiquitination
Potri.009G068400	9.9E-3	0.70	Methyltrans.	Protein methylation

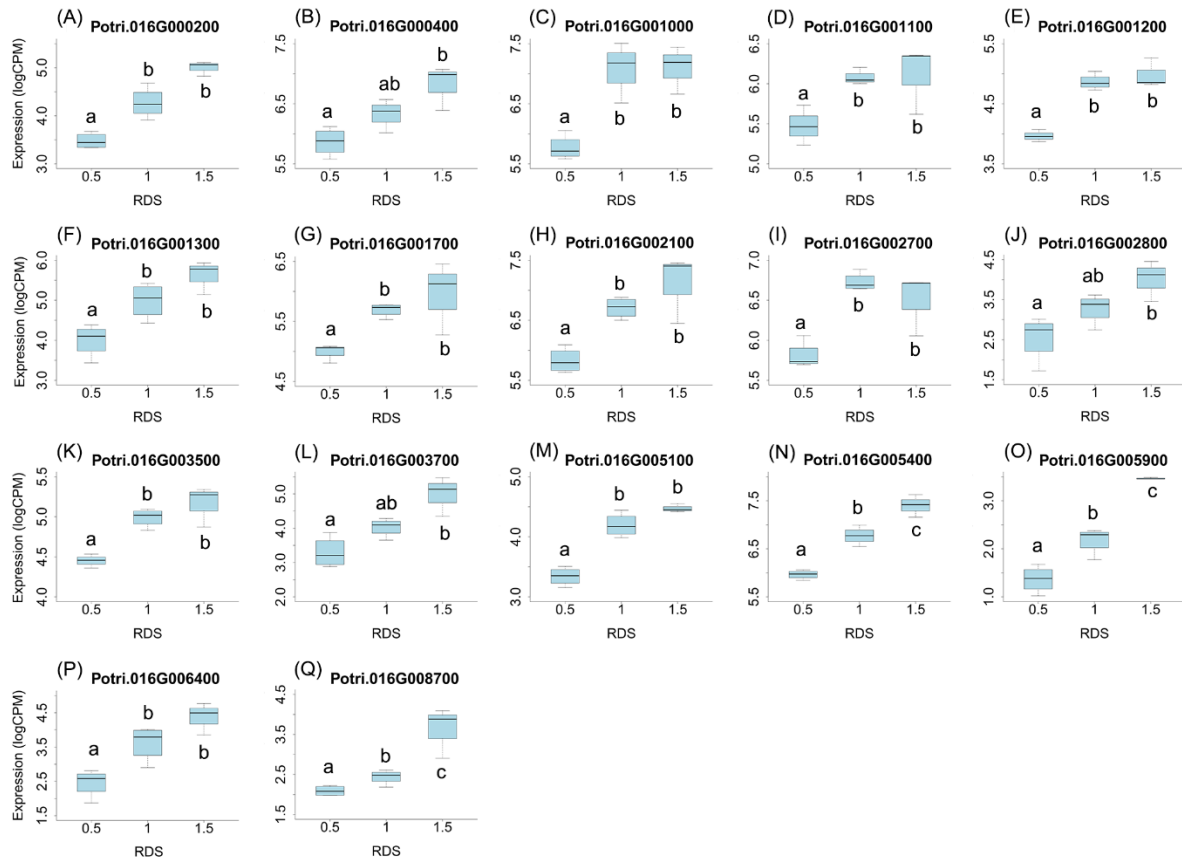


**FIGURE 3.14** | Putative dosage-sensitive genes within a previously identified dosage dependent QTL (dQTL) in chromosome 16. Each boxplot shows genotypes grouped by RDS at each gene locus within the dQTL region (0-0.5 Mbp). Only genes that had significantly different expression levels across RDS categories were included (determined by ANOVAs). Tukey pairwise comparisons were used to show significant differences in gene expression values between RDS groups; means that share a letter are not significantly different ( $p > 0.05$ ). *P. trichocarpa* genome v3.1.

**Table 3.6|** Putative dosage-sensitive genes within a previously identified dosage dependent QTL (dQTL) region in chromosome 16 (0-0.5 Mbp). Genotypes were grouped by RDS at each gene locus within the dQTL region. An ANOVA was performed using gene expression data across different RDS groups. Only genes that had significantly different expression levels across RDS categories were included ( $P < 0.05$ ). The slope obtained from the linear regression of gene expression data across RDS groups is included to show the magnitude of the effect of dosage on expression. *P. trichocarpa genome v3.1*.

Gene	P	Slope	Symbol	GO Term (BP)
Potri.016G000200	2.5E-3	1.55	NHX6	Transmembrane transport
Potri.016G000400	1.9E-2	0.94	RABA2b	GTP binding
Potri.016G001000	2.9E-3	1.76	Alpha beta-hydrolase	Hydrolase activity
Potri.016G001100	3.3E-3	0.86	PHL7	Regulation of transcript.
Potri.016G001200	4.4E-5	1.30	PHL2	Phosphate starvation resp.
Potri.016G001300	1.6E-2	1.78	Cl- channel regulator	Zinc ion binding
Potri.016G001700	2.2E-4	1.17	GAUT4	Glycosyltransferase
Potri.016G002100	7.5E-4	1.44	Autoant. RCD8	mRNA binding
Potri.016G002700	2.8E-4	1.08	PFK2	Glycolytic process
Potri.016G002800	4.4E-2	1.59	O-Glycosyl hydrolase	Carbohydrate metabolism
Potri.016G003500	7.4E-4	0.83	CBL3	Detection of calcium ion
Potri.016G003700	1.2E-2	1.64	NPH3	Protein ubiquitination
Potri.016G005100	6.9E-4	1.31	Sec14p	-
Potri.016G005400	1.5E-4	1.47	Sister chro. cohesion	-
Potri.016G005900	1.3E-3	1.91	DNA binding	-
Potri.016G006400	1.1E-2	2.13	Protein kinase	Cellular resp. to nitrogen
Potri.016G008700	1.6E-4	1.43	Ferredo. hydrogenase	-

## DISCUSSION

### Summary

The size, number, and distribution of vessels in wood are known to affect water transport efficiency, growth, and vulnerability to hydraulic failure in trees. However, the genetic regulation of these traits (described as wood anatomical traits) is not very well understood. Here, we explored the biological pathways and genes related to wood and stem anatomical traits using a 33-genotype subset of a unique poplar dosage mutant pedigree. We conducted an RNA-seq study on wood forming tissues involving three different but complementary approaches:

differential expression analysis, weighted gene correlation network analysis (WGCNA) and dosage sensitivity analysis. Broadly, we found strong evidence for the direct genetic regulation of most examined traits, were able to identify putative mechanisms associated with traits, and identified candidate genes for future study. Based on the identified mechanisms and candidate genes, we propose that differences in wood anatomy are likely related to differences in growth and proliferation rates of initials in the vascular cambium which in turn affects the timing of cell growth and expansion.

### *Approach*

An RNA-seq study on the wood-forming tissues of 33 hybrid poplar lines was undertaken to glean a better understanding of the biological pathways and genes related to the variation of stem and wood anatomical traits. These 33 lines belong to a unique poplar mutant pedigree with large-scale indels in known genomic locations developed by Henry et al. (2015). We employed this pedigree to facilitate the identification of candidate genes through its significant trait variation previously associated to a large variation in gene dosage (Bastiaanse et al. 2020; see “Chapter 2, Results”). A list of all examined traits with abbreviations and units is included in Table 3.1. Differential expression, weighted gene correlation network analyses (WGCNA) and dosage sensitivity analyses were employed as separate but complementary methods to explore the regulation of these traits. Our approach is novel in that it attempts to link whole transcriptome gene expression patterns to wood anatomical trait variation.

### *Evidence for the genetic regulation of stem and wood anatomical traits*

Differential expression analyses showed differentially expressed genes across lines with high and low TH, VF, MVD, MVC, NF and BT values. There were no differentially expressed

genes across high and low, cVF, cMVD, and VGI lines (Table 3.2). A WGCNA involving all 33 lines identified nineteen modules of highly coexpressed genes after network construction using a non indel-normalized gene expression data set (see “Network selection” below). All traits with the exception of cMVD and MVC were significantly correlated to at least one gene module (Figure 3.10a). These results suggest that most examined traits are under genetic regulation, with TH, VF, MVD, NF and BT showing associations to gene expression across both analyses.

*Correlated stem and wood anatomical traits are regulated by similar biological pathways and genes*

VF and MVD are known to predictably scale with TH, with taller trees showing wider, but less numerous vessels per unit of cross-sectional xylem area in relation to shorter trees at the same sampling height from the ground (Olson et al. 2020; Rosell et al. 2017). Explanations for the correlation between TH and MVD have been proposed in the context of hydraulic optimality models and selection. These models predict that vessels must become wider with greater tree heights to offset the increased resistance to flow that results from longer conductive pathways. Trees with vessels that scale with height would therefore be selected for as they are better able to transport water to support growth (Comstock and Sperry 2000; Olson et al. 2014). Similarly, the correlation between VF and MVD has been related to optimal partitioning between conductive vessel lumens and non-conductive xylem required for mechanical support (Taneda and Tateno 2004). The genetic and molecular nature of these correlations is not known, however. One possibility is that the correlation could result from overlapping regulatory mechanisms. Other possibilities include that the correlation is indirect, for example from biophysical or physiological conditions that affect both traits. Here we found with both differential expression and correlation network analyses that correlated stem and wood anatomical traits shared similar

biological pathways and genes. Differential expression contrasts across high and low TH, VF and MVD lines produced similar sets of genes, which was expected as they involved similar, but not identical, top and bottom lines. The WGCNA module-trait correlation analysis showed that TH, VF and MVD were significantly related to the same modules, with correlation directions between traits reflected in correlation directions to modules. The turquoise and blue modules were the largest and most strongly correlated to the three traits. BT was significantly correlated to TH, VF and MVD. Consequently, most differentially expressed genes across high and low BT lines were also found in differential expression gene sets for these traits. Interestingly, BT was not correlated to the turquoise or blue modules, pointing to at least partially diverging regulatory pathways. NF, which was not significantly correlated to any other trait, shared most of its differentially expressed genes with TH and VF sets, likely due to an existing weak but non-significant correlation to these traits. NF was correlated to both the turquoise and blue modules.

#### *High vessel frequency and low mean vessel diameter are related to decreased cambial activity*

The vascular cambium is known to respond to a variety of abiotic stressors through the reduction of secondary xylem radial growth and the production of altered wood structure (Savage and Chuine 2020; Gricar et al. 2006). Namely, shifts in temperature, water availability and salinity are linked to changes in cambial activity, with lower temperatures, drought and high salinity leading to decreased cambial proliferation and dormancy (Riding and Little 1981; Chen and Polle 2009; Zheng et al. 2013). Some trees, including those of the genus *Populus*, produce wood with smaller and more numerous vessels as a result of these stressful environmental conditions (Janz et al. 2012; Beniwal et al. 2010; Fichot et al. 2009; Arend and Fromm 2007). Accordingly, gene sets identified through our study that were related to high VF, low MVD and

low TH were all highly enriched in stress response, transcription regulation and hormone related GO terms. These gene sets include low TH, high VF and low MVD sets produced through differential expression analyses (Table 3.2) and the WGCNA-produced turquoise module (Table 3.3), which largely overlapped with the first three sets. In particular, response to cold, water deprivation and oxidative stress were the most overrepresented stress response terms. The stress response-mediating hormones abscisic acid and jasmonic acid were the most overrepresented hormone related terms. Abscisic acid concentrations have been shown to drastically increase in poplar stem wood tissues during drought. A decreased number of cambial cell layers in drought-stressed wood suggests a negative regulatory role for this hormone in cambial proliferation (Yu et al. 2021). The overrepresentation of transcription regulation related genes (many of which are related to stress, hormone, and stimulus response) broadly suggests that trees with greater VFs and smaller MVDs in our population are highly sensitive to environmental stimuli in relation to trees with lower VF and greater MVDs, which were grown under the same greenhouse conditions.

#### *Network selection*

A weighted gene correlation network analysis (WGCNA) including all 33 sampled genotypes was run as a separate but complementary analysis to the differential expression line contrasts. Network construction and subsequent analyses involved both a non indel-normalized and an indel-normalized gene expression dataset. We reasoned that the presence of many large scale indels across the 33 lines could potentially induce the formation of artificial modules, which was observed in a previous WGCNA study involving dosage mutant lines from this pedigree (Bastiaanse et al., 2021). Networks produced from the non indel-normalized and the indel normalized datasets were largely similar, both consisting of 19 gene modules of

comparable sizes (Table 3.3). Most modules had analogous equivalents across networks with similar GO enrichment analysis results. We found that in the non indel-normalized network the genes of most modules were widely distributed across the genome and were not predominantly located in any particular chromosome (Figure 3.6). The light-yellow and orange modules were the exception, with most of their genes located in chromosome 9, a high indel depth coverage region. A potential interpretation of these results is that both modules were driven completely by the physical location of indels and not by true coexpression. However, we do not favor this interpretation due to the presence of dosage sensitive genes belonging to other modules within high indel coverage regions in chromosome 9. We reasoned that if the light-yellow and orange modules are truly induced by the physical location of indels then all dosage sensitive genes in these regions should be assigned to these two modules, which was not the case (Figure 3.9, 3.14). Based on these factors we chose to only report our findings for the non indel-normalized network.

#### *Insights into putative mechanisms influencing vessel size*

The regulation of cell size is a fundamental issue for plant development but remains poorly understood. The determination of vessel element diameter is especially fascinating because it is a striking case of size regulation that is responsive to environmental conditions. Three generalized models of cell size regulation have been proposed: the “timer”, “sizer” and “adder” models (D’Ario and Sablowski 2019). Although these models were initially developed for yeast, they provide a conceptual framework for plants. The timer model predicts that cells divide at specific time intervals, while sizer model cells divide when they reach a certain size. In the sizer model, cells attain their target size after one division while timer model cells do not attain a homogenous size under exponential growth conditions. In the adder model, cells divide

after a specific amount of growth regardless of initial size and can continue to increase in size across cell divisions. The adder model thus best fits what is seen in the cambial zone, where daughter cells (also referred to as xylem mother cells) are similar in size, but daughters directly born from the fusiform initials can be smaller than older daughter cells in their final round of division prior to differentiation. Studies examining cell size determination in the Arabidopsis apical meristem have suggested that the “timer” and “sizer” models do not reflect what is observed in the apical meristem (Willis et al., 2016). Willis et al. (2016) observed cell division and expansion of individual cells in the meristem and noted that cells grew exponentially through the first ~80% of the cell cycle, and that after an asymmetric division the smaller daughter grew at a rate faster than that of the larger daughter. The latter observation was interpreted to show that the difference in growth between the daughters is driven mostly by the asymmetrical division. This was further interpreted in terms of a potential molecular mechanism in which a master growth regulator would have the following properties: 1) the regulator concentration is constant through the cell cycle and is proportional to the per unit size growth rate, 2) at mitosis the regulator is degraded or synthesized to a specific concentration, and 3) at cell division the regulator is distributed equally in number between daughter cells, potentially by titration against DNA. This would result in more of the regulator going to the smaller cell. However, these models do not account for the large difference in final size of fiber cells compared to vessel elements, and they do not account for the large variation observed in vessel element size across developmental age, height position within the stem, or in response to water stress.

Although speculative, we favor a model by which an interplay between division rates in the cambial zone and time of differentiation has an effect on final vessel size. This can be inferred in part through histological examination of poplar stems from fast growing trees in well-

watered conditions, vs trees under water stress. In the former, rapid cell division results in an expanded cambial zone which ultimately produces larger diameter vessel elements. In the latter, slower division rates result in a narrower cambial zone that produces smaller diameter vessel elements. However, the mechanisms and candidate genes identified in our study here did not have strong indications of cell cycle regulation, based on GO enrichment of differentially expressed genes (Figure 3.2), and only one module in the indel normalized network showed modest enrichment for cell cycle related genes in our WGCNA analysis. While the Arabidopsis apical meristem mechanism may be evoked to explain the size of still dividing daughter cells, upon differentiation and expansion additional mechanisms, yet to be defined, must be evoked. Thus, one future challenge is to understand vessel diameter both in terms of classical ideas about cell size regulation, as well as how environmental and developmental cues change the final size. The strong enrichment of genes associated with stress, cell wall, ABA and stress response (Figure 3.2, Figure 3.11) could suggest that these factors may be more critical in determining final size. The presence of genes encoding ubiquitin-proteasome regulators in these same analyses are intriguing and could indicate a mechanism by which the observed rapid changes in development, including size growth, could be regulated during vessel element differentiation.

## **REFERENCES**

- Anand, L., and Rodriguez Lopez, C. (2020) ChromoMap: an R package for interactive visualization and annotation of chromosomes. bioRxiv 605600, doi: <https://doi.org/10.1101/605600>
- Anders, S., Pyl, P., and Huber, W. (2015). HTSeq, a python framework to work with high-throughput sequencing data. *Bioinformatics* 31, 166-169.
- Arend, M., and Fromm J. (2007). Seasonal change in the drought response of wood cell development in poplar. *Tree Physiology* 27, 985-992.

- Baas, P., Ewers, F., Davis, S., and Wheeler, E. (2004). "Evolution of xylem physiology", in *Evolution of Plant Physiology*, ed. A. Hemsley and I. Poole (Cambridge, MA: Elsevier Academic Press), 273-295.
- Baas, P., Werker, E., and Fahn, A. (1983) Some ecological trends in vessel characters. *IAWA Bulletin new series* 4, 141-159.
- Baastianse, H., Henry, I., Tsai, H., Lieberman, M., Canning C., Comai, L., Groover, A. (2020). A systems genetics approach to deciphering the effect of dosage variation of leaf morphology in *Populus*. *The Plant Cell* 33, 940-960.
- Bechtold, U., and Field, B. (2018). Molecular mechanisms controlling plant growth during abiotic stress. *Journal of Experimental Botany* 69, 2753-2758.
- Beniwal, R., Langenfeld-Heyser, R., and Polle, A. (2010). Ectomycorrhiza and hydrogel protect hybrid poplar from water deficit and unravel plastic responses of xylem anatomy. *Environmental and Experimental Botany* 69, 189-197.
- Brodribb, T., and Field, T. (2000). Stem hydraulic supply is linked to leaf photosynthetic capacity: evidence from New Caledonian and Tasmanian rainforests. *Plant, Cell & Environment* 23, 1381-1388.
- Carlquist, S. (1984). Vessel grouping in dicotyledon wood. *Aliso* 10, 505-525.
- Cellini, J., Galarza, M., Burns, S., Martinez-Pastur, G., and Lencinas, M. (2012). Equations of bark thickness and volume profiles at different heights with easy measurement variables. *Forest Systems* 21, 23-30.
- Chen, S., and Polle, A. (2009). Salinity tolerance of *Populus*. *Plant Biology* 12, 317-333.
- Comstock, J., and Sperry, J. (2000). Theoretical considerations of optimal conduit length for water transport in vascular plants. *New Phytologist* 148, 195-218.
- D'Ario, M. and Sablowski, R. (2019). Cell size control in plants. *Annual Review of Genetics* 53, 45-65.
- Dejardin, A., Laurans, F., Arnaud, D., Breton, C., Pilate, G., and Leple, J. (2010). Wood formation in angiosperms. *Comptes Rendus Biologies* 333, 325-334.

- Dobbertin, M. (2005). Tree growth as indicator of tree vitality and of tree reaction to environmental stress: a review. *European Journal of Forest Research* 124, 319-333.
- Dobin, A., and Gingeras, T. (2015). Mapping RNA-seq reads with STAR. *Current Protocols in Bioinformatics* 51, 11.14.1-11.14.19.
- Du, Q., Gong, C., Wang, Q., Zhou, D., Yang, H., Pan, W., Bailian, L., and Zhang, D. (2016). Genetic architecture of growth traits in *Populus* revealed by integrated quantitative trait locus (QTL) analysis and association studies. *New Phytologist* 209, 1067-1082.
- Esau K: *Anatomy of Seed Plants*. New York: Wiley; 1977.
- Ewers, F., Ewers, J., Jacobsen, A. and López-Portillo, J. (2007) Vessel redundancy: modeling safety in numbers. *Iawa Journal* 28, 373.
- Feng, F., Ding, F., and Tyree, M. (2015). Investigations concerning cavitation and frost fatigue in clonal 84K poplar using high-resolution Cavitron measurements. *Plant Physiology* 168, 144-155.
- Fonti, P., Heller, O., Cherubini, P., Rigling, A., and Arend, M. (2013) Wood anatomical responses of oak saplings exposed to air warming and soil drought. *Plant Biology* 15, 210–219.
- Fichot, R., Laurans, F., Monclus, R., Moreau, A., Pilate, G., and Brignolas, F. (2009). Xylem anatomy correlates with gas exchange, water-use efficiency and growth performance under contrasting water regimes: evidence from *Populus deltoides* × *Populus nigra* hybrids. *Tree Physiology* 29, 1537-1549.
- Gleason, S., Westoby, M., Jansen, S., Choat, B., Hacke, U., Pratt R.B., et al. (2016). Weak tradeoff between xylem safety and xylem-specific hydraulic efficiency across the world's woody plant species. *New Phytologist* 209, 123–136.
- Grattapaglia, D., Plomion, C., Kirst, M., and Sederoff, R. (2009). Genomics of growth traits in forest trees. *Current Opinion in Plant Biology* 12, 148–156.
- Gricar, J., Zupancic, M., Cufar, K., Koch, G., Schmitt, U., and Oven, P. (2006). Effect of local heating and cooling on cambial activity and cell differentiation in the stem of Norway spruce (*Picea abies*). *Annals of Botany* 97, 943-951.

- Guet, J., Fichot, R., Lédée, C., Laurans, F., Cochard, H., Delzon, S., Bastien, C., and Brignolas, F. (2015). Stem xylem resistance to cavitation is related to xylem structure but not to growth and water-use efficiency at the within-population level in *Populus nigra* L. *Journal of Experimental Botany* 66, 4643-4652.
- Hajek, P., Leuschner, C., Hertel, D., Delzon, S., and Schuldt, B. (2014). Trade-offs between xylem hydraulic properties, wood anatomy and yield in *Populus*. *Tree Physiology* 34, 744-756.
- Janz, D., Lautner, S., Wildhagen, H., Behnke, K., Schnitzler, J., Rennenberg, H. et al. (2012). Salt stress induces the formation of a novel type of 'pressure wood' in two *Populus* species. *New Phytologist* 194, 129-141.
- Johnson, D., Eckart, P., Alsamadisi, N., Noble, H., Martin, C., and Spicer, R. (2018). Polar auxin transport is implicated in vessel differentiation and spatial patterning during secondary growth in *Populus*. *American Journal of Botany* 105, 186-196.
- Junghans, U., Langenfeld-Heyser, R., Polle, A., and Teichman, T. (2004). Effect of auxin transport inhibitors and ethylene on wood anatomy of poplar. *Plant Biology* 6, 22-29.
- Langfelder, P., and Horvath, S. (2008). WGCNA: an R package for weighted correlation network analysis. *BMC Bioinformatics* 9, 559.
- Law, C., Chen, Y., Shi, W., and Smyth, G. (2014). Voom: precision weights unlock linear model analysis tools for RNA-seq read counts. *Genome Biology* 15, doi:10.1186/gb-2014-15-2-r29.
- Lens, F., Sperry, J., Christman, M., Choat, B., Rabaey, D., and Jansen, S. (2010). Testing hypotheses that link wood anatomy to cavitation resistance and hydraulic conductivity in the genus *Acer*. *New Phytologist* 190, 709-723.
- Li, H., Handsaker, B., Wysoker, A., Fennell, T., Ruan, J., Homer, et al. (2009). The sequence alignment/map (SAM) format and SAMtools. *Bioinformatics* 25, 2078-2079.
- Li, S., Lin, Y., Wang, P., Zhang, B., Li, M., Chen, S., et al. (2019). The AREB1 transcription factor influences histone acetylation to regulate drought responses and tolerance in *Populus trichocarpa*. *The Plant Cell* 31, 663-686.

- Lieberman, M. (2016). Comai Lab Github. <https://github.com/Comai-Lab/allprep> [Accessed August 20, 2021].
- Lin, Y., Li, W., Chen, H., Li, Q., Sun, Y., Shi, R., et al. (2014). A simple improved-throughput xylem protoplast system for studying wood formation. *Nature Protocols* 9, 2194-2205.
- Liu, R., Holik, A., Su, S., Jansz, N., Chen, K., Leong, H., et al. (2015). Why weight? Modelling sample and observational level variability improves power in RNA-seq analyses. *Nucleic Acids Research* 43, doi: 10.1093/nar/gkv412.
- Love, J., Björklund, S., Vahala, J., Hertzberg, M., Kangasjärvi, J., and Sundberg, B. (2009). Ethylene is an endogenous stimulator of cell division in the cambial meristem of *Populus*. *PNAS* 106, 5984-5989.
- Nieminen, K., Immanen, J., Laxell, M., Kauppinen, L., Tarkowski, P., Dolezal, K. et al. (2008). Cytokinin signaling regulates cambial development in poplar. *PNAS* 105, 20032-20037.
- Olson, M., Rosell, J., Martinez-Perez, C., Leon-Gomez, C., Fajardo, A., Isnard, S. et al. (2020). Xylem vessel-diameter–shoot-length scaling: ecological significance of porosity types and other traits. *Ecological Monographs* 90, e01410.
- Olson, M., Sorianoa, D., Rosell, J., Anfodillo, T., Donoghue, M., Edwards, E. et al. (2018). Plant height and hydraulic vulnerability to drought and cold. *PNAS* 115, 7551-7556.
- Olson, M., Tommaso, A., Rosell, J., Petit, G., Crivellaro, A., Isnard, S., et al. (2014). Universal hydraulics of the flowering plants: vessel diameter scales with stem length across angiosperm lineages, habits and climates. *Ecol. Lett.* 17, 988-997.
- Riding, R., and Little, C. (1984). Anatomy and histochemistry of *Abies balsamea* cambial zone cells during the onset and breaking of dormancy. *Canadian Journal of Botany* 62, 2570-2579.
- Ritchie, M., Phipson, B., Wu, D., Hu, Y., Law, C., Shi, W. et al. (2015). Limma powers differential expression analyses for RNA-sequencing and microarray studies. *Nucleic Acids Research* 43, e47.

- Robinson, M., McCarthy, D., and Smyth, G. (2010). edgeR: a Bioconductor package for differential expression analysis of digital gene expression data. *Bioinformatics* 26, 139-140.
- Rosell, J., Olson, M., and Anfodillo, T. (2017). Scaling of xylem vessel diameter with plant size: causes, prediction and outstanding questions. *Current Forestry Reports* 3, 46-59.
- Sauter, J., and Neumann, U. (1994). The accumulation of storage materials in ray cells of Poplar wood (*Populus canadensis* “robusta”): effect of ringing and defoliation. *Journal of Plant Physiology* 143, 21-26.
- Savage, J., and Chuine, I. (2020). Coordination of spring vascular and organ phenology in deciduous angiosperms growing in seasonally cold climates. *New Phytologist* 230, 1700-1715.
- Francini, A., and Sebastiani, L. (2019). Abiotic stress effects on performance of agricultural crops. *Horticulturae* 5, 67.
- Scholz, A., Rabaey, D., Stein, A., Cochard, H., Smets, E., and Jansen, S. (2013). The evolution and function of vessel and pit characters with respect to cavitation resistance across 10 *Prunus* species. *Tree Physiology* 33, 684-694.
- Smith, M., Fridley, J., Yin, J., and Bauerle, T. (2013). Contrasting xylem vessel constraints on hydraulic conductivity between native and non-native woody understory species. *Frontiers in Plant Science* 4, 486.
- Smith, T., Heger, A., and Sudbery, I. (2017). UMI-tools: modeling sequencing errors in unique molecular identifiers to improve quantification accuracy. *Genome Research* 27, 491-499.
- Sperry, J., Meinzer, F., and McCulloh, K. (2008). Safety and efficiency conflicts in hydraulic architecture: scaling from tissues to trees. *Plant, Cell and Environment* 31, 632-645.
- Taneda, H. and Tanedo, M. (2004). The criteria for biomass partitioning of the current shoot: water transport versus mechanical support. *American Journal of Botany* 91, 1949-1959.
- Tuominen, H., Sitbon, F., Jacobsson, C., Sandberg, G., Olsson, O., and Sundberg, B. (1997). Altered growth and wood characteristics in transgenic hybrid aspen expressing *Agrobacterium tumefaciens* t-DNA indoleacetic acid-biosynthetic genes. *Plant Physiology* 109, 1179-1189.

- Tyree M., Velez V., and Dalling J. (1998). Growth dynamics of root and shoot hydraulic conductance in seedlings of five neotropical tree species: scaling to show possible adaptation to differing light regimes. *Oecologia* 114, 293-298.
- Venturas, M., Sperry, J., and Hacke, U. (2017). Plant xylem hydraulics: what we understand, current research, and future challenges. *Journal of Integrative Plant Biology* 59, 356-389.
- Wilczek, A., Wloch, W., Iqbal, M., and Kojs, P. (2011). Position of rays and lateral deviation of vessel elements in the stem wood of some dicotyledonous species with storeyed, doublestoreyed, and nonstoreyed cambia. *Botany* 89, 849-860.
- Willis, L., Refahi, Y., Wightman, R., Landrein, B., Teles, J., Huang, K. et al. (2016). Cell size and growth regulation in the *Arabidopsis thaliana* apical stem cell niche. *PNAS* 113, E8238-E8246.
- Yu, D., Wildhagen, H., Tylewicz, S., Miskolczi, P., Bhalerao, P. and Polle, A. (2019). Abscisic acid signaling mediates biomass trade-off and allocation in poplar. *New Phytologist* 223, 1192-1203.
- Yu, D., Janz, D., Zienkiewicz, K., Herrfurth, C., Feussner, I., Chen, S. et al. (2021). Wood formation under severe drought invokes adjustment of hormonal and transcriptional landscape in poplar. *International Journal of Molecular Sciences* 22, 9899.
- Zhao, X., Guo, P., and Peng, H. (2019). An ignored anatomical variable: pore shape shows a nonrandom variation pattern in xylem cross sections. *Nordic Journal of Botany* 37, e02249.
- Zheng, J., Xi, M., Lu, Y., Lu, Y., and Shi, J. (2013). Transcriptional analysis provides new insights into cold and dehydration tolerance signaling pathways and on regulation of stem cell activity in the vascular cambium of poplar. *Plant Molecular Biology Reporter* 31, 75-86.

## **Chapter 4. The effects of genotype and drought on tree physiology and wood anatomy**

**F. Daniela Rodriguez-Zaccaro, Courtney Canning, Andrew Groover**

### **Abstract**

Trees can respond to drought through the production of wood with altered anatomy and through physiological adjustments including stomatal closure, both of which are directly tied to growth and productivity. These responses have been shown to differ in magnitude across genotypes, with varying degrees of altered wood anatomy and stomatal closure. The genetic regulation of these responses, however, is not very well understood. Here, we selected a subset of 8 hybrid poplar genotypes included in a previous screen. Three of these lines have deletions and 3 have insertions spanning a previously identified wood anatomy dosage QTL. Two additional lines were randomly selected as non-lesion controls. Our aim was to make a preliminary evaluation of the effects of drought on growth, physiology and wood anatomy across genotype and lesion category. We found that most measured traits significantly differed across both genotype and lesion category. Most of these traits, however, were unaffected by the drought treatment. Some evidence points to possible drought sensitivity in the deletion lines.

### **INTRODUCTION**

Vessel elements are highly lignified, tube-like cells that allow for the upward and lateral flow of water in angiosperm xylem under tension. These cells form larger pipe-like structures known as vessels, which provide a low resistance water pathway linking roots to leaves. The loss of water vapor through open stomata (transpiration) generates capillary forces that drive the continuous upward flow of water through the xylem network (Pickard 1981). The variation of vessel anatomical traits in wood is significantly tied to tree hydraulic function. In particular, the diameter of vessels is directly related to water transport efficiency, with small increases in

diameter translating to large increases in the upward volumetric flow rate of sap (Tyree et al. 1994; Zwieniecki et al. 2001). The degree of interconnectivity between vessels through pit structures (often assessed through vessel grouping indices) has likewise been related to water transport efficiency, with greater vessel grouping linked to increased stem conductivity (Lens et al. 2010). Water transport efficiency in tree stems is in turn tied to other important functional traits including stomatal conductance, chlorophyll content, photosynthetic capacity and growth (Zhang et al. 2013; Zhang and Cao 2009; Santiago et al. 2004; Campanello et al. 2008). Stomatal conductance, or the degree of stomatal opening (measured through the rate of leaf gas exchange), controls both the rate of water loss and carbon gain through leaves and increases with stem hydraulic conductivity. Stomatal conductance, along with leaf chlorophyll content (often estimated through leaf absorbance) have been used as reliable proxies for photosynthetic capacity (Croft et al. 2016; Kumar et al. 2002). Wood that allows for more efficient water transport, however, can be more vulnerable to freeze-thaw and water stress induced cavitation and embolism (Pockman and Sperry 2000; Gleason et al. 2016; Sperry and Sullivan 1992). Larger diameter vessels in poplar wood have been shown to embolize at lower levels of water stress in relation to narrow vessels (Jacobsen et al. 2019; Cai and Tyree 2010). During drought, progressively lower water potentials can result in runaway embolism that impedes the flow of water through the xylem network, leading to hydraulic failure (Pittermann 2010). The water potential at which 50% of hydraulic conductivity has been lost in a stem due to embolism ( $P_{50}$ ) is often used as a measure of vulnerability to drought (Fichot et al. 2015).

Trees, however, can respond to drought through the production of wood with smaller and more numerous vessels, potentially reducing the risk of cavitation at the cost of water transport efficiency and growth. The magnitude of this response depends on environment, genotype and

growth season (Yu et al. 2021; Arend and Fromm 2007; Fichot et al. 2009). Similarly, the modulation of stomatal conductance under drought conditions varies widely across species and genotypes, with plants displaying different degrees of isohydric or anisohydric water management behaviors (Attia et al. 2015). Isohydric behavior involves avoidance of hydraulic failure through stomatal closure (at the cost of growth), while anisohydric behavior involves maintaining open stomata at the risk of hydraulic failure to maintain high growth rates (Sade et al. 2012).

The genetic regulation of vessel anatomy and related physiological traits, however, is not very well understood. In a previous screen using a mutant poplar hybrid population, we found that some wood anatomical traits were significantly correlated to specific areas of the genome in a dosage-dependent manner. In particular, height-corrected mean vessel diameter (cMVD) and height-corrected vessel frequency (cVF) showed the strongest relationship of any examined trait to any genomic region, both showing a strong correlation to a 1.2 Mb region in chromosome 9. Genotypes with deletions spanning this region showed increased cMVD and decreased cVF in relation to controls, while those with insertions showed the opposite pattern (see “Chapter 2, Results”). Here, we selected a subset of 8 genotypes included in the previous screen to assess previously unexamined physiological traits. Three of these lines have deletions and 3 have insertions spanning the aforementioned genomic region. Two additional lines were randomly selected as non-lesion controls. Our aim is to make a preliminary evaluation of general growth, physiological and wood anatomical traits across genotype, lesion category and watering regimes. A list of all measured traits is included in Tables 4.1 and 4.2. We hypothesize that both genotype and lesion category will have a significant effect on measured traits under well-watered conditions. In addition, we hypothesize that a chronic drought treatment will significantly affect

the measured traits and that the effect of drought will be dependent on genotype and lesion category. We predict that the deletion lines will be the most detrimentally affected by drought and that the insertion lines will be the most resilient. Lastly, we hypothesize that the measured traits will correlate to each other as shown in previous studies. In particular, mean vessel diameter and vessel frequency are expected to correlate to water transport efficiency and vulnerability to cavitation.

## **MATERIALS AND METHODS**

### **Plant materials and growing conditions**

Eight hybrid poplar genotypes were selected from a larger group of lines included in two previous studies (see “Chapters 2 and 3”). These lines originate from a larger group of interspecific F1 hybrids produced through crosses between two female *Populus deltoides* and the gamma-irradiated pollen of a male *Populus nigra*. The F1 hybrids were analyzed to detect radiation-induced large-scale insertions and deletions (indel mutations) after complete sequencing through Illumina short reads (Henry et al. 2015). The complete pedigree consists of approximately 800 lines, many of which have large indel mutations (ranging in size from 0.1 MB to whole chromosomes) with known genomic locations. These lines are kept in an outdoor garden at the US Forest Service Institute of Forest Genetics (IFG) in Placerville, CA. The eight genotypes studied during the current project were selected based on the presence of indel lesions spanning a previously identified dosage QTL (dQTL) region related to height-corrected mean vessel diameter and height-corrected vessel frequency. The region consists of 4 contiguous genomic bins in chromosome 9, starting at 6.3 and ending at 7.5 MB (see “Chapter 2”). Three genotypes have deletions, and 3 genotypes have insertions spanning this location; 2 additional genotypes were randomly selected as non-lesion controls (Table 4.1).

Multiple replicates (ramets) of the 8 lines were clonally propagated through stem cuttings from the field during the Spring of 2020. Cuttings were planted in individual tubes containing horticultural soil (Sungro Sunshine Mix #4) and rooting hormone (Bontone). Cuttings were kept inside an IFG greenhouse at a temperature of  $\sim 24^{\circ}\text{C}$  and watered through diurnal interval misting. After a period of 3 ½ months, 8 clonal replicates per line (n=64) were selected for transfer into eight 94.6 L pots. Each pot was filled with a mix of peat moss, gravel and perlite in a 2:1:1 ratio, along with fertilizer (Osmocote) at a concentration of 14 g/Kg of soil. One replicate per line was planted in each pot, with a total of 8 plants per pot spaced  $\sim 20$  cm apart in a circular arrangement. This particular design was chosen to minimize the effect of genotype size differences on soil drying rate. The field capacity of this soil mix was estimated prior to planting (see “Soil field capacity estimation” below). Plants were allowed to become established in the pots for a period of 3 weeks inside the same greenhouse and watered by hand to saturation every 4-5 days. Pot positions within the greenhouse were randomly shuffled once a week.

### **Soil field capacity estimation**

The field capacity of the peat moss, gravel and perlite soil mix (2:1:1) was estimated through an adapted version of Cassel and Nielsen’s procedure for measuring container capacity (1986). Three 94.6 L pots were filled with the soil mix and left to dry under the sun for a minimum of 1 week. Volumetric water content was then measured using a time domain refractometer (HydroSense II, Campbell Scientific). Soil with greater than 0% volumetric water content (VWC) was left to dry for a longer period of time until reaching this value. The three soil-filled pots were then weighed, and dry soil weight was obtained after subtracting the pot weight. Pots were then watered to saturation, covered, and allowed to drain for 2 days before

obtaining soil weight at saturation. The field capacity of the soil within each pot was calculated by subtracting the dry soil weight from the water-saturated soil weight (Cassel and Nielsen 1986). An average value of 0.41 Kg of water/ Kg of soil was obtained from the 3 pots.

### **Drought treatment**

After a 3-week establishment period, each of the 8 pots was randomly assigned to either a drought or a well-watered control treatment. The drought treatment consisted of withholding water until reaching a soil water content target range of 25 to 35% of field capacity, with the aim of maintaining this range for a minimum of 4 weeks. This was assessed by weighing pots every 3-4 days. All drought pots reached the desired soil moisture range by week 2 of the experiment (Figure 4.1). Control pots were watered to saturation every 4-5 days and monitored by weighing once a week to obtain percentage of field capacity. The effect of the drought treatment was assessed every week by monitoring tree height and tree diameter (see “5-week experiment period: trait measurements and data analysis” below). By week 3 it was determined that these traits were not significantly different across drought and control treatments. The target soil water content was thus lowered to 10 to 15% of field capacity during weeks 4 and 5 (Figure 4.1). Pot locations within the greenhouse were randomly shuffled once a week during this time period.

### **5-week experiment period: trait measurements and data analysis**

The following traits, included in Table 4.2, were measured once a week on all trees (n=64) during the course of a 5-week experiment period: stomatal conductance (Gs), SPAD values (SPAD), tree height (TH), tree diameter (TD), total leaf number (LN) and average leaf area (LA). Drought and control assigned pots did not differ significantly in soil moisture content during week 1 measurements (Figure 4.1). Our aim during week 1 was to focus on testing for trait differences across genotype and lesion category under well-watered conditions with the

maximum amount of replication for each line (8/line). Drought and control assigned pots differed significantly in soil moisture content from week 2 to week 5 (Figure 4.1). Here, our aim was to test for trait differences across treatment type, and to test for interactions between treatment and line.

#### *Stomatal conductance measurements*

Stomatal conductance to water vapor ( $\text{mmol m}^{-2} \text{s}^{-1}$ ) and leaf temperature were measured once a week using a steady state porometer (SC-1, Meter Group). The 4<sup>th</sup> and 5<sup>th</sup> fully expanded leaves from the shoot apex on each tree were tagged for Gs measurements every week on the day prior to measuring. An average Gs value for each tree was obtained from two measurements (1/leaf). During week 1, Gs was measured across 3 different time blocks: 9:00-11:00 AM, 12:00-2:00 PM, and 3:00-5:00 PM across 2 consecutive days. Thirty-two plants were sampled on each day to allow for enough time to measure all 64 plants within each 2-hour block. Gs was compared across time blocks to determine the length of the midday Gs measurement time window for weeks 2 through 5. As there was no significant difference in Gs between time blocks on both days (Figure 4.2) we established an 11:00 AM to 3:00 PM measurement time window in which all 64 plants could be sampled in the same day. Gs was not measured during week 4 due to a porometer malfunction.

#### *SPAD, tree height, tree diameter, total leaf number and average leaf area measurements*

SPAD values were obtained once a week with a chlorophyll meter (SPAD 502, Spectrum Technologies) by sampling the same leaves that were tagged for Gs measurements. One SPAD value was obtained from each leaf (2 values/tree) from which an average was obtained for analysis. SPAD values are the ratio of red light to infrared light transmittance across a leaf and

are used to estimate relative leaf chlorophyll content (Jiang et al. 2017). Tree height was measured from the point of emergence from the original cutting to the shoot apex. Tree diameter was measured at 10 cm from the point of emergence from the original cutting, obtaining an average from two measurements using digital calipers. Total leaf number was obtained by manually counting all unfolded leaves from the shoot apex to the base of each tree. Lastly, average leaf area was obtained non-destructively by photographing 4-5 leaves on each tree against a handheld white flat background with a ruler. Leaves were selected for photographing starting with the 4<sup>th</sup> fully expanded leaf and then photographing every other leaf towards the base of the tree. Photographs were processed using Fiji ImageJ software (v2) to obtain an average leaf area per tree. Only photographs taken during week 1 were processed to obtain leaf area data.

#### *Data analysis*

Trait data obtained throughout all 5 weeks were transformed, when necessary, through Box-Cox power transformations. Pearson's correlation tests between all trait combinations were run using week 1 data. Two-way ANOVA tests were run with trait data from each week, with genotype and lesion category as independent factors during week 1, and an additional treatment factor during weeks 2 through 5. Gs ANOVA tests involved an additional collection time factor. ANOVA tests using week 1 Gs data were run to determine an appropriate Gs collection time window for weeks 2 through 5. Here, sampling time-block, collection date, pot, leaf temperature and genotype (or lesion category) were independent factors in the model. Tukey's HSD tests were used to show pairwise significant differences across groups. All data were processed and analyzed in base R.

## **Post-harvest trait measurements and data analysis**

The traits included in Table 4.3 were measured after a 5-week experiment period on harvested trees. As the drought treatment did not significantly affect tree growth traits (TH, TD, LN), only control group trees were sampled for Ks and P<sub>50</sub>. An exception was made for non-lesion lines, for which both control and drought plants were sampled to test for trait differences between treatments. A total of 31 trees were sampled (25 control and 6 drought group plants), with at least 3 replicates per line and treatment. Wood anatomical traits were measured on the control group samples used to measure Ks and P<sub>50</sub> (n=25).

### *Stem specific hydraulic conductivity measurements*

Stem specific hydraulic conductivity (Ks) and vulnerability to cavitation (P<sub>50</sub>) were obtained from harvested trees after the 5-week experiment period, between September and October of 2020. Final height and diameter were measured for each tree before cutting at ~10 cm from the point of emergence from the original propagated stem. Each tree was immediately placed under water and cut down into a 14 cm stem segment using single-edged razorblades. The midpoint of each 14 cm sample coincided with the final height midpoint of the original tree (50% of final tree height). To remove emboli, samples were immersed in a 20 mM KCL solution and vacuum infiltrated at -71 kPa for a minimum of 4 hours. This solution was made with DI water that had been previously degassed using a 0.2 µm filter membrane contactor (Liqui-Cell Minimodule, Membrana). Ks was then measured gravimetrically using a conductivity apparatus based on a design first described by Sperry et al. (1988). Briefly, a stem sample was connected with tubing to an elevated IV bag reservoir on one end and a graduated pipette on the other. A degassed 20 mM KCL solution was then allowed to flow from the IV bag, through the stem

sample, and out through the pipette. The flow rate of solution through the stem ( $Q$ , kg/s) was obtained by timing the movement of a water meniscus through the pipette.  $K_s$  was calculated using the equation below (equation 1), where  $Q$  is the flow rate of the solution through the stem,  $L$  is the length of the sample,  $\Delta P$  is the pressure difference across the sample and  $A_{sw}$  is the cross-sectional area of conducting wood (Melcher et al. 2012).

$$K_s = Q \times L / (\Delta P \times A_{sw}) \quad \text{equation 1}$$

#### *Vulnerability to cavitation curves and $P_{50}$ estimates*

Vulnerability to cavitation curves were constructed using the standard centrifuge method described by Alder et al. (1997) and modified by Tobin et al. (2013). After obtaining  $K_{s_{max}}$  values ( $K_s$  measured after removing emboli, described above), stems were spun in a custom centrifuge rotor at progressively greater speeds (rpm) to induce increasingly negative pressures inside the xylem.  $K_s$  was measured after every spin until reaching a percent loss of conductivity (PLC) of at least 90%. An equation for PLC is included below, where  $K_{s_i}$  is the current conductivity after spinning and  $K_{s_{max}}$  is the maximum flow rate prior to any spinning (equation 2). A PLC value at every induced xylem pressure was obtained for each stem (at -0.25, -0.50, -1.0, -1.5, and -2.0 MPa). The R package “fitplc” was then used to fit vulnerability curves from PLC data using a Weibull model.  $P_{50}$ , or the pressure at which 50% of  $K_s$  has been lost, was then estimated from these curves, along with 95% confidence intervals (Duursma and Choat, 2017). Three types of vulnerability curves were constructed with the same data: genotype level curves, lesion category level curves and treatment group level curves. For genotype level curves, a single curve was fitted for each separate genotype, obtaining a single  $P_{50}$  estimate per line. For lesion category level curves, a single curve was fitted for each lesion category, estimating one  $P_{50}$  value

per lesion group. Treatment group level curves were produced with data from control and drought plants from non-lesion lines. Stem samples were then stored at -20°C before processing for wood anatomical measurements.

$$PLC = 100(1 - K_{Si}/K_{S_{max}}) \quad \text{equation 2}$$

#### *Wood anatomical trait measurements*

Wood anatomical traits were measured on the same 25 control group samples used for vulnerability curves (8 lines, with a minimum of 3 replicates per line). Stems were cut in 40 µm thick cross-sections using a vibratome (Vibratome Series 1000) and stained with a mixture of phloroglucinol and Astra Blue dyes. Dye-mounted sections were placed under a microscope at ×5 or ×10 magnification and photographed with a digital camera with standardized settings (Leica Microsystems). A scale bar was included in each image, adjusted for specific magnification. A single micrograph of each stem sample was selected for image analysis. Wood anatomical trait data were then obtained by processing the selected images through Fiji ImageJ software (v2). To establish the scale of the image, the known scale bar length was used to determine the number of pixels per micrometer. Xylem thickness (XT) was obtained by calculating the average distance between the edge of the pith and the vascular cambium. Images were then converted to grayscale and segmented into a vessel lumen particle foreground and a non-vessel lumen area background. Vessel number, lumen areas and circularities were automatically obtained through the Analyze Particles tool, with equivalent circle vessel diameters calculated from vessel areas. Mean vessel diameter (MVD) and hydraulic mean vessel diameter (hMVD) were obtained from each image. Hydraulic MVD was calculated by assigning a greater weight to larger diameter conduits, as these conduits contribute disproportionately to stem conductivity (Scholz et al., 2013). Mean vessel circularity (MVC) was calculated as the

simple mean of all vessel circularities in an image. Circularity is a unitless value ranging from 0 to 1 which describes the cross-sectional shape of vessels. Values closer to 0 represent highly elongated shapes and values closer to 1 represent shapes approaching perfect circularity. Vessel frequency (VF) was calculated by dividing the number of vessels by the total xylem area (mm<sup>2</sup>). A vessel grouping index (VGI) was obtained for each image by dividing the number of vessels by the number of vessel groups. Vessel groups were counted manually using the Multi-point tool. A vessel group consists of anything from a solitary vessel to any number of clustered vessels with secondary walls that are in contact (Carlquist, 2001).

### *Data analysis*

Post-harvest measured traits (Table 4.3) were transformed, when appropriate, through Box-Cox power transformations. Pearson's correlation coefficients and values of P were obtained for all trait combinations excluding P<sub>50</sub>, as a single P<sub>50</sub> value was estimated per genotype. A second set of correlation tests was performed between P<sub>50</sub> values and the average genotype values of all other traits. ANOVA based tests were run with all non P<sub>50</sub> trait data, with pot and genotype (or lesion category in a separate model) as independent factors. Tukey's HSD tests were used to show pairwise significant differences across groups. Significant differences between the P<sub>50</sub> values of genotypes, lesion categories and treatment groups were determined based on the 95% confidence intervals around each estimate. Non-overlapping intervals indicate a significant difference. All data were processed and analyzed in R.

## **RESULTS**

### **5-week experiment period**

The traits included in Table 4.2 were measured once a week on 8 hybrid poplar genotypes (8 replicates per line, lines described in Table 4.1) during a 5-week drought experiment period.

During week 1 measurements, there was no significant difference in soil moisture content across control and drought group-assigned pots (Figure 4.1). Control and drought group pots had a moisture content average of 84 and 78% of field capacity, respectively.

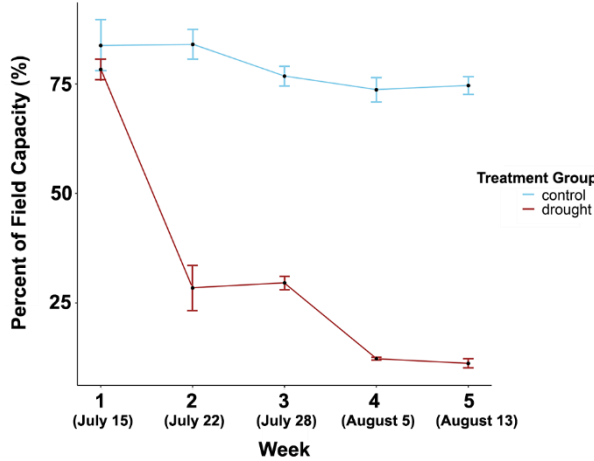


**FIGURE 4.1** | Percentage of field capacity obtained for soil in 8 (94.6 L) pots across 5 weeks (from July to August 2020). Four pots were assigned to a well-watered control group and four to an increasingly severe drought treatment. The dots represent the means, and the bars depict the standard errors.

**TABLE 4.1** | Indel lesion locations of eight *P. deltoides* × *nigra* genotypes selected for the current project. Lesion types include deletions (dl) and insertions (in) spanning a previously identified dQTL region in chromosome 9. Non lesion (nl) genotypes were selected as controls.

Genotype	Lesion type	Lesion start (MB)	Lesion end (MB)
GWR_100_283	dl	5.6	10.4
XXX_100_043	dl	0	12.95
XXX_100_093	dl	0	12.95
XXX_100_179	nl	-	-
GWR_100_158	nl	-	-
GWR_100_369	in	6.8	12.95
GWR_100_447	in	6.3	7.1
XXX_100_250	in	6.3	10.1

**TABLE 4.2** | Traits examined across 8 hybrid poplar lines (*P. deltoides* × *P. nigra*, n=64) over the course of a 5-week drought treatment from July 13 to August 15, 2020.

Trait	Abbr.	Units
Stomatal conductance	Gs	mmol m <sup>-2</sup> s <sup>-1</sup>
SPAD value	SPAD	unitless
Tree height	TH	cm
Tree diameter	TD	mm
Total leaf number	LN	number of leaves
Average leaf area	LA	cm <sup>2</sup>

### *Stomatal conductance across three time blocks*

During week 1, stomatal conductance (Gs) was measured across three 2-hour time blocks (9:00-11:00 AM, 12:00-2:00 PM, and 3:00-5:00 PM) over the course of two consecutive days. Half of all plants were sampled on each day (32 per day). Gs did not change significantly across the three examined time blocks during either day (Figure 4.2), despite a difference in leaf temperature across time blocks. Leaf temperatures were significantly greater during the 3:00-5:00 PM time window on both days. There was no significant difference in Gs across the 2 collection days. Genotype and lesion category, however, had a statistically significant effect on Gs. Across all three time periods, the deletion lines (dl) showed significantly greater Gs compared to non-lesion (nl) and insertion (in) lines (Figure 4.2). A time block factor was included in this analysis to determine the maximum length of the midday Gs collection time window for the drought treatment (weeks 2-5). A time window of 11:00 AM to 3:00 PM was thus chosen to allow for the collection of Gs from all 64 plants on the same day, without time of day as a confounding factor.

### *Pearson's correlation tests between traits*

Pearson's correlation tests were run between all trait combinations using week 1 data. Significant correlations ( $P < 0.05$ ) were found between many of the measured traits (Figure 4.3). Namely, all tree growth parameters: tree height (TH), tree diameter (TD), total leaf number (LN), and average leaf area (LA) were highly positively correlated to each other. Correlations ranged from  $R = 0.44$  between LA and LN to  $R = 0.93$  between TH and TD. Midday stomatal conductance (collected between 12:00 to 2:00 PM) was weakly to moderately negatively correlated to TH, TD and LN, but not to LA or SPAD. SPAD values were not significantly correlated to any other trait (Figure 4.3).

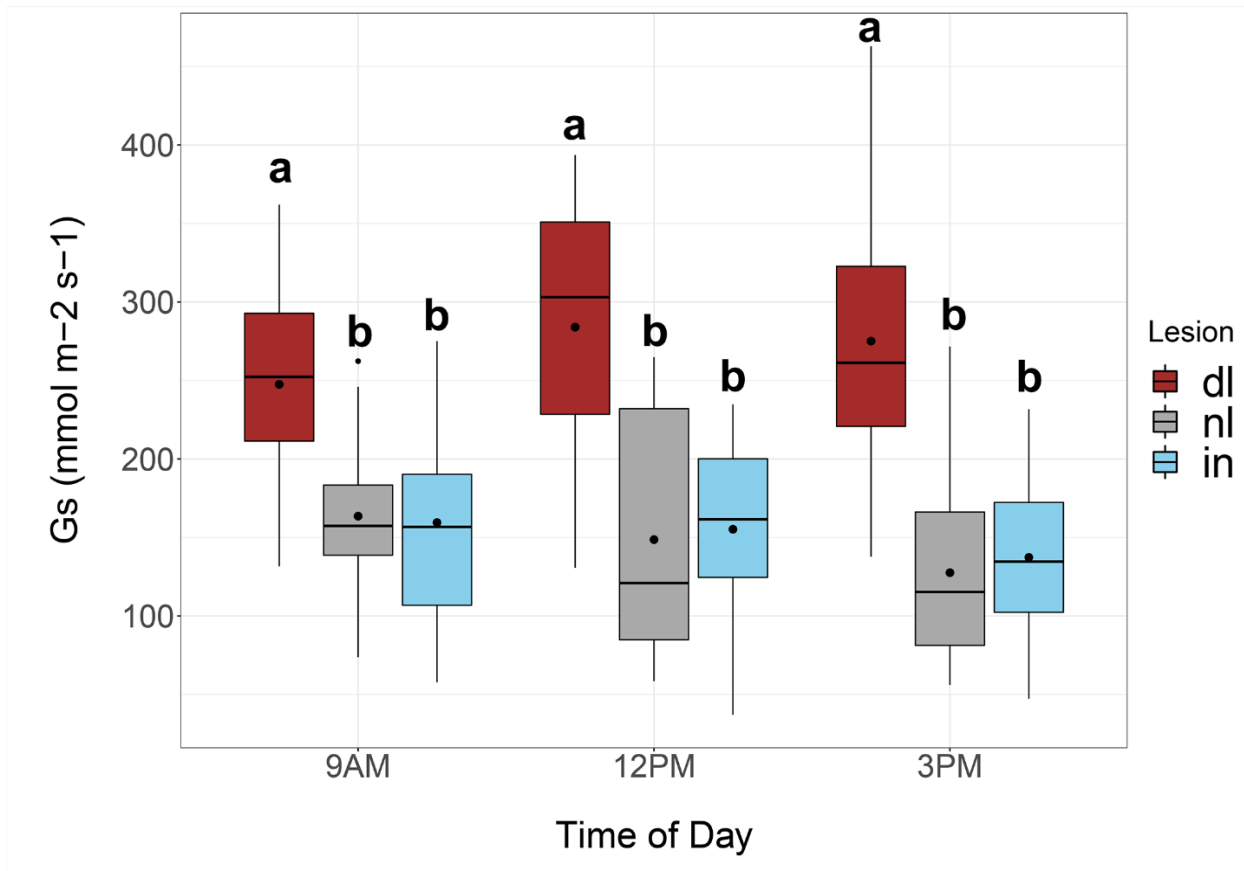


**FIGURE 4.2** | Stomatal conductances (Gs) of 8 hybrid poplar genotypes (n=64) sampled across 3 time blocks on July 14 and 15, 2020. Time blocks range from 9AM to 11AM, 12PM to 2PM and 3PM to 5PM. Genotypes are grouped into 3 lesion categories: **dl** (3 genotypes with a deletion spanning a dQTL in Chr09), **nl** (2 control genotypes with no lesions) and **in** (3 genotypes with an insertion spanning a dQTL in Chr09). The horizontal lines represent the medians and the dots represent the means. Tukey’s honestly significant difference (HSD) test was used to show significant differences of Gs means across lesion categories and time blocks; means that share a letter are not significantly different ( $P_{adj} > 0.05$ ).

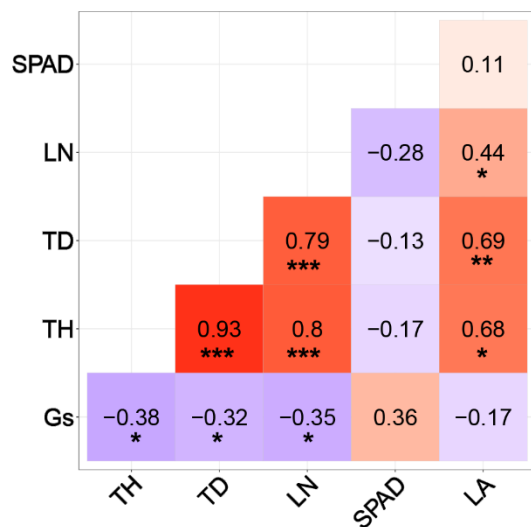


**FIGURE 4.3** | Pearson correlation coefficients between traits across 8 hybrid poplar genotypes during the week of July 13, 2020 (week 1 of current study). Traits include tree height (TH), tree diameter at 10 cm from the ground (TD), total leaf number (LN), SPAD value (SPAD), average leaf area (LA), and midday stomatal conductance (Gs). Asterisks indicate significant correlations between traits (\* $p \leq 0.05$ ; \*\* $p \leq 0.01$ ; \*\*\* $p \leq 0.001$ ).

### *Growth and physiological traits across genotype and lesion category*

An ANOVA test was run for each measured trait, using week 1 data to determine the effects of genotype and lesion category under well-watered conditions. Only Gs data from the 12:00-2:00 PM time window were used in this analysis. Pot and genotype, and pot and lesion category were treated as independent factors in separate models. Genotype and lesion category had a significant effect ( $P < 0.0001$ ) on almost all measured traits. The exception was LA, which differed across genotype, but not lesion category. Pot did not have a statistically significant effect on any trait ( $P > 0.05$ ). Tukey HSD post hoc tests determined that deletion (DL) lines had significantly greater Gs and SPAD values than non-lesion (NL) and insertion (IN) lines, which did not differ between each other. NL lines had significantly greater TH, TD and LN (Figures 4.4, 4.5). LA was significantly different between genotypes within the DL and IN lesion categories (Figure 4.4). Additional ANOVA and post hoc tests were run using week 2 through 5 data from control group plants. Broadly, the results obtained from week 1 data were similar to those obtained from control plants for the rest of the 5-week period (Figures 4.6-4.13). NL lines were taller in week 1, but no different from IN lines by week 2.

### *Growth and physiological traits across genotype, lesion category and treatment*

Control and drought treatment assigned pots differed significantly in soil moisture content from weeks 2 to 5 (Figure 4.1). Drought pots were kept within a soil moisture content range of 25 to 35% of field capacity during week 2 and 3 measurements. During weeks 4 and 5, drought pots were kept within a moisture range of 10 to 15% of field capacity (Figure 4.1). An ANOVA test was run for each measured trait during each week (weeks 2-5) to determine the effects of genotype, lesion category and treatment. Treatment and genotype, and treatment and lesion category were treated as independent factors in separate models. LA is excluded from

these analyses, as this trait was only obtained for week 1. Treatment did not significantly affect SPAD, TH, or TD throughout this period. Treatment, however, had a significant effect on Gs during weeks 2 through 5, and on LN during week 5. Gs ANOVAs showed significant interactions between genotype and treatment, and between lesion category and treatment during all weeks, which suggests that treatment affected only some genotypes and lesion categories. Tukey HSD post hoc tests determined that Gs was significantly lower in drought-treated DL lines compared to control DL lines across all weeks (Figures 4.6-4.9, 4.12-4.13). Gs did not differ between drought and control NL plants across all weeks. Gs was significantly lower in drought-treated IN lines only until week 5 (Figure 4.13a). In addition, the DL drought group started to show significantly lower LN only until week 5 (Figure 4.13e). Both genotype and lesion category had a statistically significant effect on all traits during all weeks. DL lines had the greatest Gs and SPAD values regardless of treatment group, while NL lines had significantly greater TD and LN, regardless of treatment (Figures 4.6-4.13).

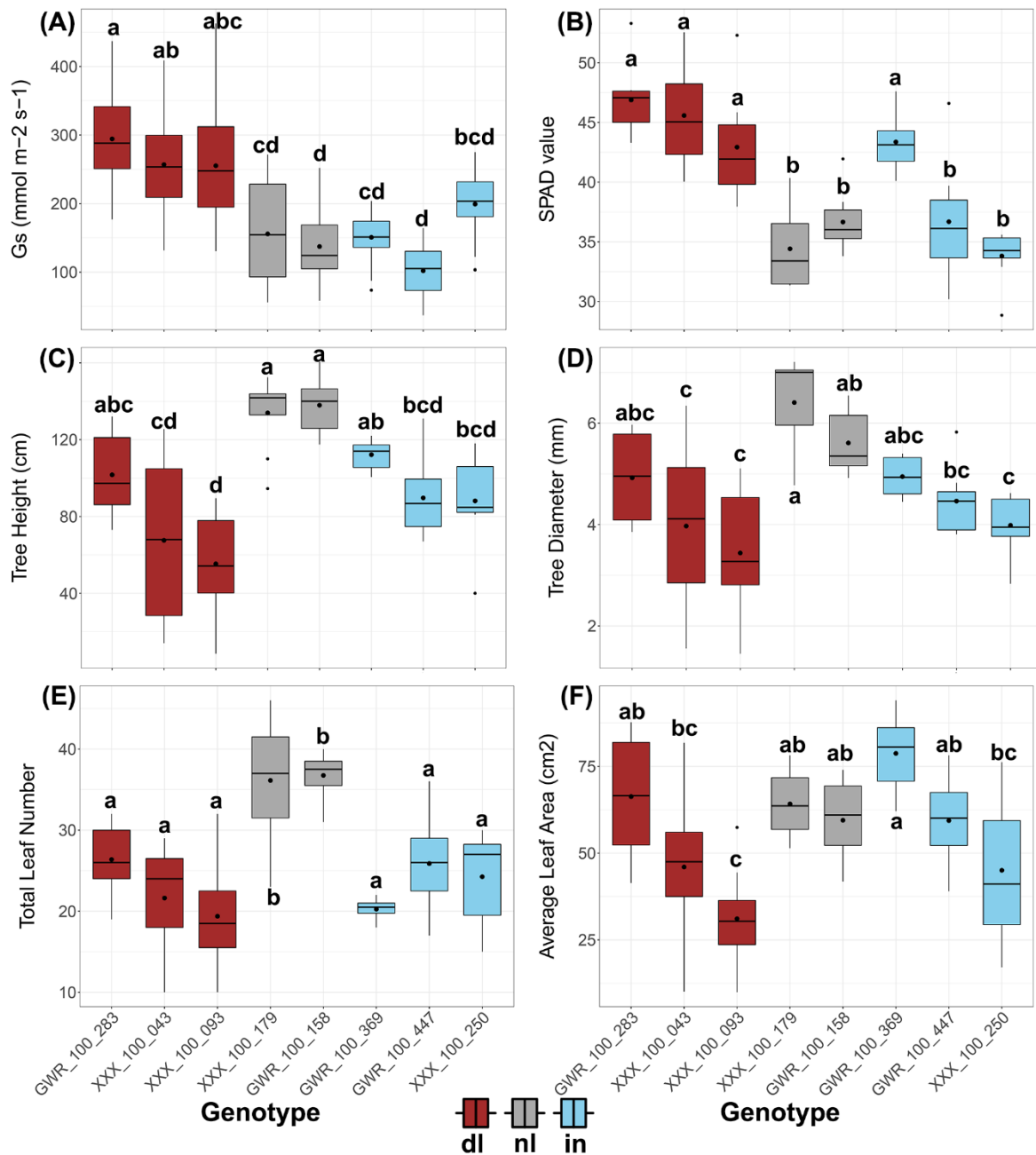


**FIGURE 4.4** | Traits measured on 8 hybrid poplar genotypes (n=64) collected during the week of July 13, 2020 (week 1 of current study). Genotypes are grouped into 3 lesion categories: **dl** (3 genotypes with a deletion spanning a dQTL in Chr09), **nl** (2 control genotypes with no lesions) and **in** (3 genotypes with an insertion spanning a dQTL in Chr09). The horizontal lines represent the medians, and the dots represent the means. Tukey's HSD test was used to show significant differences of means across genotypes; means that share a letter are not significantly different ( $P_{adj} > 0.05$ ). \*Gs (A) data shown collected on July 14 and 15, 2020, from 12 to 2PM.

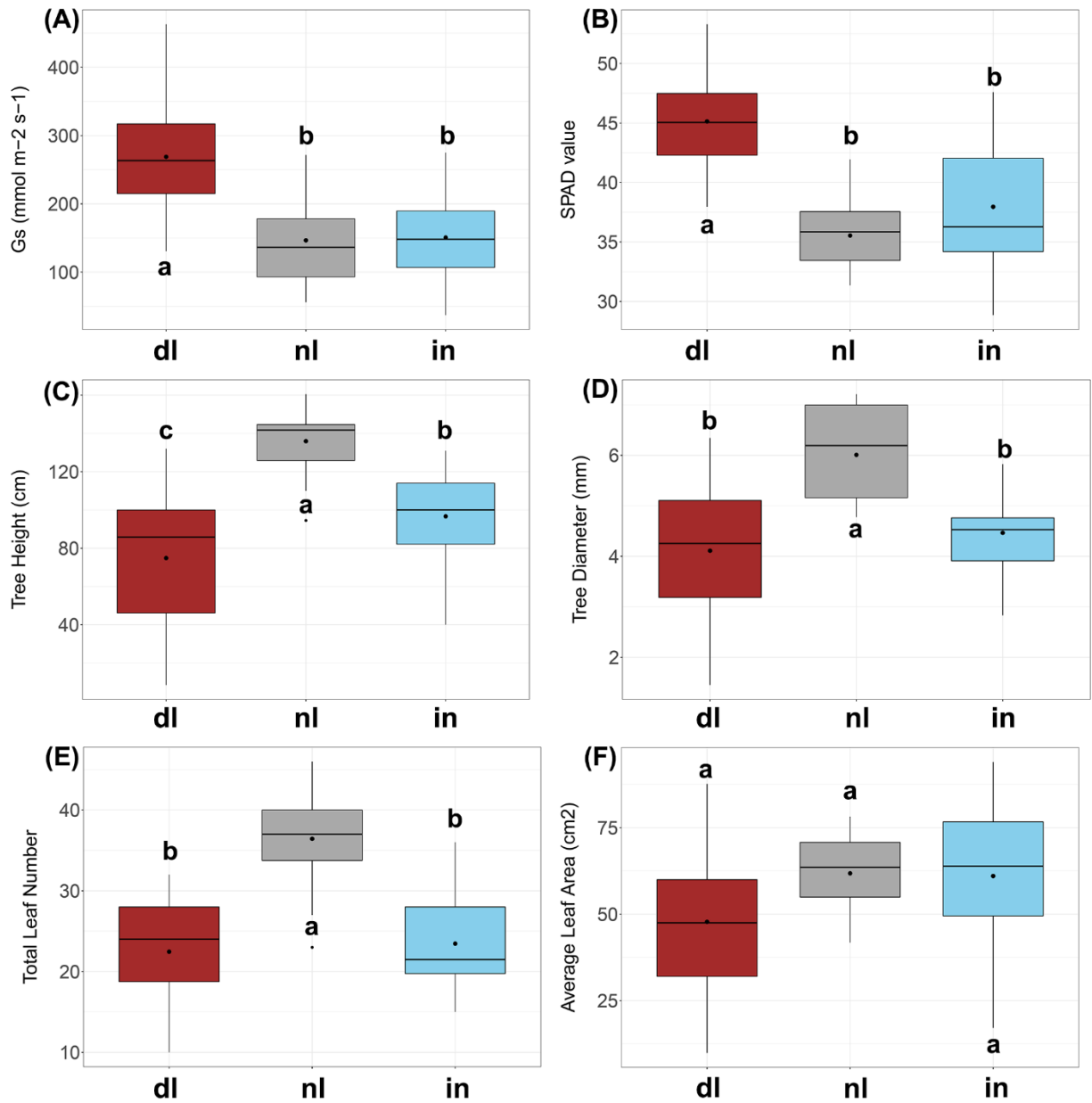


**FIGURE 4.5** | Traits measured on 8 hybrid poplar genotypes (n=64) collected during the week of July 13, 2020 (week 1 of current study). Genotypes are grouped into 3 lesion categories: **dl** (3 genotypes with a deletion spanning a dQTL in Chr09), **nl** (2 control genotypes with no lesions) and **in** (3 genotypes with an insertion spanning a dQTL in Chr09). The horizontal lines represent the medians, and the dots represent the means. Tukey's HSD test was used to show significant differences of means across lesion groups; means that share a letter are not significantly different ( $P_{adj} > 0.05$ ). \*Gs (A) data shown collected on July 14 and 15, 2020, from 12 to 3PM.

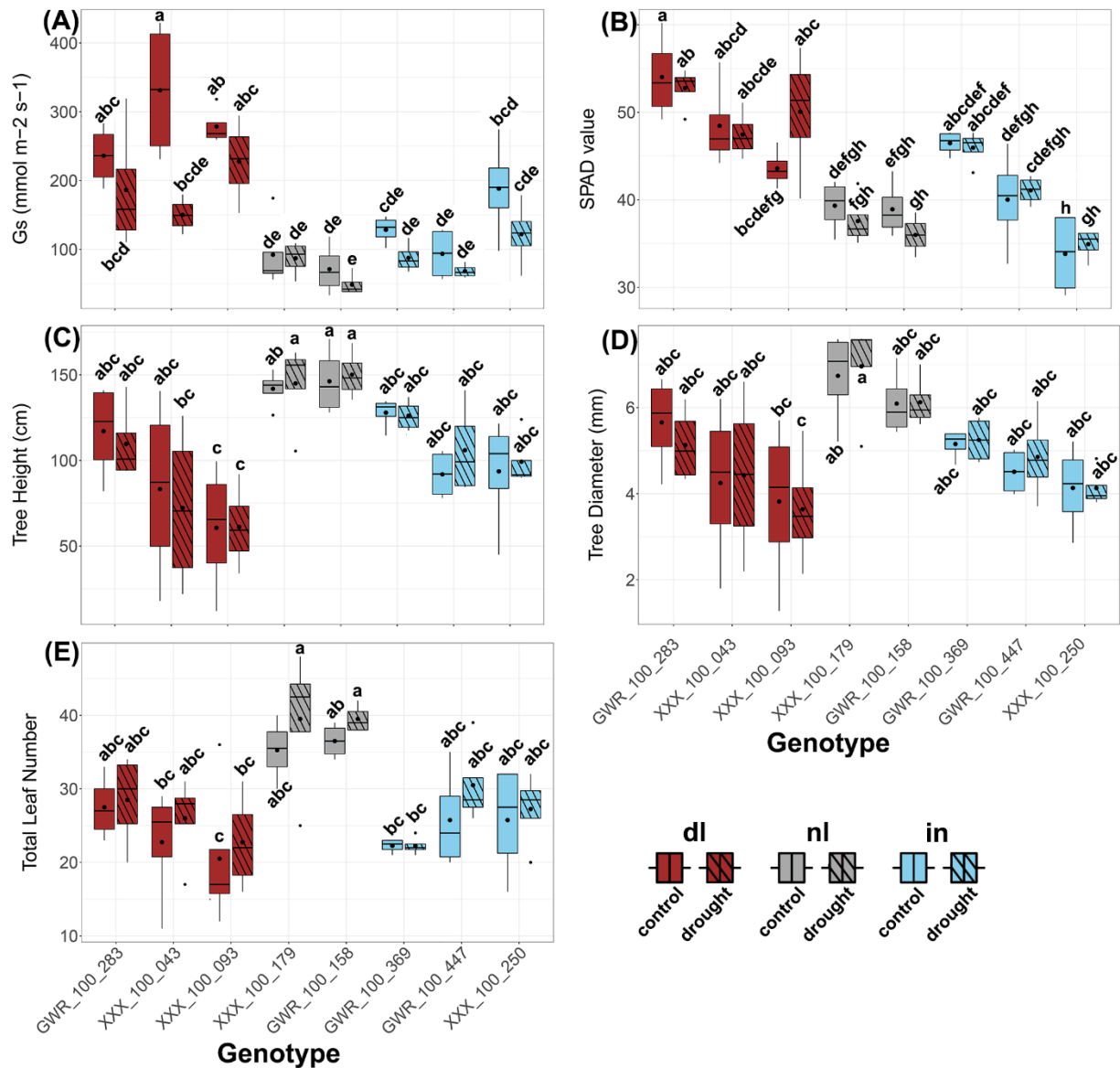


**FIGURE 4.6** | Traits measured on 8 hybrid poplar genotypes (n=64) collected during the week of July 20, 2020 (week 2 of current study). Genotypes are grouped into 3 lesion categories: **dl** (3 genotypes with a deletion spanning a dQTL in Chr09), **nl** (2 control genotypes with no lesions) and **in** (3 genotypes with an insertion spanning a dQTL in Chr09). Solid color boxes depict well-watered control trees (n=32), and diagonal line boxes show drought-treated trees (n=32). The horizontal lines represent the medians, and the dots represent the means. Tukey's HSD test was used to show significant differences of means across genotypes; means that share a letter are not significantly different (P adj > 0.05). \*Gs (A) data shown collected on July 22, 2020, from 11 to 3PM.

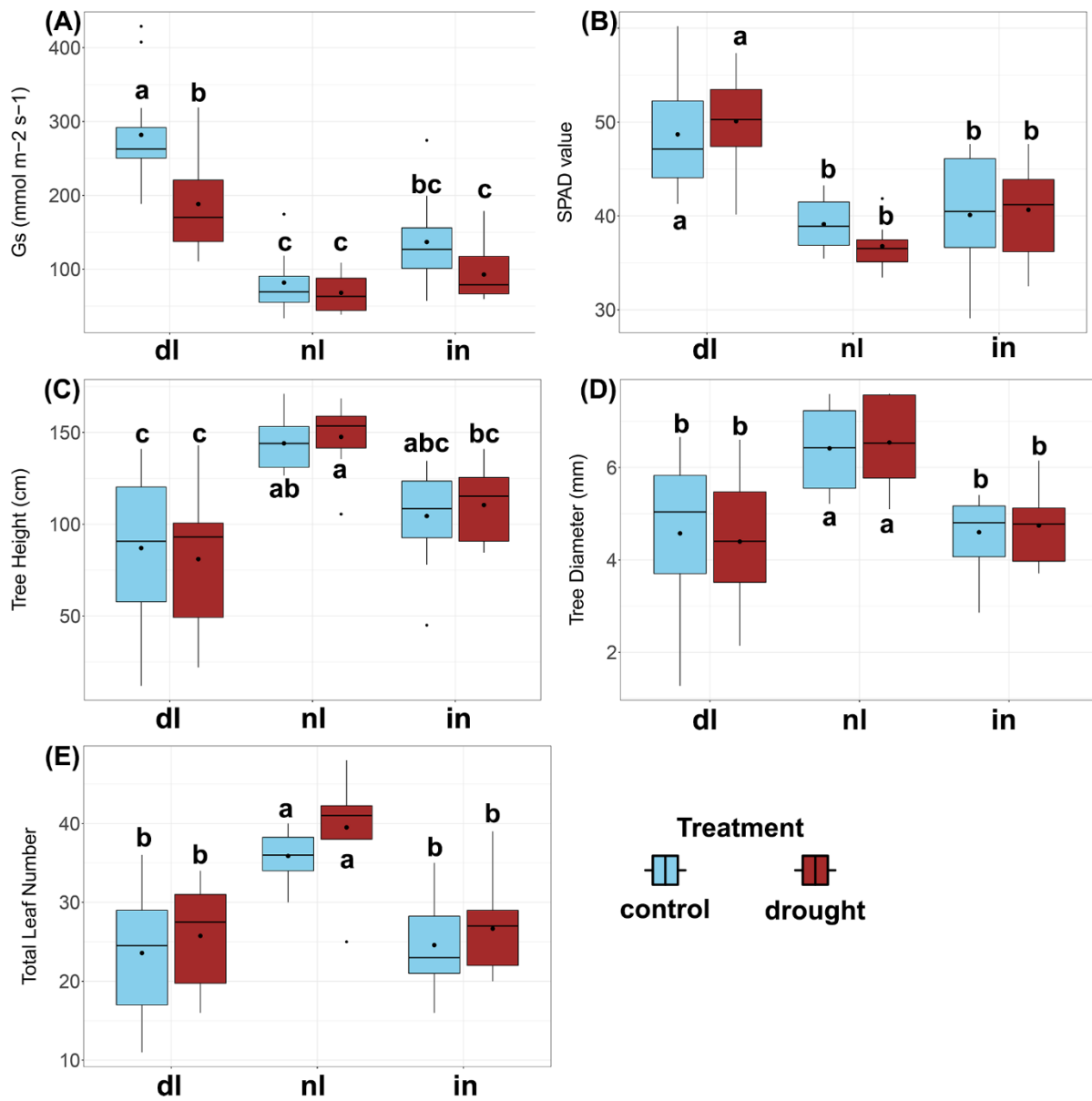


**FIGURE 4.7** | Traits measured on 8 hybrid poplar genotypes (n=64) collected during the week of July 20, 2020 (week 2 of current study). Replicates of each genotype are grouped into a well-watered control (n=32) or a drought treatment group (n=32) by week 2. Genotypes are grouped into 3 lesion categories: **dl** (3 genotypes with a deletion spanning a dQTL in Chr09), **nl** (2 control genotypes with no lesions) and **in** (3 genotypes with an insertion spanning a dQTL in Chr09). The horizontal lines represent the medians, and the dots represent the means. Tukey's HSD test was used to show significant differences of means across lesion groups; means that share a letter are not significantly different ( $P_{adj} > 0.05$ ). \*Gs (A) data shown collected on July 22, 2020, from 11AM to 3PM.

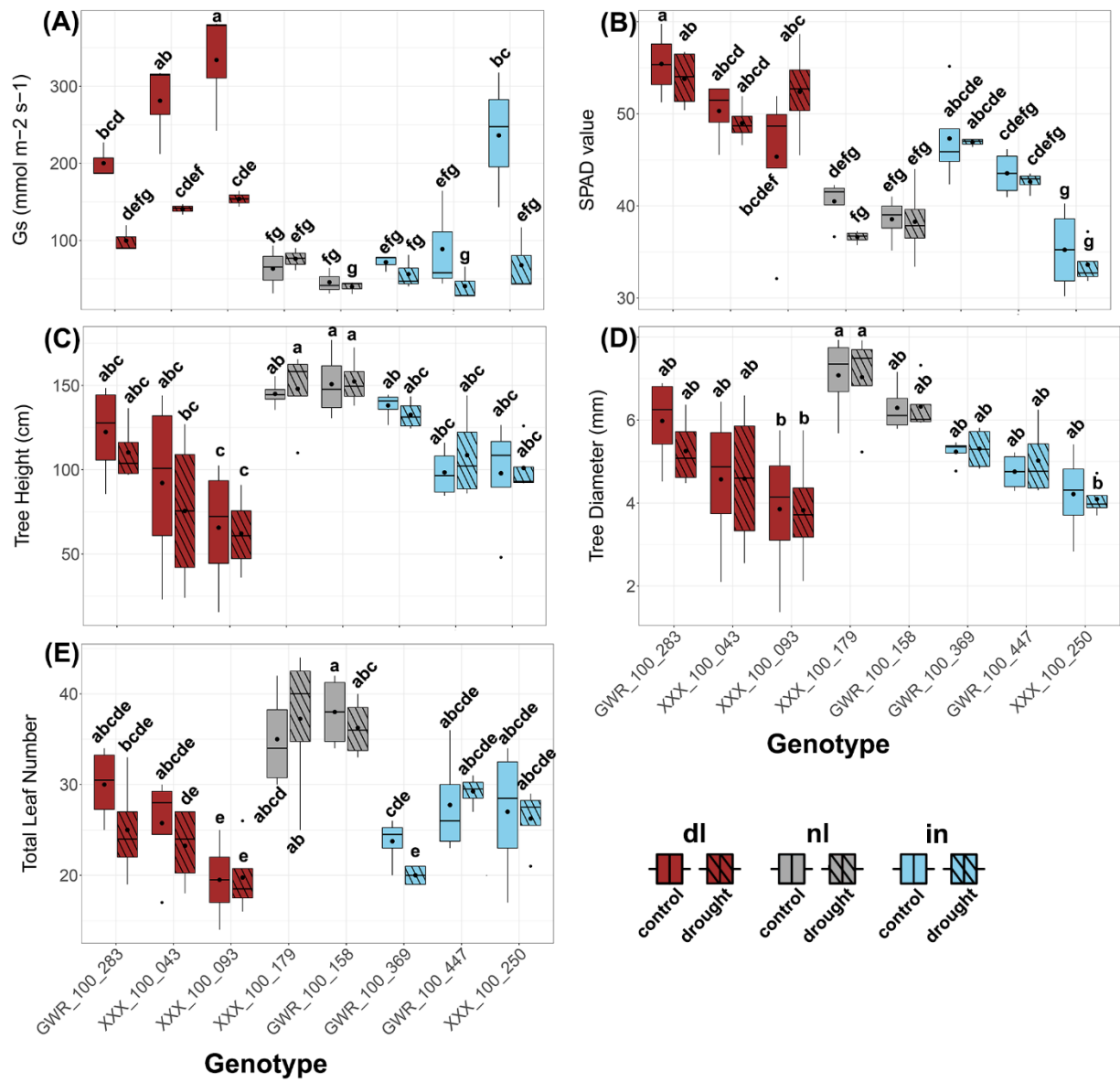


**FIGURE 4.8** | Traits measured on 8 hybrid poplar genotypes (n=64) collected during the week of July 27, 2020 (week 3 of current study). Genotypes are grouped into 3 lesion categories: **dl** (3 genotypes with a deletion spanning a dQTL in Chr09), **nl** (2 control genotypes with no lesions) and **in** (3 genotypes with an insertion spanning a dQTL in Chr09). Solid color boxes depict well-watered control trees (n=32), and diagonal line boxes show drought-treated trees (n=32). The horizontal lines represent the medians, and the dots represent the means. Tukey’s HSD test was used to show significant differences of means across genotypes; means that share a letter are not significantly different (P adj > 0.05). \*Gs (A) data shown collected on July 28, 2020, from 11 to 3PM.

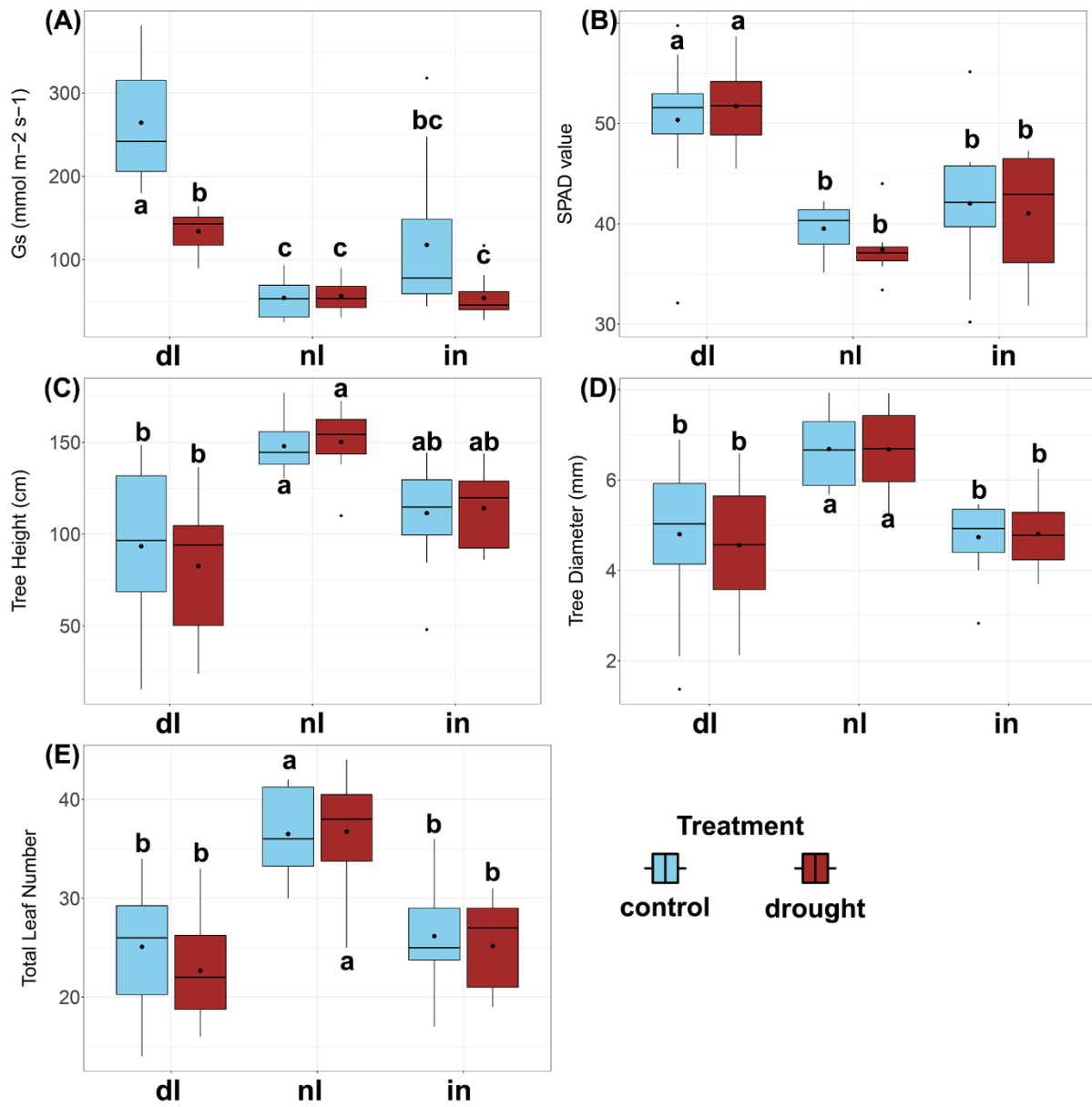


**FIGURE 4.9** | Traits measured on 8 hybrid poplar genotypes (n=64) collected during the week of July 27, 2020 (week 3 of current study). Replicates of each genotype are grouped into a well-watered control (n=32) or a drought treatment group (n=32) by week 2. Genotypes are grouped into 3 lesion categories: **dl** (3 genotypes with a deletion spanning a dQTL in Chr09), **nl** (2 control genotypes with no lesions) and **in** (3 genotypes with an insertion spanning a dQTL in Chr09). The horizontal lines represent the medians, and the dots represent the means. Tukey's HSD test was used to show significant differences of means across lesion groups; means that share a letter are not significantly different (P adj > 0.05). \*Gs (A) data shown collected on July 28, 2020, from 11AM to 3PM.

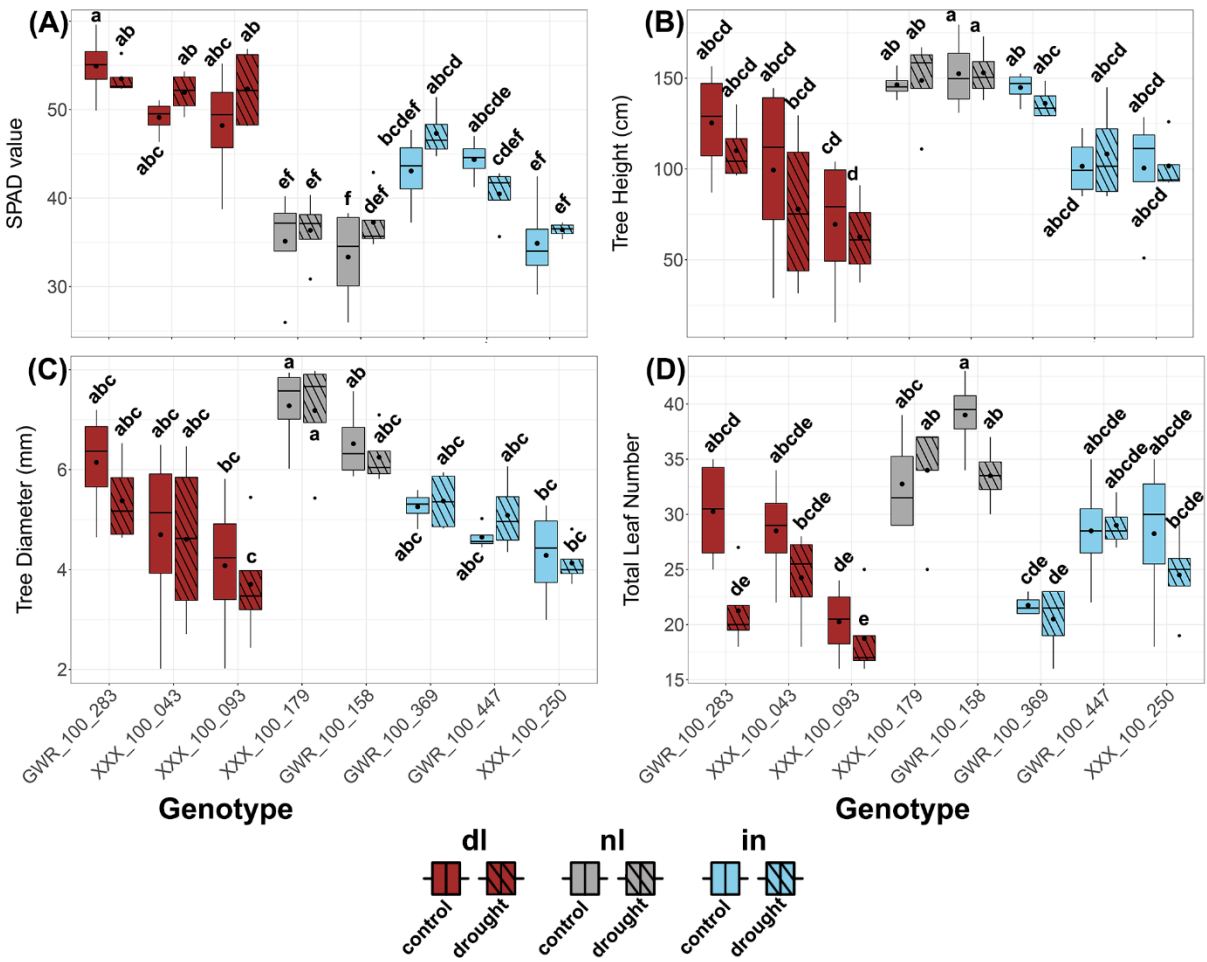


**FIGURE 4.10** | Traits measured on 8 hybrid poplar genotypes (n=64) collected during the week of August 3, 2020 (week 4 of current study). Genotypes are grouped into 3 lesion categories: **dl** (3 genotypes with a deletion spanning a dQTL in Chr09), **nl** (2 control genotypes with no lesions) and **in** (3 genotypes with an insertion spanning a dQTL in Chr09). Solid color boxes depict well-watered control trees (n=32), and diagonal line boxes show drought-treated trees (n=32). The horizontal lines represent the medians, and the dots represent the means. Tukey’s HSD test was used to show significant differences of means across genotypes; means that share a letter are not significantly different ( $P_{adj} > 0.05$ ).

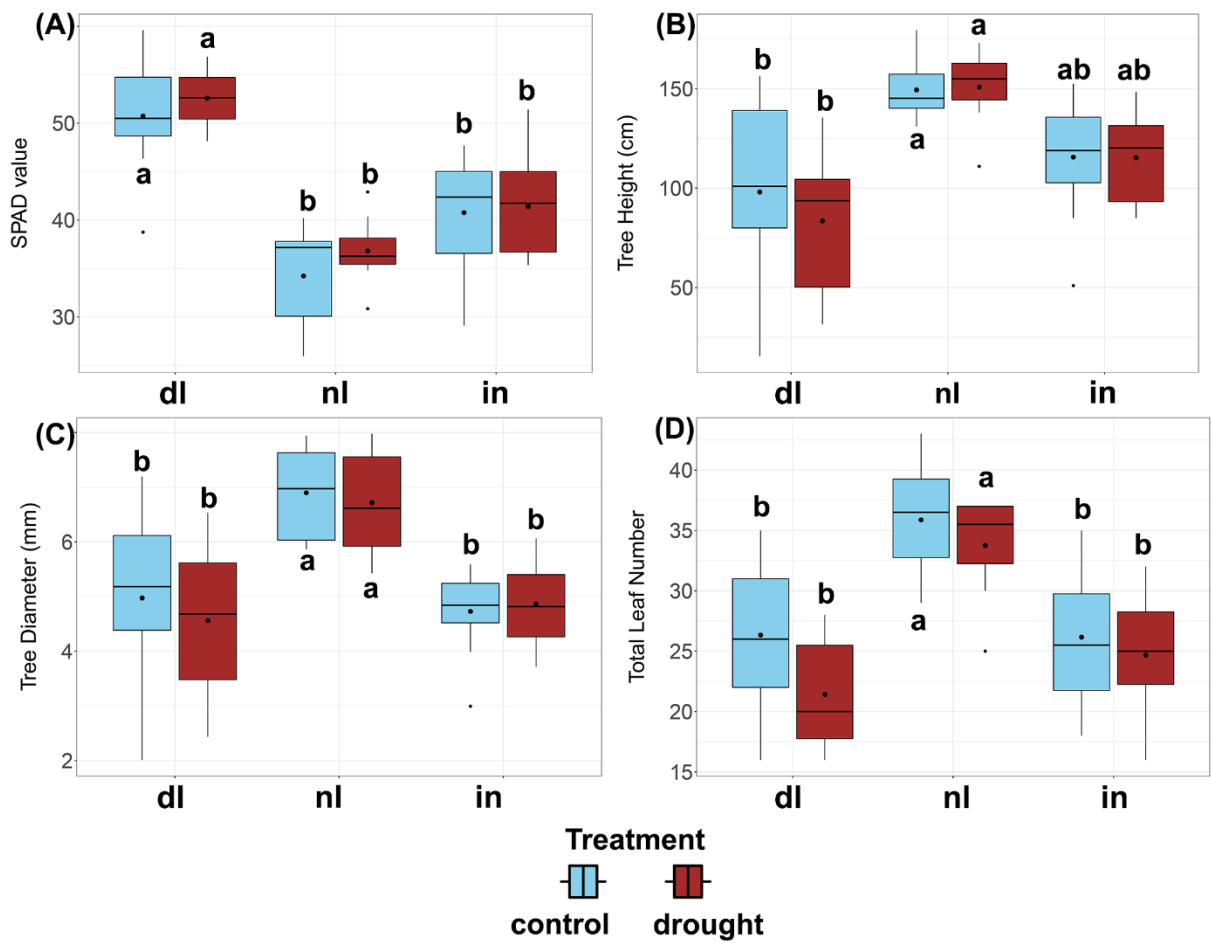


**FIGURE 4.11** | Traits measured on 8 hybrid poplar genotypes (n=64) collected during the week of August 3, 2020 (week 4 of current study). Replicates of each genotype are grouped into a well-watered control (n=32) or a drought treatment group (n=32) by week 2. Genotypes are grouped into 3 lesion categories: **dl** (3 genotypes with a deletion spanning a dQTL in Chr09), **nl** (2 control genotypes with no lesions) and **in** (3 genotypes with an insertion spanning a dQTL in Chr09). The horizontal lines represent the medians, and the dots represent the means. Tukey's HSD test was used to show significant differences of means across lesion groups; means that share a letter are not significantly different ( $P_{adj} > 0.05$ ).

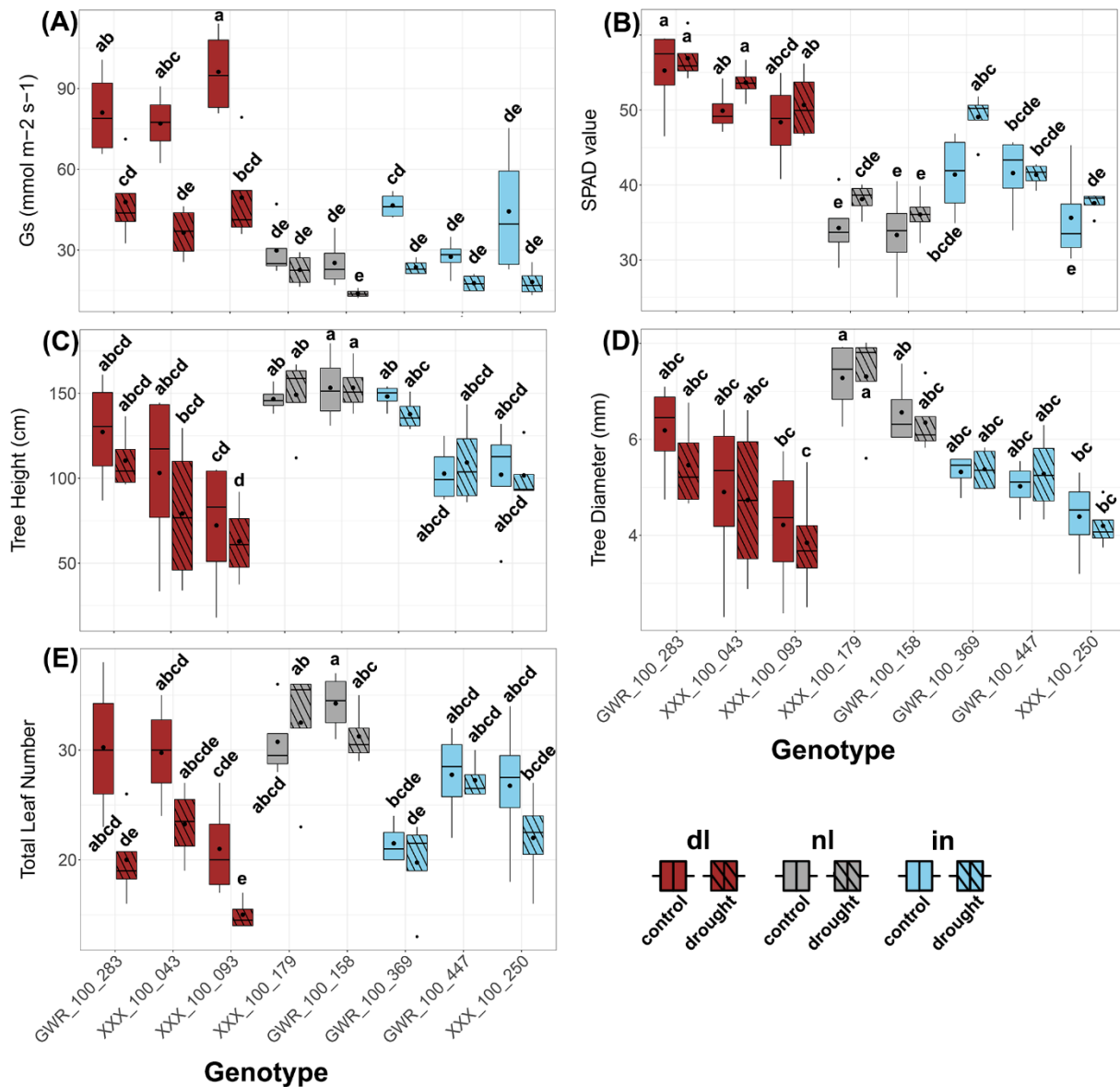


**FIGURE 4.12** | Traits measured on 8 hybrid poplar genotypes (n=64) collected during the week of August 10, 2020 (week 5 of current study). Genotypes are grouped into 3 lesion categories: **dl** (3 genotypes with a deletion spanning a dQTL in Chr09), **nl** (2 control genotypes with no lesions) and **in** (3 genotypes with an insertion spanning a dQTL in Chr09). Solid color boxes depict well-watered control trees (n=32), and diagonal line boxes show drought-treated trees (n=32). The horizontal lines represent the medians, and the dots represent the means. Tukey's HSD test was used to show significant differences of means across genotypes; means that share a letter are not significantly different ( $P_{adj} > 0.05$ ). \* $G_s$  (A) data shown collected on August 13, 2020, from 11 to 3PM.

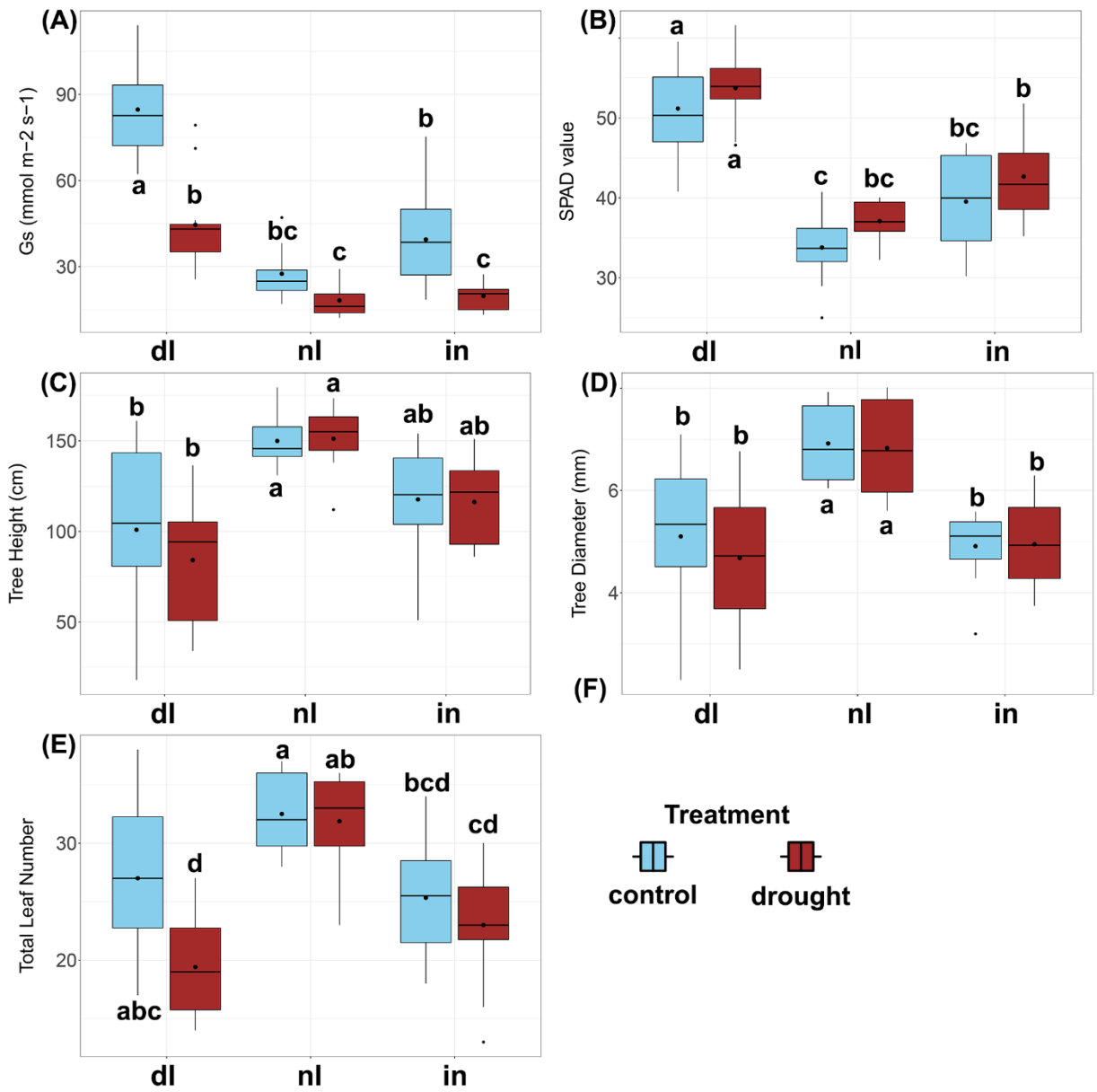


**FIGURE 4.13** | Traits measured on 8 hybrid poplar genotypes (n=64) collected during the week of August 10, 2020 (week 5 of current study). Replicates of each genotype are grouped into a well-watered control (n=32) or a drought treatment group (n=32) by week 2. Genotypes are grouped into 3 lesion categories: **dl** (3 genotypes with a deletion spanning a dQTL in Chr09), **nl** (2 control genotypes with no lesions) and **in** (3 genotypes with an insertion spanning a dQTL in Chr09). The horizontal lines represent the medians, and the dots represent the means. Tukey's HSD test was used to show significant differences of means across lesion groups; means that share a letter are not significantly different ( $P_{adj} > 0.05$ ). \*Gs (A) data shown collected on August 13, 2020, from 11AM to 3PM.

## Post-harvest trait measurements

### *P<sub>50</sub> estimates across control and drought treatments*

The traits described in Table 4.3 were measured on harvested trees after the 5-week experiment period. Control and drought-treated NL trees were harvested to estimate vulnerability to cavitation ( $P_{50}$ ) values from vulnerability curves. A control and a drought group curve were each fitted with data obtained from 6 samples ( $n=12$ ). This was done as a preliminary test to compare vulnerability curves between treatment groups, despite the lack of drought-induced changes for most traits measured during the 5-week period. Significantly different  $P_{50}$  values would justify sampling drought-treated stems within all other lesion categories.  $P_{50}$  estimates from control and drought plant curves were 1.29 and 1.09 MPa, respectively. These estimates were not significantly different, as evidenced by overlapping 95% confidence intervals (Figure 4.14). These findings confirm that the drought treatment had no obvious effects on wood growth. As effects of drought on growth traits were minimal (Figure 4.15), all analyses from here on involve only well-watered control plants.

**TABLE 4.3** | Traits examined on harvested trees ( $n=25$ ) after the end of a 5-week drought treatment across 8 hybrid poplar lines (*P. deltoides* × *P. nigra*) during the fall of 2020.

Trait	Abbr.	Units
Tree height at harvest	TH	cm
Xylem thickness	XT	mm
Mean vessel diameter	MVD	$\mu\text{m}$
Hydraulic mean vessel diameter	hMVD	$\mu\text{m}$
Vessel frequency	VF	vessels/ $\text{mm}^2$ xylem
Mean vessel circularity	MVC	unitless
Vessel grouping index	VGI	vessels/vessel group
Stem-specific hydraulic conductivity	Ks	$\text{Kg s}^{-1} \text{MPa}^{-1} \text{m}^{-2}$
Vulnerability to cavitation	$P_{50}$	-MPa

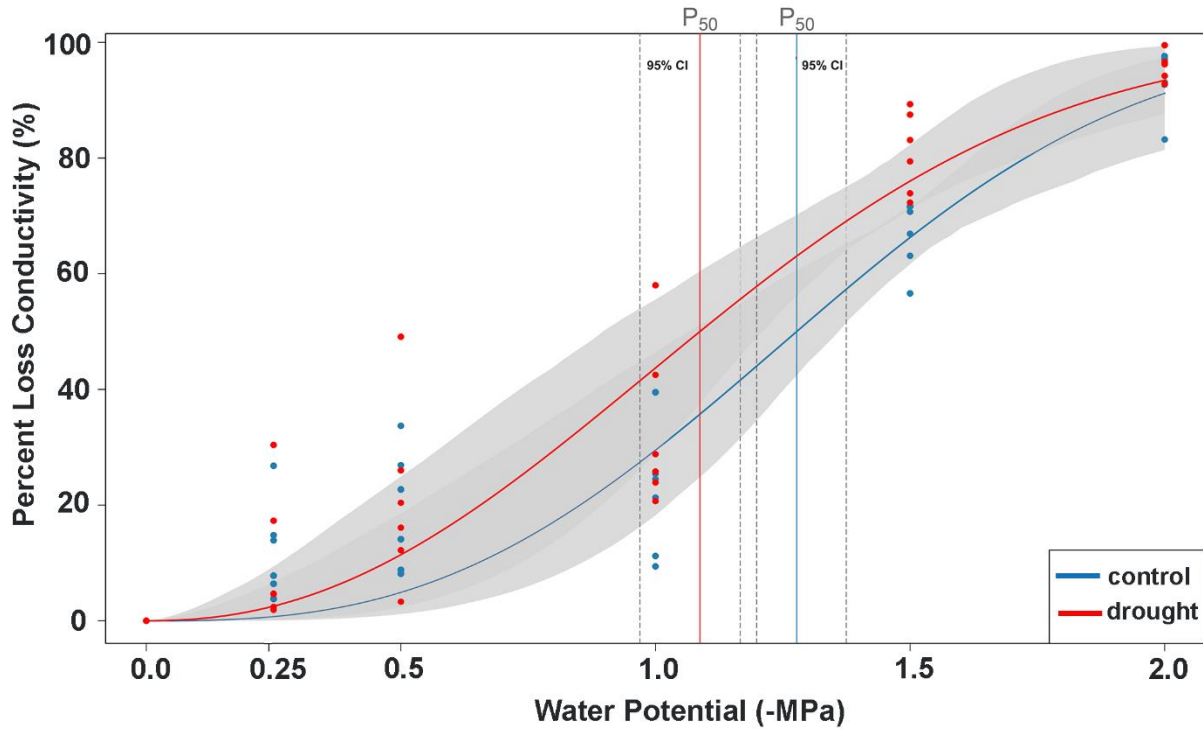


**FIGURE 4.14** | Vulnerability curves\* constructed from 2 non-lesion (nl) hybrid poplar genotypes (n=12) harvested in the fall of 2020. Trees were kept in well-watered conditions or an increasingly severe drought before harvest. P<sub>50</sub> value estimates for each lesion group are shown with upper and lower 95% confidence limits depicted with dotted vertical lines. \*Fitted using a Weibull model

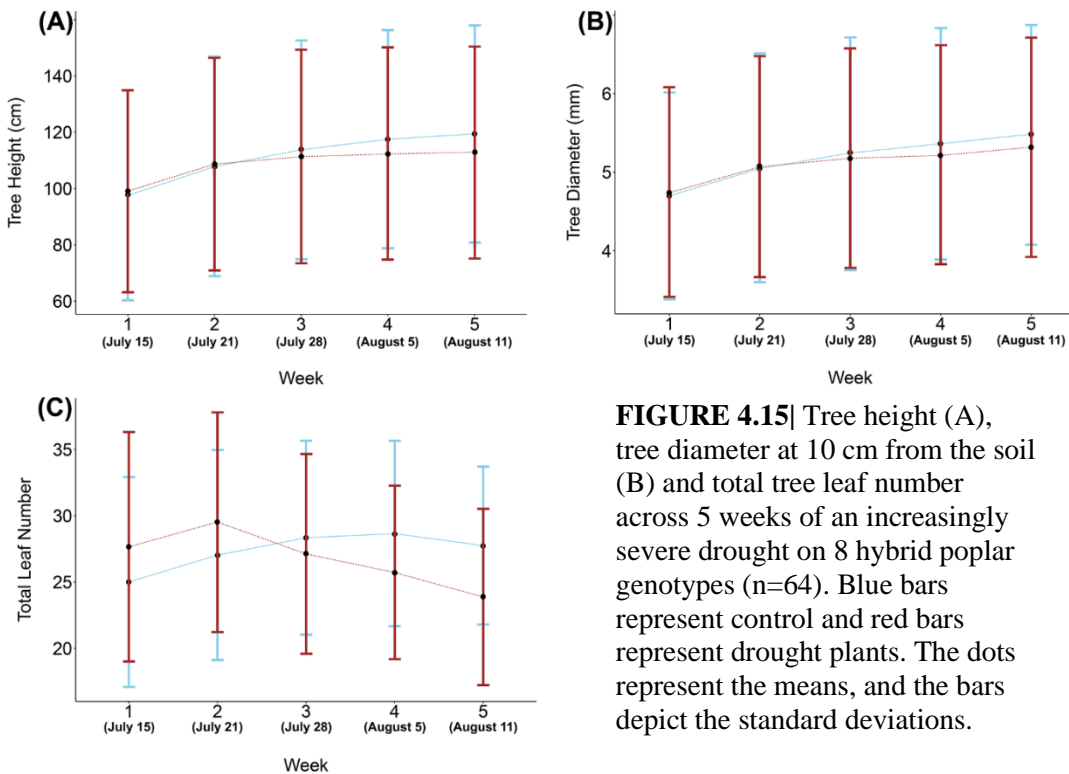


**FIGURE 4.15** | Tree height (A), tree diameter at 10 cm from the soil (B) and total tree leaf number across 5 weeks of an increasingly severe drought on 8 hybrid poplar genotypes (n=64). Blue bars represent control and red bars represent drought plants. The dots represent the means, and the bars depict the standard deviations.

*P<sub>50</sub> estimates across genotype and lesion category*

Stem specific hydraulic conductivity (K<sub>s</sub>) and P<sub>50</sub> were obtained from well-watered control group trees after the 5-week experiment period. Stems from all genotypes were sampled, with a minimum of 3 replicates (trees) per genotype (n=25). Final tree height at harvest was obtained from all trees before sampling. Two types of vulnerability curves were fitted using the same data: lesion category level curves and genotype level curves. DL, NL and IN line curves produced P<sub>50</sub> estimates of -0.92, -1.18, and -1.28 MPa, respectively.

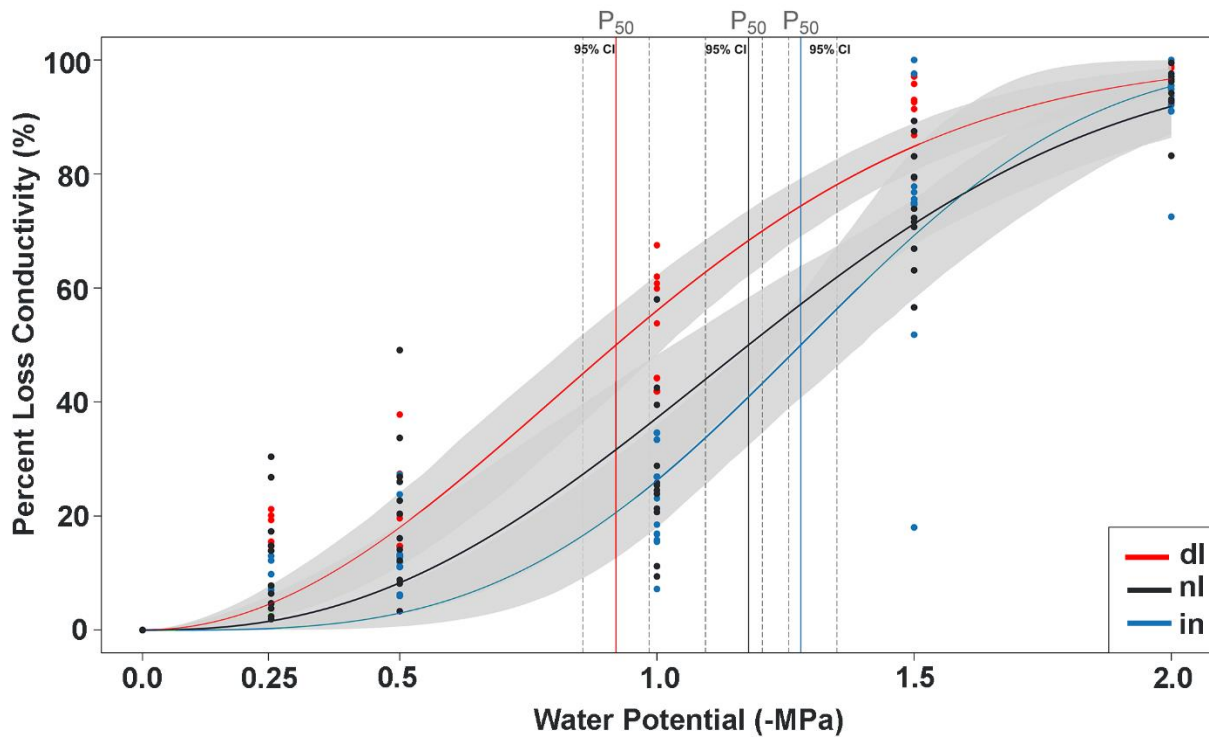


**FIGURE 4.16** | Vulnerability curves\* constructed from 8 hybrid poplar genotypes (n=25) harvested in the fall of 2020. Genotypes are grouped into 3 lesion categories: **dl** (3 genotypes with a deletion spanning a dQTL in Chr09), **nl** (2 control genotypes with no lesions) and **in** (3 genotypes with an insertion spanning a dQTL in Chr09). P<sub>50</sub> value estimates for each lesion group are shown with upper and lower 95% confidence limits depicted with dotted vertical lines. \*Fitted using a Weibull model

The 95% confidence intervals around each estimate indicate that DL lines have a significantly greater (less negative) P<sub>50</sub> than the other two lesion categories, suggesting a greater vulnerability to cavitation. NL and IN line P<sub>50</sub> estimates were not significantly different (Figure 4.16). Genotype level curves were also constructed to determine P<sub>50</sub> value differences between

individual lines. The greatest  $P_{50}$  estimate was for the DL genotype GWR\_100\_283, at -0.89 MPa, while the lowest was for the IN genotype XXX\_100\_250, at -1.41 MPa (Table 4.4). Significant differences between genotype  $P_{50}$  values largely reflected differences seen between lesion categories. Maximum  $K_s$  value differences across lesion category and genotype are reported below.

#### *Pearson's correlation tests between traits*

Wood anatomical traits (Table 4.3) were measured on the same 25 control group stems sampled for  $K_s$  and  $P_{50}$  (8 lines, with a minimum of 3 replicates per line). Pearson's correlation tests were performed between all trait combinations including final tree height at harvest (TH) and previously obtained  $K_s$  values.  $P_{50}$  estimates were excluded from this analysis as only a single value could be obtained for each genotype. We found significant correlations ( $P < 0.05$ ) between many of our measured traits (Figure 4.17). TH was positively correlated to mean vessel diameter (MVD), hydraulic mean vessel diameter (hMVD), vessel grouping index (VGI) and  $K_s$ . However, TH showed only weak and non-significant correlations to xylem thickness (XT) and vessel frequency (VF). As expected, XT was strongly directly correlated to MVD, hMVD and  $K_s$ , and strongly inversely related to VF. VF was the wood anatomical trait with the strongest correlation to  $K_s$  ( $R = -0.67$ ), followed by hMVD ( $R = 0.66$ ). No relationship was found between  $K_s$  and VGI, even though a positive correlation was expected. The strongest correlation in any direction was between MVD and VF ( $R = -0.87$ ). MVD and hMVD showed very similar relationships with other traits, with hMVD showing slightly stronger correlations to  $K_s$  and TH. Interestingly, there was an unexpected moderate to strong correlation between VGI and MVC ( $R = 0.57$ ). A second set of correlation tests was performed between the absolute values of  $P_{50}$  estimates and the average genotype values of all other traits.  $P_{50}$  was uncorrelated to most traits

and showed non-significant relationships to VF (R=0.46), VGI (R=0.43) and XT (R=-0.38). As the analysis had a low sample size, it lacked statistical power to make meaningful predictions about P<sub>50</sub>. These trends could tentatively point to a positive relationship between VF and VGI and resistance to cavitation, a relationship found in previous studies (Lens et al. 2011; Robert et al. 2009). The negative trend between P<sub>50</sub> and XT could suggest that vulnerability to cavitation increases with greater stem xylem width, which is also in line with previous studies (Cochard 1992).

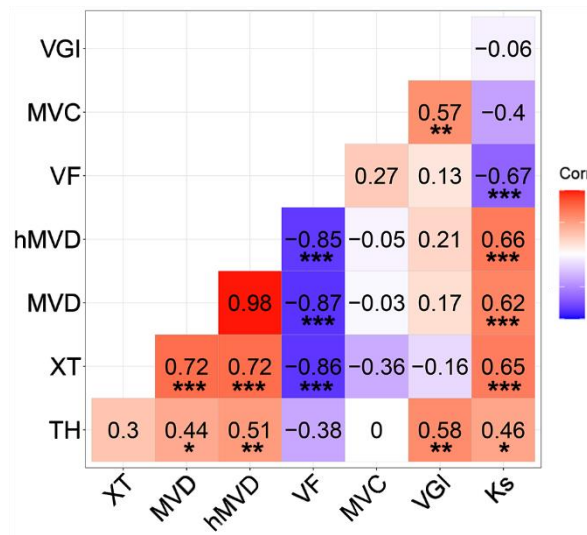


**FIGURE 4.17** | Pearson correlation coefficients between traits across 8 hybrid poplar genotypes harvested in the fall of 2020 (n=25). Traits include final tree height at harvest (TH), xylem thickness (XT), mean vessel diameter (MVD), hydraulic mean vessel diameter (hMVD), vessel frequency (VF), mean vessel circularity (MVC), vessel grouping index (VGI) and stem-specific hydraulic conductivity (Ks). Asterisks indicate significant correlations between traits (\*p ≤ 0.05; \*\*p ≤ 0.01; \*\*\*p ≤ 0.001).

*Wood anatomical traits, TH and Ks across genotype and lesion category*

ANOVA tests were performed on each measured trait (Table 4.3) to test for statistically significant differences across genotypes and lesion categories. P<sub>50</sub>, which was analyzed in previous tests, was excluded (see “P<sub>50</sub> estimate” sections above). Pot and genotype, and pot and lesion category were treated as independent factors in separate models. Pot did not have a significant effect on any trait (P>0.05). Genotype and lesion category had a statistically significant effect on all traits (P<0.0001) except MVC. TH was not significantly different across lesion categories (P=0.13, Figure 4.19a) but was different across genotypes (P=0.007). Tukey

HSD post hoc tests determined that within the DL group only genotype XXX\_100\_093 was significantly shorter than other lines (Figure 4.18a). NL lines had significantly greater MVD and Ks, while DL and IN lines were not different from each other (Figures 4.19c, g). Across genotypes, only the NL line XXX\_100\_179 had a significantly larger MVD (Figure 4.18c), while both NL lines had a significantly greater Ks compared to other lines (Figure 4.18g). IN lines had the lowest XT, greatest VF and greatest VGI (Figures 4.18, 4.19).

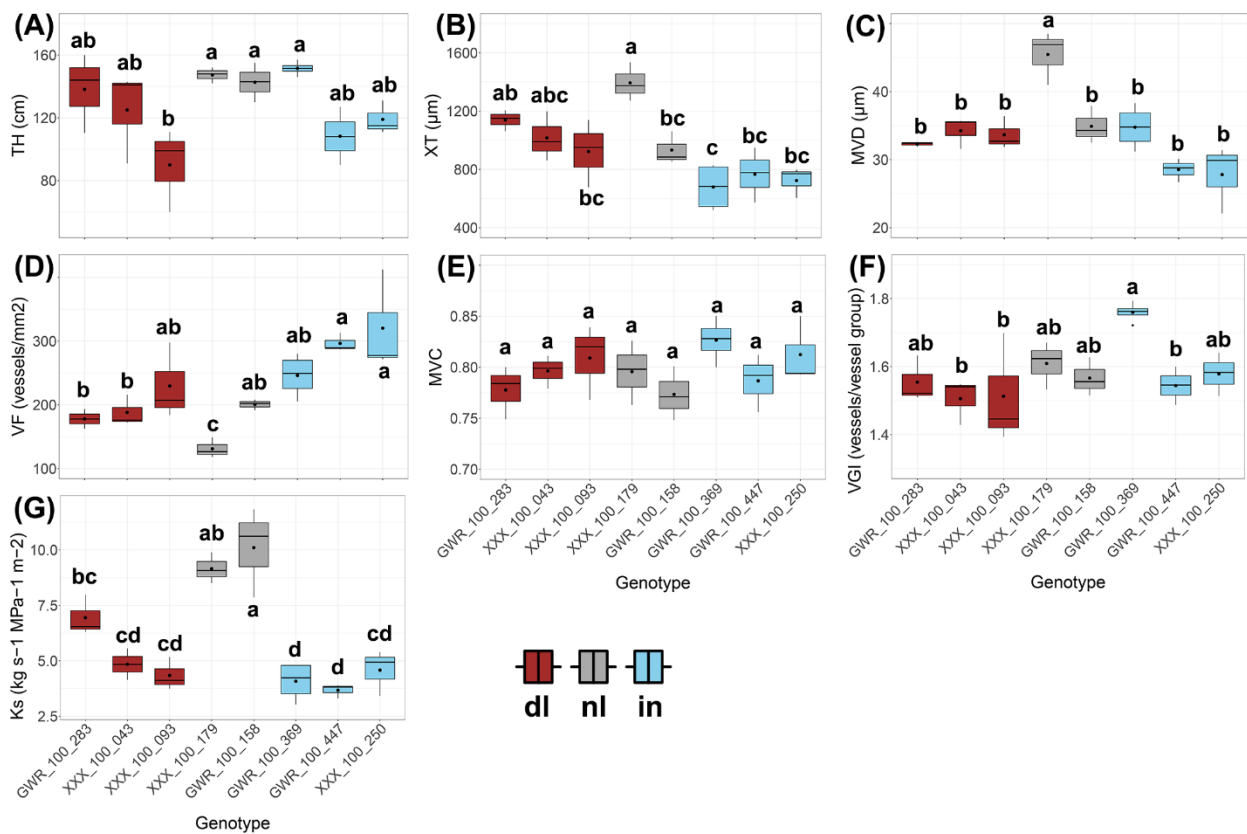


**FIGURE 4.18** | Wood traits measured on 8 hybrid poplar genotypes (n=25) harvested in the fall of 2020. Genotypes are grouped into 3 lesion categories: **dl** (3 genotypes with a deletion spanning a dQTL in Chr9), **nl** (2 control genotypes with no lesions) and **in** (3 genotypes with an insertion spanning a dQTL in Chr9). The horizontal lines represent the medians, and the dots represent the means. Tukey’s HSD test was used to show significant differences of means across genotypes; means that share a letter are not significantly different (P adj > 0.05).

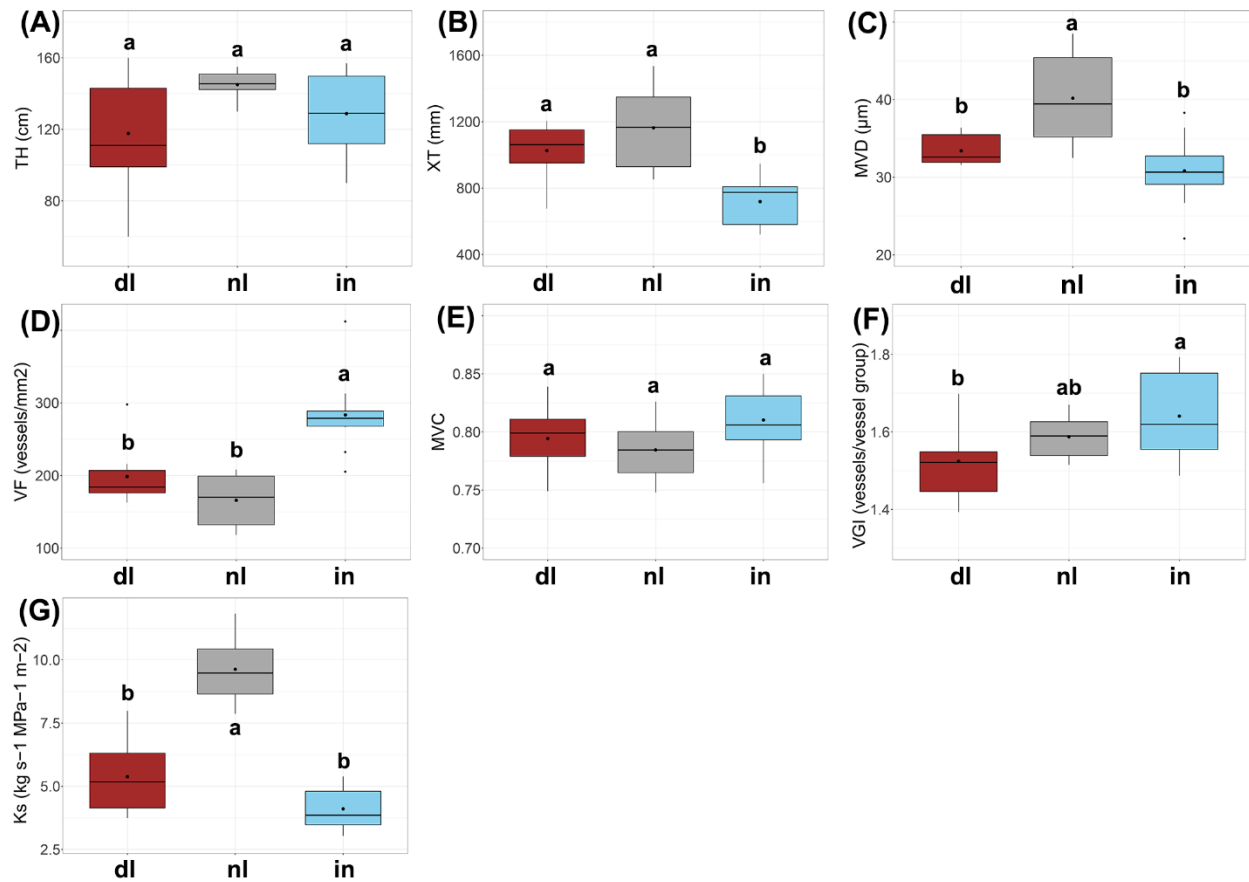


**FIGURE 4.19** | Wood traits measured on 8 hybrid poplar genotypes (n=25) harvested in the fall of 2020. Genotypes are grouped into 3 lesion categories: **dl** (3 genotypes with a deletion spanning a dQTL in Chr09), **nl** (2 control genotypes with no lesions) and **in** (3 genotypes with an insertion spanning a dQTL in Chr09). The horizontal lines represent the medians, and the dots represent the means. Tukey’s HSD test was used to show significant differences of means across lesion groups; means that share a letter are not significantly different ( $P_{adj} > 0.05$ ).

## DISCUSSION

Tree height (TH), tree diameter (TD), total leaf number (LN) and average leaf area (LA) were significantly positively correlated to each other. Tree height and diameter, in particular, reflect the most fundamental tree growth processes, which include axial growth from the shoot apical meristem and radial growth from secondary meristems (Baucher et al. 2007). Tree height is widely known to predictably scale with tree diameter, a correlation that is often interpreted as arising from mechanical, hydraulic and biophysical constraints (Hulshof et al. 2015). Mechanical

constraint hypotheses state that taller trees require wider stems to provide mechanical support against buckling (King 2005). Previous studies have shown that leaf area, tree height and cross-sectional sapwood area (which contributes to tree diameter) are positively correlated (Ceulemans et al. 1993). Hydraulic constraint models suggest that because the upward flow of water is driven by transpiration at the leaves, leaf mass must be proportional to the conductive cross-sectional area of stems (Niklas and Spatz 2004). Stomatal conductance ( $G_s$ ) was weakly but significantly inversely correlated to TH, TD, and LN, but not to LA.  $G_s$  has been shown to decrease with increasing tree height to regulate minimum water potentials in the xylem (Schafer et al. 2000). SPAD values, which are used to estimate relative leaf chlorophyll content, were not significantly correlated to any other trait. Positive correlations to our measured tree growth parameters were expected, as chlorophyll content has been extensively linked to photosynthetic capacity and growth (Carter 1998; Croft et al. 2002, Zarco-Tejada et al. 2004).

Most measured traits differed significantly across genotype and lesion category. In particular, deletion (DL) lines showed consistently greater  $G_s$  and SPAD values across a 5-week measurement time period compared to non-lesion (NL) and insertion (IN) lines.  $G_s$  has been experimentally and mathematically linked to structural and functional traits, including the ratio of leaf area to sapwood area (LA/SA), stem hydraulic conductivity ( $K_s$ ) and flow path length (Whitehead et al. 1984). Although not directly tested, high  $G_s$  in DL lines could be attributed to a genotype-dependent difference in one or more of these parameters. A lower LA/SA, a shorter flow path length, or a greater  $K_s$  could lead to increased  $G_s$  (Buckley and Roberts 2005). DL lines were generally shorter across the 5-week period (which translates to shorter flow path lengths), but not significantly shorter than IN lines during most weeks. DL lines did not show the highest  $K_s$  values.

Consequently, a future direct examination of LA/SA across these genotypes could help explain differences in Gs.

Leaf chlorophyll content (often estimated through SPAD values) has been directly related to photosynthetic capacity and growth (Croft et al. 2017; Gitelson et al. 2006). Although DL lines showed significantly greater estimated chlorophyll content, they did not exhibit the greatest productivity (as assessed through TH, TD, LN and LA). Differences in carbon assimilation ( $A_{\max}$ ) to chlorophyll content ratios across lines could help explain these findings. Hypothetical lower  $A_{\max}$  to chlorophyll content ratios in DL lines could have resulted in relatively less growth, with less carbon assimilated for every unit of chlorophyll, despite a greater chlorophyll content. A plant that maintains a low  $A_{\max}$  to chlorophyll content ratio under high growth irradiance levels (a feature seen in shade-adapted species) could become less efficient at assimilating carbon dioxide (Sims and Pearcy 1989).

DL lines also showed significantly greater  $P_{50}$  estimates from harvested stems, suggesting a greater vulnerability to drought stress-induced cavitation. The species and hybrids within the *Populus* genus are among the most drought vulnerable trees, with  $P_{50}$  estimate means of -1.44 and -1.55 MPa across pure species and hybrids, respectively (Fichot et al. 2015). The poplar hybrid examined in this study, *P. deltoides* × *P. nigra*, has been previously shown to vary widely in  $P_{50}$  across genotypes, ranging from -1.6 to -2.4 MPa in 1 year old stems (Fichot et al. 2011). Studies on 4-month-old *P. deltoides* × *P. nigra* potted trees found mean  $P_{50}$  estimates of -1.56 and -1.40 MPa (Fichot et al. 2015). In contrast, DL genotypes in our study showed unusually high  $P_{50}$  values ranging from -0.89 to -0.96 MPa. We speculate that more extreme  $P_{50}$  estimates could be a result of gene dosage variation induced by the large-scale deletions present in these lines. Broadly, the presence of indel mutations has been previously associated with increased phenotypic variation

for many poplar traits (Bastiaanse et al. 2019). Our lines were selected based on the presence of indels spanning a previously identified dQTL region, with deletions associated with greater height-corrected vessel widths (see “Chapter 2, Results”), and possibly to greater vulnerability to cavitation. Although DL lines were the most vulnerable to cavitation, they were not the lines with the greatest MVD or Ks, despite the commonly reported trade-off between hydraulic safety and efficiency (Gleason et al. 2016). Allelic variation across these highly heterozygous lines could alternatively account for observed trait variation, regardless of the presence of large-scale lesions. Future studies involving transformed trees with an identical genetic background could help disentangle gene dosage effects from the effects of allelic variation. NL lines showed greater biomass related trait values compared to DL and IN lines across the 5-week measurement period. Namely, TD and LN were significantly greater in NL lines across all 5 weeks. NL lines were taller during this period, but not significantly taller than IN lines after week 1. Gene dosage alterations have been previously linked to effects on plant biomass phenotypes, with an inverse correlation between biomass and the proportion of genotype covered in insertions and deletions (Guo and Birchler 1994; Birchler 2010). This effect has been interpreted through the gene balance hypothesis, which states that altering the stoichiometry of protein subunits (through changes in gene dosage) will affect the function of the whole complex, which can result in whole-plant level detrimental effects (Birchler and Veitia 2009).

Line specific trait responses were assessed throughout an increasingly severe 4-week drought treatment (weeks 2 through 5). Compared to well-watered DL lines, drought-treated DL lines showed a significant drop in Gs throughout this period, while NL and IN lines showed little to no response. Only until week 5 did drought-treated IN lines show a significant drop in Gs compared to their well-watered counterparts. High levels of xylem embolism, which can lead to

catastrophic hydraulic failure, can be avoided through the regulation of stomatal conductance. Namely, a reduction in  $G_s$  can help maintain minimum xylem water potentials above a threshold of runaway embolism (Tyree and Sperry 1988). Stomatal response to water deficit can vary widely across poplar species and populations, which display varying degrees of isohydric and anisohydric behaviors (Hacke 2015). Greater stomatal sensitivity to drought points to a possible isohydric water conserving strategy in DL lines. In contrast, overall lack of stomatal sensitivity in NL and IN lines points to potential anisohydric behavior. Although not examined during this study, DL lines might be able to maintain a constant minimum leaf water potential as soil dries, while NL and IN lines might decrease in leaf water potential due to lack of stomatal closure. Greater overall  $G_s$  and stomatal sensitivity in DL lines also provide some evidence for greater sensitivity to drought. Silim et al. (2009) found that drought-sensitive poplar genotypes had greater  $G_s$  values than drought tolerant genotypes under well-watered conditions. In addition, drought-sensitive genotypes showed rapid stomatal closure at greater leaf water potentials (Silim et al. 2009). We found that the lines with the lowest  $G_s$  values (NL and IN) also had the lowest  $P_{50}$  estimates, providing evidence for a previously reported link between low stomatal responsiveness to drought and resistance to stem xylem cavitation (Arango-Velez et al. 2011). With the exception of LN in DL lines, most of the other measured traits were unaffected by the drought treatment across all genotypes. In particular, drought was expected to significantly inhibit both axial and radial growth, as reported in numerous poplar studies (Cao et al. 2014; Beniwal et al. 2010; Attia et al. 2015). The start of our drought treatment during the late summer could have contributed to the lack of difference in growth. A previous study on hybrid poplar found that most drought-induced effects on radial growth and wood anatomy occurred during the early summer, with trees becoming less sensitive to the effects of drought during late summer (Arend and Fromm 2007).

## REFERENCES

- Alder, N., Pockman, W., Sperry, J., and Nuismer, S. (1997). Use of centrifugal force in the study of xylem cavitation. *Journal of Experimental Botany* 48, 665-674.
- Arango-Velez, A., Zwiazeka, J., Thomas, B., and Tyree, M. (2011). Stomatal factors and vulnerability of stem xylem to cavitation in poplars. *Physiologia Plantarum* 143, 154-165.
- Arend, M., and Fromm, J. Seasonal change in the drought response of wood cell development in poplar. (2007). *Tree Physiology* 27, 985-992.
- Attia, Z., Domec, J., Oren, R., Way, D., and Moshelion, M. (2015). Growth and physiological responses of isohydric and anisohydric poplars to drought. *Journal of Experimental Botany* 66, 4373-4381.
- Baastianse, H., Zinkgraf, M., Canning, C., Tsai, H., Lieberman, M., Comai, L., et al. (2019). A comprehensive genomic scan reveals gene dosage balance impacts on quantitative traits in *Populus* trees. *PNAS* 116, 13690-13699.
- Baucher, M., Jaziri, M., and Vandeputte, O. (2007). From primary to secondary growth: origin and development of the vascular system. *Journal of Experimental Botany* 58, 3485-3501.
- Beniwal, R., Langenfeld-Heyser, R., and Polle, A. (2010). Ectomycorrhiza and hydrogel protect hybrid poplar from water deficit and unravel plastic responses of xylem anatomy. *Environmental and Experimental Botany* 69, 189-197.
- Birchler, J. (2010). Reflections on studies of gene expression on aneuploids. *Biochemical Journal* 426, 119-123.
- Birchler, J., and Veitia, R. (2009). The gene balance hypothesis: implications for gene regulation, quantitative traits and evolution. *New Phytologist* 186, 54-62.
- Buckley, T., and Roberts, D. (2005). How should leaf area, sapwood area and stomatal conductance vary with tree height to maximize growth? *Tree Physiology* 26, 145-157.
- Cai, J., and Tyree, M. (2010). The impact of vessel size on vulnerability curves: data and models for within species variability in saplings of aspen, *Populus tremuloides* Michx. *Plant, Cell and Environment* 33, 1059-1069.

- Campanello, P., Gatti, G., and Goldstein, G. (2008). Coordination between water transport efficiency and photosynthetic capacity in canopy tree species at different growth irradiances. *Tree Physiology* 28, 85-94.
- Cao, X., Jia, J., Zhang, C., Li, H., Liu, T., Jiang, X., et al. (2014). Anatomical, physiological and transcriptional responses of two contrasting poplar genotypes to drought and re-watering. *Physiologia Plantarum* 151, 480-494.
- Carlquisy, S. (1984). Vessel grouping of dicotyledon wood. *Aliso* 10, 505-525.
- Carter, G. (1998). Reflectance wavebands and indices for remote estimation of photosynthesis and stomatal conductance in pine canopies. *Remote Sensing of Environment* 63, 61-72.
- Cassel, D. and Nielsen, D. (1986). "Field capacity and available water capacity," in *Methods of Soil Analysis* 2 ed. A, Klute (Madison, WI: American Society of Agronomy), 901-926.
- Ceulemans, R., Pointailler, J., Mau, F., and Guittet, J. (1993). Leaf allometry in young poplar stands: Reliability of leaf area index estimation, site and clone effects. *Biomass and Bioenergy* 4, 315-321.
- Cochard, H. (1992). Vulnerability of several conifers to air embolism. *Tree Physiology* 11, 73-83.
- Croft, H., Chen, J., Luo, X., Bartlett, P., Chen, B., and Staebler, R. (2002). Leaf chlorophyll content as a proxy for leaf photosynthetic capacity. *Global Change Biology* 23, 3513-3524.
- Duursma, R., and Choat, B. (2017). *fitplc*- an R package to fit vulnerability curves. *Journal of Plant Hydraulics* 4, e002.
- Fichot, R., Brignolas, F., Cochard, H., and Ceulemans R. (2015). Vulnerability to drought induced cavitation in poplars: synthesis and future opportunities. *Plant, Cell and Environment* 38, 1233-1251.
- Fichot, R., Chamaillard, S., Depardieu, C., Le Thiec, D., Cochard, H., Barigah, T., et al. (2011). Hydraulic efficiency and coordination with xylem resistance to cavitation, leaf function, and growth performance among eight unrelated *Populus deltoides* × *Populus nigra* hybrids. *Journal of Experimental Botany* 62, 2093-2106.

- Fichot, R., Laurans, F., Monclus, R., Moreau, A., Pilate, G., and Brignolas, F. (2009). Xylem anatomy correlates with gas exchange, water-use efficiency and growth performance under contrasting water regimes: evidence from *Populus deltoides* × *Populus nigra* hybrids. *Tree Physiology* 29, 1537-1549.
- Gitelson, A., Vina, A., Verma, S., Rundquist, D., Arkebauer, T., Keydan, G. et al. (2006). Relationship between gross primary production and chlorophyll content in crops: implications for the synoptic monitoring of vegetation productivity. *Journal of Geophysical Research* 111, doi:10.1029/2005JD006017.
- Gleason, S., Westoby, M., Jansen, S., Choat, B., Hacke, U., Pratt, B., et al. (2016). Weak tradeoff between xylem safety and xylem-specific hydraulic efficiency across the world's woody plant species. *New Phytologist* 209, 123-136.
- Guo, M., and Birchler, J. (1994). Trans-acting dosage effects on the expression of model gene systems in maize aneuploids. *Science* 266, 1999-2002.
- Hacke, U. (2015). "The hydraulic architecture of *Populus*," in *Functional and Ecological Xylem Anatomy*, ed. U. Hacke (New York, NY: Springer Publishing), 103-131.
- Hulshof, C., Swenson, N., and Weiser, M. (2015). Tree height-diameter allometry across the United States. *Ecology and Evolution* 5, 1193-1204.
- Jacobsen, A., Pratt, B., Venturas, M., and Hacke, U. (2019). Large volume vessels are vulnerable to water-stress induced embolism in stems of poplar. *IAWA Journal* 40, 4-22.
- Jiang, C., Johkan, M., Hohjo, M., Tsukagoshi, S., and Maruo, T. (2017). A correlation analysis on chlorophyll content and SPAD value in tomato leaves. *Horticultural Research* 71, 37-42.
- King, D. (2005). Linking tree form, allocation and growth with an allometrically explicit model. *Ecological Modelling* 185, 77-91.
- Kumar, R., Marimuthu, S., Jayakumar, D., and Jeyaramraja, P. (2002). In situ estimation of leaf chlorophyll and its relationship with photosynthesis in tea. *Indian Journal of Plant Physiology* 7, 367-371.

- Lens, F., Sperry, J., Christman, M., Choat, B., Rabaey, D., and Jansen, S. (2011). Testing hypotheses that link wood anatomy to cavitation resistance and hydraulic conductivity in the genus *Acer*. *New Phytologist* 190, 709-723.
- Melcher, P., Holbrook, N., Burns, M., Zwieniecki, M., Cobb, A., Brodribb, T. et al. (2012). Measurements of stem xylem hydraulic conductivity in the laboratory and field. *Methods in Ecology and Evolution* 3, 685-694.
- Niklas, K., and Spatz, H. (2004). Growth and hydraulic (not mechanical) constraints govern the scaling of tree height and mass. *PNAS* 101, 15661-15663.
- Pickard, W. (1981) The ascent of sap in plants. *Progress in Biophysics and Molecular Biology* 37, 181-229.
- Pittermann, J. (2010). The evolution of water transport in plants: an integrated approach. *Geobiology* 8, 112-139.
- Pockman, W., and Sperry, J. (2000). Vulnerability to xylem cavitation and the distribution of Sonoran Desert vegetation. *American Journal of Botany* 87, 1287-1299.
- Robert, E., Koedam, N., Beeckman, H., Schmitz, N. (2009). A safe hydraulic architecture as wood anatomical explanation for the difference in distribution of the mangroves *Avicennia* and *Rhizophora*. *Functional Ecology* 23, 649-657.
- Sade, N., Gebremedhin, A., and Moshelion, M. (2012). Risk-taking plants. *Plant Signaling and Behavior* 7, 767-770.
- Santiago, L., Goldstein, G., Meinzer, F., Fisher, J., Machado, K., Woodruff, D., and Jones, T. (2004). Leaf photosynthetic traits scale with hydraulic conductivity and wood density in Panamanian forest canopy trees. *Oecologia* 140, 543-550.
- Schafer, K., Oren, R., Tenhunen, J. (2000). The effect of tree height on crown level stomatal conductance. *Plant, Cell and Environment* 23, 365-375.
- Scholz, A., Klepsch, M., Karimi, Z., and Jansen, S. (2013). How to quantify conduits in wood? *Frontiers in Plant Science* 4, 56.

- Silim, S., Nash, R., Reynard, D., White, B., and Schroeder, W. (2009). Leaf gas exchange and water potential responses to drought in nine poplar (*Populus* spp.) clones with contrasting drought tolerance. *Trees* 23, 959-969.
- Sims, D. and Percy, R. (1989). Photosynthetic characteristics of a tropical forest understory herb, *Alocasia macrorrhiza*, and a related crop species *Colocasia esculenta* grown in contrasting light environments. *Oecologia* 79, 53-59.
- Sperry, J., and Sullivan, J. (1992). Xylem embolism in response to freeze-thaw cycles and water stress in ring-porous, diffuse-porous and conifer species. *Plant Physiology* 100, 605-613.
- Sperry, J., Donnelly, J., and Tyree, M. (1988). A method for measuring hydraulic conductivity and embolism in xylem. *Plant, Cell and Environment* 11, 35-40.
- Tobin, M., Pratt, R., Jacobsen, A., and De Guzman, M. (2013). Xylem vulnerability to cavitation can be accurately characterized in species with long vessels using a centrifuge method. *Plant Biology* 15, 496-504.
- Tyree, M., Davis, S., and Cochard, H. (1994). Biophysical perspectives of xylem evolution: is there a tradeoff of hydraulic efficiency for vulnerability to dysfunction? *IAWA Journal* 15, 335-360.
- Tyree, M., and Sperry, J. (1988) Do woody plants operate near the point of catastrophic xylem dysfunction caused by dynamic water stress? Answers from a model. *Plant Physiology* 88, 574-580.
- Whitehead, D., Edwards, W., and Jarvis, P. (1984). Conducting sapwood area, foliage area, and permeability in mature trees of *Picea sitchensis* and *Pinus contorta*. *Canadian Journal of Forestry Research* 14, 940-947.
- Yu, D., Janz, D., Zienkiewicz K., Herrfurth, C., Feussner, I., Chen, S. et al. (2021). Wood formation under severe drought invokes adjustment of the hormonal and transcriptional landscape in Poplar. *International Journal of Molecular Sciences* 22, 9899.

- Zarco-Tejada, P., Miller, J., Morales, A., Berjon, A., and Aguera, J. (2004). Hyperspectral indices and model simulation for chlorophyll estimation in open-canopy tree crops. *Remote Sensing of Environment* 90, 463-476.
- Zhang, J., and Cao, K. (2009). Stem hydraulics mediates leaf water status, carbon gain, nutrient use efficiencies and plant growth rates across dipterocarp species. *Functional Ecology* 23, 658-667.
- Zhang, Y., Meinzer, F., Qi, J., Goldstein, G., and Cao, K. (2013). Midday stomatal conductance is more related to stem rather than leaf water status in subtropical deciduous and evergreen broadleaf trees. *Plant, Cell and Environment* 36, 149-158.
- Zwieniecki, M., Melcher, P., and Holbrook, N. (2001) Hydraulic properties of individual xylem vessels in *Fraxinus americana*. *Journal of Experimental Botany* 52, 257-264.

## **Conclusions**

### *General conclusions*

Some of the major findings presented in this dissertation include the following. Wood vessel anatomical traits are under genetic control, as evidenced by trait heritabilities, dosage-dependent QTL mapping (dQTL) and gene expression analyses. Gene dosage is an important and previously unexplored source of stem and wood anatomical trait variation. We found significant associations between most examined traits and relative dosage across the genome, as well as dosage sensitive genes within dQTL. Smaller and more numerous vessels are related to increased transcriptional, hormonal and stress response signals in wood forming tissues. In contrast, larger and less numerous vessels are related to increased Golgi vesicle mediated transport and cell wall synthesis and modification signals. We found evidence of genetic regulation of vessel diameter and frequency that is unrelated to tree height, with candidate genes involved in cell cycle function. Lastly, we found evidence of gene dosage-dependent variation in tree physiological traits, including sensitivity to drought.

### *Hypotheses on wood vessel trait regulation*

Differences in vessel anatomy across lines could be related to an antagonistic relationship between Golgi vesicle transport activity and stress and hormone related activity. Trees with smaller and more frequent vessels showed strong transcriptional, stress response, and stress hormone related signals, even under well-watered conditions that were identical to those of larger trees. These signals were coupled with significant downregulation of Golgi transport, cell wall synthesis and modification related genes. The disruption of vesicle transport across the trans Golgi network (TGN) has been linked to hypersensitivity to water and salt stress, likely through the inhibition of stress resistance-inducing cargo transport (Rosquete and Drakakaki 2018). This

includes transport disruption of cell wall deposition and modification related cargo, with alterations in cell wall construction related to different degrees of drought tolerance (Piro et al. 2003). We broadly speculate that line-dependent variations in TGN transport capacity confer different levels of baseline cell desiccation resistance. Namely, less efficient transport of cell wall related cargo could result in desiccation-prone wall structures that lead to water stress in mesic conditions. This could ultimately induce strong stress response and hormone signals that contribute to the development of the observed wood vessel phenotype.

Ubiquitin-mediated protein degradation could also have an important role in the control of vessel size and frequency in wood. Through dQTL mapping and subsequent gene expression analyses we found that specific cell cycle associated E3 ligases are highly related to wood vessel traits. E3 ligases are components within the ubiquitin proteasome system that confer substrate degradation specificity (Stone and Callis 2007). The BIG BROTHER E3 ubiquitin ligase (BB) gene was previously characterized in *Arabidopsis* as a negative regulator of organ size. Decreased BB gene dosage was linked to increased cell growth, leading to a longer cell proliferation phase and larger organs (Disch et al. 2006). In our own poplar study, decreased BB gene ortholog dosage was linked to increased vessel element size. Preliminary immunolocalizations in woody stems suggest that this gene is primarily expressed in cells that are no longer proliferating or expanding (Gerttula and Groover, unpublished). We speculate that the poplar BB gene restricts terminal cell expansion through the targeting of expansion-promoting factors.

Interestingly, the dosage and expression of the BB gene in poplar is unrelated to tree height, a trait that is often highly correlated to vessel size and number. This correlation could be the result of common genetic pathways that affect all three traits, or pathways that directly affect

height, and indirectly affect wood traits. Because of this correlation, attempting to modify vessel traits to improve resistance to cavitation can come at the expense of tree size and wood production (Eller et al. 2017). The identification and study of genes related to height-independent vessel variation could help us determine if and to what degree wood vulnerability to drought can be modified without affecting biomass.

### *Future Steps*

The direct functional characterization of identified candidate genes will help us further understand the regulation of vessel traits in wood. Immunolocalization analyses will help us determine the exact locations of proteins coded for by candidate genes across stem sections. These will provide valuable information about cell types, cell developmental stages and broad regions of secondary xylem that are influenced by candidate genes products (Gerttula and Groover 2017). Immunoprecipitation approaches can help us determine what proteins or DNA regions our candidate gene products physically associate with. For instance, the role of ubiquitination-associated proteins such as E3 ubiquitin ligase could be elucidated through the identification of their target substrates (Yoshida et al. 2015). The dosage of specific candidate genes can be altered through *Agrobacterium*-mediated CRISPR/Cas9 transformations (Fan et al. 2015). This approach can help us causally link the dosage of a particular gene to a specific vessel development effect across trees of identical genetic background.

Single cell RNA sequencing (scRNA-seq) has been recently adapted for poplar woody stems (Chen et al. 2021) and could allow for the specific and in-depth study of developing vessel elements across lines of varying conduit dimensions and across developmental stages. Spatial transcriptomic methods involve the mapping of high-resolution expression profiles on to sectioned tissues (Giacomello and Lundeberg 2018). Although this method has not yet been

applied to woody tissues, it could help elucidate differences in expression across cell types and clusters in the context of intact xylem tissue. In addition, the development and application of a novel microendoscopic approach could allow for the visualization of cambial and wood forming cells within living stems (Groover, unpublished). This could provide an unprecedented view of real-time vessel development.

A study that expands on the findings of Chapter IV could be conducted to more closely examine the relationship between decreased dosage at a wood anatomy dQTL and sensitivity to drought. Comparing transformed poplar clones (with deletions of candidate genes within the dQTL) to wildtypes of identical genetic background could provide more conclusive evidence that dosage is related to drought sensitivity. As natural poplar stands often experience periods of prolonged drought (Anderegg et al. 2013), a significantly longer, slow-developing drought treatment could elicit responses that were not observed in the severe short-term drought applied in our previous experiment. If transformed lines show greater sensitivity through changes in growth and stomatal conductance, our aim will be to examine the contribution of wood anatomy and hydraulic failure to this response.

## **REFERENCES**

- Anderegg, L., Anderegg, W., Abatzoglou, J., Hausladen, A., and Berry, J. (2013). Drought characteristics' role in widespread aspen forest mortality across Colorado, USA. *Global Change Biology* 19, 1526-1537.
- Chen, Y., Tong, S., Jiang, Y., Ai, F., Feng, Y., Zhang, J., et al. (2021). Transcriptional landscape of highly lignified poplar stems at single cell resolution. *Genome Biology* 22, 319.
- Disch, S., Anastasiou, E., Sharma, V., Laux, T., Fletcher, J., and Lenhard, M. (2006). The e3 ubiquitin ligase BIG BROTHER controls *Arabidopsis* organ size in a dosage-dependent manner. *Current Biology* 16, 272-279.

- Eller, C., Barros, F., Bittencourt, P., Rowland, L., Mencuccini, M., and Oliveira, S. (2017). Xylem hydraulic safety and construction costs determine tropical tree growth. *Plant, Cell and Environment* 41, 548-562.
- Fan, D., Liu, T., Li, C., Jiao, B., Li, S., Hou, Y., et al. (2015). Efficient CRISPR/Cas9-mediated targeted mutagenesis in *Populus* in the first generation. *Scientific Reports* 5, 12217.
- Gerttula, S., and Groover, A. (2017). "Immunolocalization in Secondary Xylem of *Populus*," in *Xylem: Methods in Molecular Biology*, ed. M. de Lucas, J., Etchhells, (New York, NY: Humana Press), 83-90.
- Giacomello, S. and Lundeberg, J. (2018). Preparation of plant tissue to enable spatial transcriptomics profiling using barcoded microarrays. *Nature Protocols* 13, 2425-2446.
- Piro, G., Leucci, M., Waldron, K., and Dalessandro, G. (2003). Exposure to water stress causes changes in the biosynthesis of cell wall polysaccharides in roots of wheat cultivars varying in drought tolerance. *Plant Science* 165, 559-569.
- Rosquete, M., and Drakakaki, G. (2018). Plant TGN in the stress response: a compartmentalized overview. *Current Opinion in Plant Biology* 46, 122-129.
- Stone, S., and Callis, J. (2007). Ubiquitin ligases mediate growth and development by promoting protein death. *Current Opinion in Plant Biology* 10, 624-632.
- Yoshida, Y., Saeki, Y., Murakami, A., Kawawaki, J., Tsuchiya, H., Yoshihara, H., et al. (2015). A comprehensive method for detecting ubiquitinated substrates using TR-TUBE. *PNAS* 112, 4630-4635.